الجمهورية الجزائرية الديمقراطية الشعبية
République Algérienne Démocratique et Populaire
وزارة التعليم العالي و البحث العلمي
Ministère de l'enseignement supérieur et de la recherche scientifique

Université Mohamed Khider - Biskra
Faculté des Sciences et de la technologie
Département : Génie électrique
Ref :……

جامعة محمد خيضر - بسكرة
كليـــة العلـــوم و التكـنولوجـــيا
قسم : الهـندسة الكهربائية
المرجع:

Thèse présentée en vue de l'obtention
Du diplôme de
Doctorat LMD en électronique
Spécialité: Micro-électronique

Intitulé

Contribution to the numerical modeling and simulation of multilayer heterojunction light-emitting diodes

Contribution à la modélisation et à la simulation numériques des diodes électroluminescentes à hétérojonction multicouches

Présentée par :
AHMID Djelloul

Soutenue publiquement le : 20/02/2024
Devant le jury composé de :

SENGOUGA Nouredine	**Professeur**	**Président**	**Université de Biskra**
HAMAIZIA Zahra	**Professeur**	**Encadreur**	**Université de Biskra**
MEFTAH Afak	**Professeur**	**Examinateur**	**Université de Biskra**
HIMA Abdelkader	**MCA**	**Examinateur**	**Université de El oued**
LAKHDAR Nacereddine	**Professeur**	**Examinateur**	**Université de Batna**

Dedications

To my parents
To my wife
To my daughters and sons
To my sisters and brothers
To AHMID family
To all my friends

Acknowledgement

In the name of God, the most merciful.

My sincere gratitude and thanks to my supervisor Pr.HAMAIZIA Zahra for her support, research guidance and patience.

I would like to extend my appreciation to Pr.SAADOUNE Achour for his guidance and support.

I would like to express my gratitude to Pr.SENGOUGA Nouredine, Dr.GEUSBAYA Tahar and Dr.BECKHOUCH Khaled for their expert guidance, patience and constant encouragement.

I would like to acknowledge the technical and personal support provided by Pr.BENCHABANE Adel, Dr. HIMA Abdelkader, Pr.NACEREDINE Lakhdar and Pr.MAJOURI Abdelkader.

Thx to Dr.BOULILA Mohamed, Pr.AJGOU Riadh and Dr.BELMIR Okba for their encouragement.

To the president of the jury.

I extend my thanks to the members of the jury who honored me by their acceptance to examine my thesis.

my gratitude is also to the reporters of this work, for helpful comments and advices on the manuscript. Showing interest to the work and for interesting discussions after the presentation.

ملخـــص

ملخص:

تتـميز مــواد أشباه الموصلات القائمة على Nitride-III بفجوة واسعة في نطاق الطــاقة حيث يمــكن أن تغــطي الطـيف بين الأشعة فوق البنفسجية والأشعة تحت الحمراء، مما يجعــلها قادرة على توليد جميع نطـاق الألوان المرئية، وبرزت كمادة رائدة في تكنولوجيا الإلكترونيك الضوئية، وتستخدم عالميًا تقريبًا لصنع الشاشات الملونة، و توليد الضوء الأبيض و الليزر البنفسجي، حيث ظلت هيمنتها دون منازع حتى الآن.

في هذه الأطروحة، تم تصـميم ومحاكاة العديد من الثـنائيات الضوئية، مـن ضمنها الثنائيات الضـوئية الخـضراء والبنفسجية و القابلة لتوليد مجال مـتغير من الألوان بما فيها الضوء الأبــيض ، في الـــبداية قمنا بمـــحاكاة الـثنائيات الضوئية الخضراء والبنفسجية وبعد ذلك قمنا بمحاكاة ثنائيات ضوئية تتكون من طـبقتين متراكمتين باستخدام التصميم التقليدي لتوليد الضوء البنفسجي و الأخضر. ثم قمنا بتصـميم ومحاكاة نوعين من الـثنائيات الضوئية الأولى تحوي طبقتين مرتبتين أفقيا والثانية تحوي طـبقتين مرتبتين عــموديا، كليهما يولدان الضوء البنفســجي و الأخــضر و قابلتين للضبط و تــغيير الألوان.

في هذا العمل، تـــم استـخدام مـــــواد أشباه المـوصلات من نـوع III-Nitride بــحكم ميزاتها الضوئيــة. وتم تصميم هذه الثنائيات الضوئية باســتخدام برنامج المحاكاة الرقـــــــمية TCAD SILVACO-Atlas يحتوي التصميمان الأخيران على ثلاثة أقطاب كـهربائية وهذا يعطي إمكانية إصــدار الضــوء البنفــسجي (410-420 نانومتر) أو الضوء الأخضر (561-562 نانومتر) على حدة، علاوة على ذلك، يمكنهما إصــدار مزيج من كلا اللونين، وعند نسبة خليط معينة يتم الحصول على الضوء الأبيض قريبا من المعيار القياسـي، في تصميم الثنائي الضوئي المرتب أفقياً، يتم الحصول على ألوان خـليط أفضل. في تصميم الثنائي الضوئي المرتب عموديا يتم الحد من الــتأثير السلبي لامتصاص الضوء، ممــا يعــطي كفاءة خارجية جيدة. يكــتسي التصميمان الأخــيران أهمية كبيرة في تـــطبيق الإضاءة باستعمال أشباه الموصلات ، خاصة لـتوليد الضوء الأبيض والضوء متغيرالألوان قابل للضــبط.

الكلمات المفتاحــية: شواهد ضوئية باستــعمال نترات-III، امتصاص ضــوئي، بئر كمومي بنترات الانـديوم غاليوم، نظام1931 E I C ، شواهد ضوئية قابلة للضبط، المحاكاة الرقمية، أقطاب.

Abstract:

Nitride-based semiconductor materials have wide energy band gap that can cover the spectrum between the deep ultraviolet and the infrared. Meaning that they can generate all the spectrum color in the visible region and they are almost universally used for making full color displays, white light (LED) and violet lasers. They emerged as the leading material in the optoelectronic technology. Their dominance have remained unchallenged until now.

In this thesis, many structures of quantum wells light emitting diodes are designed, and simulated. They are a Green and violet SQW LEDs, dual color LEDs with two staked QWs using conventional structure, two vertically arranged SQW LED, and two laterally arranged SQW LED. Where, III-nitride materials are used.

The structures have been numerically investigated using TCAD SILVACO-Atlas simulation software. The two last proposed structures have both three electrodes. This gives the opportunity to emit violet (410-420 nm) or green (561-562 nm) light individually. Furthermore, they can emit simultaneously mixture of both colors, and at certain mixture ratio, the white light is obtained with chromaticity coordinate close to the standard norm. In the structure, where a two (SQW) are vertically arranged, better mixture colors is obtained. In the structure, where (SQW) are laterally arranged, a reduction of the negative effect of photon absorption is obtained, which will give a good external quantum efficiency (EQE).

The two last designed structures have a big importance in the application of the solid-state lighting, especially for white and multicolor light generation.

Keywords: III–nitride based LED, InGaN/GaN quantum well, system CIE1931, Color tunable LED, Numerical simulation, Electrodes, optical Absorption.

Résumé:

Les semi-conducteur à base de nitrure ont une large bande interdite d'énergie qui peut couvrir le spectre entre l'ultraviolet et l'infrarouge, ce qui signifie qu'ils peuvent générer toutes les régions de couleur visibles, on plus ils sont utilisé universellement pour fabriquer des écrans couleur et pour générer la lumière blanche (LED). Ils sont devenus les matériaux préférée de la technologie optoélectronique jusqu'à présent.

Dans cette thèse, des nombreuses structures des diodes électroluminescentes à puits quantiques sont conçues et simulées. Au début, nous avons simulé des LEDs SQW vertes et violets, après nous avons simulé un LED bicolores avec deux QW en utilisant une structure conventionnelle. Enfin, nous avons conçu et simulé un LED a deux SQW disposées verticalement et un LED a deux SQW disposées latéralement.

Dans ce travail, des matériaux de nitrure-III sont utilisés. Les structures ont été étudiées numériquement à l'aide du logiciel de simulation TCAD SILVACO-Atlas. Les deux dernières structures proposées possèdent trois électrodes. Cela donne la possibilité d'émettre une lumière violette (410-420 nm) ou verte (561-562 nm) individuellement. De plus, ils peuvent émettre simultanément un mélange des deux couleurs et à un certain rapport de mélange, la lumière blanche est obtenue avec une coordonnée de chromaticité proche de la norme standard. Dans la structure, où les deux (SQW) qui sont disposés verticalement, un meilleur mélange de couleurs est obtenu. Dans la structure, où les deux (SQW) sont disposés latéralement, une réduction de l'effet négatif de l'absorption des photons est atteinte, ce qui donnera une bonne efficacité quantique externe (EQE). Les deux structures à trois électrodes qui sont proposées ont une grande importance dans l'application de l'éclairage à semi-conducteurs, et pour la génération de lumière blanche et multi-couleur.

Mots clés : LED à base de III–Nitride, puits quantique à base de InGaN/GaN, system CIE1931, LED a couleur ajustable, Simulation numérique, Electrodes, absorption optique.

Table of Contents

List of Figure

List of Tables

*List of abbreviation*s

AlGaN	Aluminium Gallium Nitride
AlN	Aluminium Nitride
CIE	Comission Internationale de l'Eclairage
CL	Cathodoluminescence
CT	Color Temperature
CRI	Color Rendering Index
EQE	External Quantum Efficiency
FWHM	Full Width at Half Maximum
GaN	Gallium Nitride
III-N	III Nitrides
IQE	Internal Quantum Efficiency
LED	Light Emitting Diode
MBE	Molecular Beam Epitaxy
MOCVD	Metal Organic Chemical Vapor Deposition
MOVPE	Metal Organic Vapor Phase Epitaxy
MQW	Multiple Quantum Wells
PAMBE	Plasma Assisted Molecular Beam Epitaxy
PL	Photoluminescence
QD	Quantum Dot
QB	Quantum Barrier
QCSE	Quantum Confined Stark Effect
QW	Quantum Well
InGaN	Indium Gallium Nitride
InN	Indium Nitride
RGB	Red Green Blue
SAG	Selective Area Growth
SL	Super Lattice
TCAD	Technology Computer Aided Design

TD	Threading Dislocation
XRD	X-ray Diffraction
WPE	Wall Plug Efficiency
YAG	Yttrium Aluminum Garnet

List of symbols

a_0	Lattice constant
a_B	Bohr radius
A	Area
D	Diffusion constant of dopants
Dn, Dp	Diffusion constant of electrons, holes
Δn, Δp	Change in electron concentration, hole concentration
ΔE_C, ΔE_V	Band discontinuity of conduction band, valance band
α	Absorption coefficient
α0	Absorption coefficient at $h\nu = 2\,Eg$
χ	Electron affinity
λ	Wavelength
ω	(XRD) Angle of incident X-ray beam
Φ	(Semiconductors) Electrostatic potential
Eg	Semiconductor band-gap energy
J	Current density
k	Boltzmann constant
n	Density of electrons
p	Density of holes
q	Elementary charge
T	Temperature (in Kelvin)
NA, ND	Acceptor, donor concentration
Nc	Effective density of states at conduction band edge
NT	Concentration of trap or deep level
Nv	Effective density of states at valence band edge
B	Bimolecular recombination coefficient
V	Voltage
h	Planck's constant
ε	Material Permittivity
c	Light velocity

μ	Carrier mobility
η	Efficiency
η_{ext}	External quantum efficiency
$\eta_{extraction}$	Extraction efficiency
η_{int}	Internal quantum efficiency
η_{power}	Power efficiency

Physical constants.

Avogadro's number	NA = 6.02214×10^{23} atoms/g mol
Bohr radius	a_B = 0.52917 ˚ A
Boltzmann constant	kB = 1.38066×10^{-23}J/K
Electronic charge	e = 1.60218×10^{-19}C
Free electron rest mass	m_0 = 9.11×10^{-31} kg
Gas constant	R = 1.98719 cal/mol K
Permittivity in vacuum	ε_0 = 8.85418×10^{-14}F/cm
Planck constant	h = 6.62607×10^{-34}Js
Reduced Planck constant	ħ(h/2π) = 1.05457×10^{-34} Js
Proton rest mass	m_p = 1.67262×10^{-27}kg
Speed of light in vacuum	c = 2.99792×10^{8} m/s
Thermal voltage	kBT = 0.025852 eV

International system of units (SI units).

Quantity	Unit	Symbol	Dimension
Current	Ampere	A	
Current density	Ampere/m2	A/m2	
Length	Meter	m	
Mass	Kilogram	kg	
Time	Second	s	
Temperature	Kelvin	K	
Luminous	Intensity	Candela	Cd
Luminous	Fux	Lumen	lm
Frequency	Hertz	Hz	1/s
Force	Newton	N	kg m/s^2
Pressure	Pascal	Pa	N/m^2
Energy	Joule	J	N m
Power	Watt	W	J/s
Electric charge	Coulomb	C	A s
Potential	Volt	V	J/C
Conductance	Siemens	S	A/V
Resistance	Ohm	Ω	V/A
Capacitance	Farad	F	C/V
Inductance	Henry	H	Wb/A
Magnetic	Flux	Weber	Wb V s
Magnetic flux	Density	Tesla	T

General introduction

General introduction

Over the past two centuries, the development of semiconductor materials started with the invention of the first transistor at 1947.

On the other hand, in 1907 R. Henry Joseph noticed that a light was emitted from a crystallite silicon carbide, a new semiconductor applications appear and the first light-emitting diode (LED) had been born. He immediately reported his observations. In 1928, Oleg Losev reported that the luminescence phenomenon observed with SiC materials was not caused by incandescence but by a phenomenon termed electroluminescence. Since then, many semiconductors materials have been used in LED manufacturing, in 1960 SiC p-n junction blue LED, next in 1962, the infrared GaAs LEDs was produced. Also, the year of 1962 has seen, the appearance of visible-spectrum LEDs, using GaAsP junctions. Between 1963-1964, used GaP p-n junction LEDs to emit efficient red light that is clearly seen with the eyes. Then in 1967, visible red LED was fabricated using AlGaAs materials. in 1968 Green LEDs were formed with efficiencies. The Monsanto team attains emission in the red, orange, yellow, and green wavelength range using GaAsP [6-8]. Moreover, in 1968, researchers started working on GaN, until they obtain the first single-crystal film of GaN, which is n-type without intentional doping. But they failed to find a p-type dopant so that they could make a p-n junction. The first example of electroluminescence from GaN was announced in 1971, where blue light centered at 475 nm was emitted. This diode was the first current-injected GaN light emitter, where green and blue light was generated. In 1972 the magnesium has been used as second choice of p-type dopant, the blue and violet emission centered at 430 nm has been obtained. This method did not exhibit p-type conductivity, so that the luminescence of these devices were inefficient, and as a consequence this hard work is terminated. However, in 1989 the first p-type doping and p-type conductivity in GaN has been obtained. These p-type doping paved the way to efficient III-nitride based p-n junction LEDs. And the first GaN p-n-homojunction LED was reported. it emits light in the ultraviolet (UV) and blue. In 1994, Nakamura et al reported a high luminosity blue LED, from GaN and related alloys. This was possible after the achievement of good p-type GaN. LEDs have been produced in blue, violet, and UV. This achievement give the possibility to manufacture full color LED displays and color temperature tunable white light emitting diodes (LEDs) [11-17]. Where extensive research has been done to improve the design of light emitting diodes (LEDs), in such way that they acquire an extremely long life and good light quality [6]. Where a great energy saving was achieved, this makes them as a promising technological solution to replace conventional light sources such as incandescent bulbs and fluorescent lamps, and excellent candidates for visible light communication (VLC).

But GaN based LEDs encounter limitations due to many problems in the family of nitrides and associated alloys. For visible LEDs, the conversion efficiency decreases with increasing current density. In addition the sapphire which is generally used as substrates for III–nitride LEDs, shows several disadvantages such as the thermal expansion coefficient mismatch. Moreover, the QW LEDs grown on sapphire substrate have large polarization electric field, which leads to the quantum confined Stark effect (QCSE), this will lower the internal quantum efficiency [13,14]. Also it has a poor thermal conductivity which limit heat dissipation, and because it is an insulator, the LEDs must have a lateral configuration. Those problems becomes more significant for longer wavelength devices such as green LEDs.

In addition the phosphor has been used as wavelength converter in the white light and multicolor LEDs [16] generation, but this technique shows many draw backs such as high correlated color temperature (CCT), low color rendering index (CRI), and slow frequency response limitation. Hence many researchers have proposed phosphor free LEDs [11-15], in which a multi-quantum well (MQW) with different In content active layer was used [11-15,17], those structures suffer from low performance because of inhomogeneous carriers distribution as reported in many works [18]. In addition the chromaticity coordinates depend on the injection current due to the wavelength blue shift. Moreover a critical problem is encountered where a part of the photon generated by the higher band gap active layer will be absorbed by the lower band gap active layer [19]. It is also reported that the radiative recombination efficiency decreases with increasing Indium composition [20], all of those drawbacks will make the conception of white light and different emissions colors MQW LEDs very difficult. Some researchers have designed a color-tunable LED, generally with three terminals structure [21], where QW are vertically staked, which suffer from the photon absorption effect as the ordinary multi-color emitting MQW LED.

The main goal of the thesis

The purpose of this work is expressed through the need of inorganic LED devices that have low internal electric field, high luminous efficiency, low wavelength blue shift, which is phosphor free, and that can generate broad emission band and make the carriers distribution homogenous, also limits the absorption effect. Where many structures are propose and designed to improve the optical and electrical performances of III-nitride based LEDs, using the InGaN active layer, GaN barriers, AlGaN electron blocking layers (EBL), single (SQW) or multiple quantum wells (MQW). We focus our objectives on the study of the theories and models for the description of inorganic semiconductors electroluminescence, investigate the mechanisms of injection, transport and

recombination of charges in inorganic materials. In addition the defects present in the structures will be analyzed in order to determine the physical mechanisms responsible for the degradation of the injection efficiency. Where the ATLAS simulator was utilized for this purpose, it is a powerful tool for understanding and designing electronic devices, it determines the key parameters affecting performance. In this work different models have been used to simulate complete structures of LEDs, this TCAD tool predicts many physical properties in different operating conditions without actual fabrication, and makes the optimization very easy which will save time, money and energy [23].

The main achieved works of this thesis was the design and simulation of many structure, they are Green and violet SQW LEDs, dual color LEDs with two staked QWs using conventional structure, also, two vertically arranged SQWs LED [21], finally two laterally arranged SQWs LED.

Organization of this thesis

The thesis consist of five chapters as follows:

Chapter one is reserved to III–nitride materials, especially the properties that have a relation and influence on the LEDs.

Chapter two discuses the light characteristics, mainly the color representations by CIE method**,** and the color rendering, the black body temperature CCT**,** finally the Color mixing in the LEDs is explained.

Chapter three is devoted to Light emitting diodes, where the different theories and laws of the semiconductor physics are presented, the used semiconductors and structures for LEDs are described, finally LEDs characteristics are presented.

Chapter four presents TCAD Device Simulation Tools, where the different simulators are listed, the models and the parameters are investigated, also the Order of he Commands in ATLAS simulator which used in our design are presented.

Chapter five presents the numerical simulation results of the comparative study between violet and green InGaN-based SQW LEDs, and that of the proposed devices, which are dual wavelength LED with two QWs, color tunable vertically stacked QW LED, and color tunable laterally arranged quantum well LED.

Chapter I

III–Nitride Materials

I.1. Introduction

Based on the electrical properties there are three classes of materials that are conductors, insulators and semiconductors [24] as seen in Figure I.1. The conductors have high conductivity of heat and electricity such as copper, aluminum and silver. Their valence band and conduction band generally overlap, they have a resistivity ρ smaller then $10^{-5}\Omega$.cm. Whereas the insulators have low conductivity of heat and electricity such as glass, paper and plastic. They are characterized by a valence and a conduction band that are separated by energy band gap greater then 5eV, they have a resistivity ρ greater then $10^{8}\Omega$.cm. Finally the semiconductors that can be good conductor of electricity by many ways such as heat, light and doping. Silicon, germanium and gallium nitride are different kind of semiconductors. Their valence and conduction band are separated by energy band gap between 0.7eV and 3eV, they have a resistivity ρ between $10^{-3}\Omega.\text{cm}$ and $10^{-4}\ \Omega$.cm.

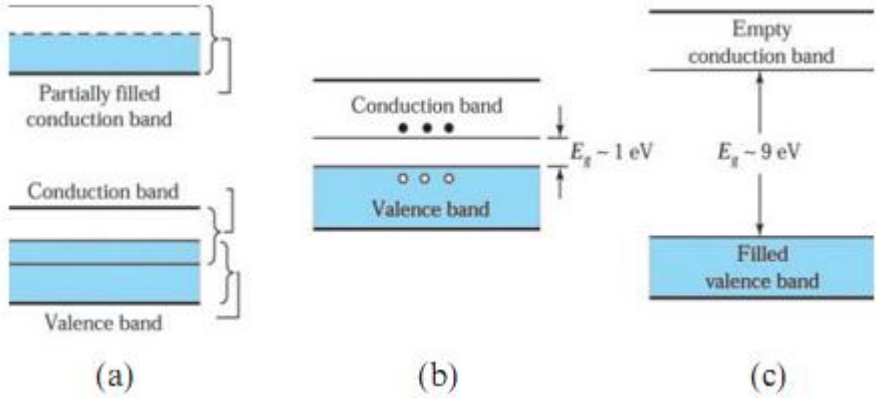

Figure I.1: energy band diagram (a) a conductor band gap

(b) a semiconductor band gap (c) an insulator band gap [24].

The semiconductors have two categories, the Organic materials which are comprised mostly of carbon and hydrogen atoms [25,26], their conductivity could be increased up to a level close to that of a typical metal, after exposure to special chemical vapors, which leads to high conductivity. This has encouraged the growth of organic electronics field. And the inorganic materials like Si, Ge, ZnO, and III-nitrides semiconductors.

In this chapter we will see many inorganic semiconductors, and we will concentrate our study on the III–nitride materials, in addition the properties of the III–nitride materials will be covered. The investigation will focus on the properties that have a relation and influence on the LEDs, especially the crystal structure types and the atom arrangement in semiconductors, where the single-crystalline semiconductor characteristics are sited and explained in detail. After that we will cover the elastic properties and the influence of the polarization on the GaN based LEDs. Also optical, electrical and thermal properties will be studied. Moreover, we will deal with the doping and its

influence on the Fermi level and quasi Fermi level. Finally the electrical contacts and the substrates used for LEDs will be interpreted.

I.2. Inorganic semiconductor

There are many inorganic semiconductors types [24]. Which are the elemental category such as Si and Ge, they are from Group IV, the Compound category like GaN and GaAs, which are formed from one group III element and one group V element. ZnO and HgSe are another's compound, they are constituted from one group II element and one group VI element. Finally the alloys category, they are Binary alloy such as $Si_{1-x}Ge_x$, ternary alloy like $Al_{1-x}Ga_xN$ and $Al_{1-x}Ga_xAs$, which are composed of two element from group III and one element from group V, and Quaternary alloy like AlGaInN constituted of three element from group III and one element from group V and InGaAsP constituted of two element from group III and two element from group V.

The inorganic semiconductor can be obtain from the elements sited in periodic table as listed in Table I.1.

	III	**IV**	**V**	**VI**
	B Boron	C Carbon	N Nitrogen	O Oxygen
II	Al Aluminum	Si Silicon	P Phosphors	S Sulfur
Zn Zinc	Ga Gallium	G Germanium	As Arsenic	Se Selenium
Cd Caduim	In Indium	Sn Tin	Sb Antimony	Te Tellurium
Hg Mercury	Ti Thallium	Pb Lead	Bi Bismuth	Po Polnium

Table I.1: A portion of the periodic table elements that can form semiconductors [3].

The III-nitrides semiconductors such as AlN, GaN, and InN and their ternary (AlGaN and InGaN), and quaternary (AlGaInN) alloys, are widely used for the optoelectronic devices. They are characterized by the wider direct band-gap among the other semiconductor groups, ranging from 0.7 eV to 6.2 eV. They can be used for optoelectronic applications such as light detectors, solar cells, laser diodes (LDs), and LEDs with wavelengths ranging from the near infrared to the deep ultraviolet, including visible light, they have high efficacy in satellite technology and nuclear reactors where others semiconductors cannot accomplish the mission**.**

I.3 The III–nitride properties

The study of the semiconductors properties will help to design, simulate and manufacture the needed devices. Hence the structural, electrical, thermal, and optical properties of the III–nitride materials will be investigated. Whereas the properties of ternary compounds(AlGaN and InGaN), and quaternary (AlGaInN) alloys, generally depend on the alloy composition, and they are

calculated by the Vegards law. But in some cases there is a bowing parameter which have to be taken in consideration, hence modeled using a quadratic polynomial with a nonlinear coefficient. Such as the band gap where the bowing parameter, b, accounts for the deviation from a linear interpolation.

I.3.1. The III–nitride structural properties

The atoms in semiconductors have three types of arrangement. They are amorphous semiconductors where the atoms are randomly arranged, also the polycrystalline semiconductor, where the regions of crystalline separated by grain boundary, in addition the single-crystalline semiconductor, characterized by repeating arrangement of atoms.

I.3.1.a The single-crystalline semiconductor characteristics:

A crystal is a periodic arrangement of base in three dimensions space. This base can consist of a single or group of atoms. One base is located at each lattice point. where a set of translation vectors a_1 , a_2 and a_3 can represent any point R in the crystal lattice [1-5], given by:

$$R = n_1 a_1 + n_2 a_2 + n_3 a_3 \qquad \text{I.1}$$

The unit cell concept: Unit cell is a region of space which can generate the entire crystal lattice by repetition through lattice translations, where The smallest volume unit is called the primitive unit cell.

Bravais lattices: It is three-dimensional classification of the lattice depending on their angles and basis vectors ,where the unit cells which are translated in all directions to form the entire space, they are 14 different types, and seven systems. They are sited in Table I.2.

Lattice systems	Angles and basis vectors	Bravais lattices
Triclinic	b1 ≠ b2 ≠ b3 α ≠ β ≠ γ	Simple
Monoclinic	b1 ≠ b2 ≠ b3 α = β = 90◦≠ γ	Simple base-centered
Orthorhombic	b1 ≠ b2 ≠ b3 α = β = γ = 90◦	Simple, base-centered, body-centered face-centered
Tetragonal	b1 = b2 ≠ b3 α = β = γ = 90◦	Simple body-centered
Trigonal	b1 = b2 = b3 α = β = γ ≠ 90◦	Simple
Cubic	b1 = b2 = b3 α = β = γ = 90	Simple body-centered, face-centered
Hexagonal	b1 = b2 ≠ b3 α = β = 90◦,γ = 120◦	Simple

Table I.2: Seven lattice systems and fourteen Bravais lattices [4].

The semiconductors can be found in four important crystal structures which are diamond structure, zinc-blende structure, wurtzite structure, hexagonal close-packed structure as seen in Figure I.2.

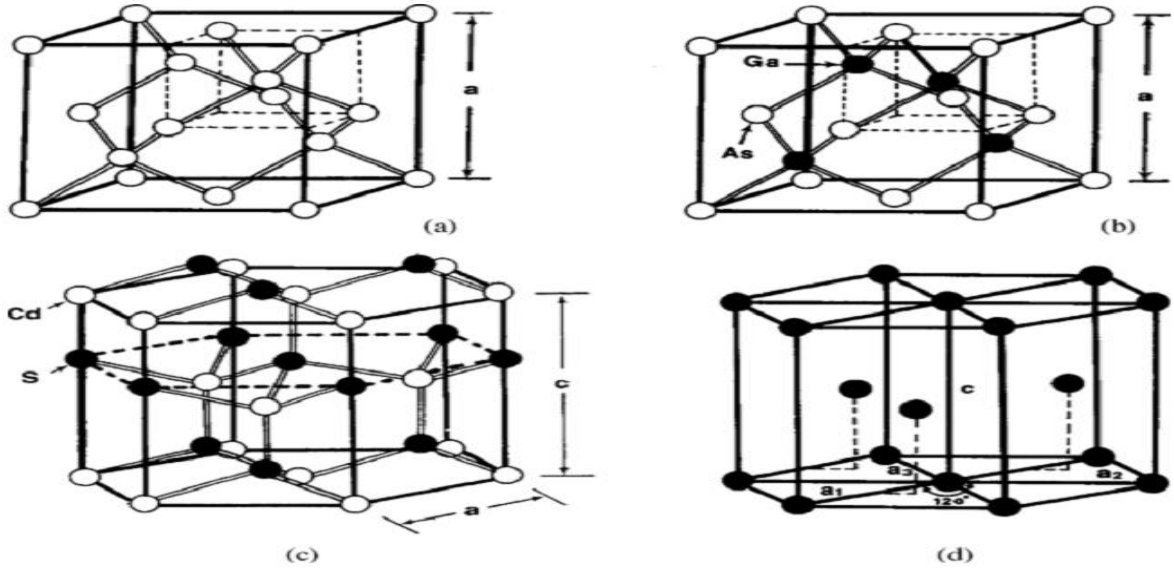

Figure I.2: The crystal structures for elemental and compound semiconductors[4].

Semiconductors	Elements	Lattice structure	Lattice constant
III-V compound semiconductors	GaN	Zinc blende	4.50
	GaN	Wurtzite	a = 3.189, c = 5.185
	AIN	Wurtzite	a = 3.11, c = 4.98
	InN	Wurtzite	a = 3.54, c = 5.70

Table I.3: The crystal structures and lattice constants for the III-V semiconductors [4].

Miller indices: The crystals are terminated at a surface, which has a big influence on the device characteristics, the three Miller indices (hkl) described mathematically the directions and planes surface of atoms in a crystal. Whereas the hexagonal system, has four crystallographic axes.

The reciprocal lattice: In a crystal lattice, all physical quantities have the periodicity of the lattice, in all directions. The wave vector K has the dimension of an inverse distance and for a periodic function, it can take discrete values in a three dimension. The concept of reciprocal or momentum space is important for the classification of electron states in quantum theory. There is a relation between lattice planes and reciprocal lattice vectors, since the plane crosses the x_1 axis at $x_1 = 1/l_1$, where the distance is measured in units of a1. Similarly, for the two others axis. Hence, the Miller indices l_1, l_2, l_3 of a lattice place is the reciprocals of its intercepts on the axes x_1, x_2, x_3.

The Brillouin zone: We can construct unit cells in the reciprocal lattice as the same manner for the real lattice, where the smallest unit cell in k-space is called the "first Brillouin zone".

I.3.1.b The III–nitride structure types

As structural point of view, there are mainly two types of crystal structures for group-III nitrides, cubic zincblende which is thermodynamically metastable. Whereas the hexagonal wurtzite, is thermodynamically stable [10], as seen Figure 1.3 and Figure I.4.

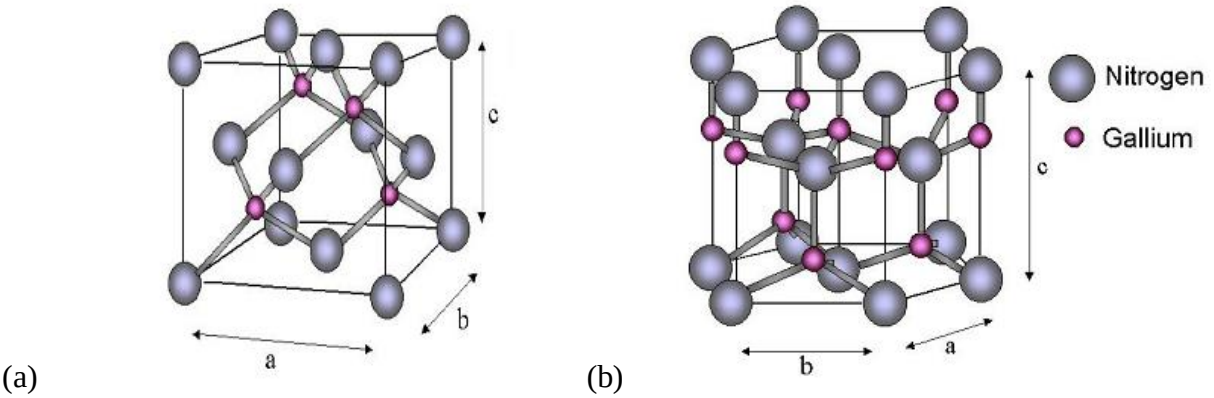

(a) (b)

Figure I.3: (a) Zincblend crystalline structure. (b)Wurzite crystalline structure.

The III–nitride Wurtzite structure:

Many III-V semiconductor compounds such as III–nitride can have the wurtzite structure shown in Figure I.4. This structure has two hexagonal close-packed lattices, each one consist of different atoms, they are interpenetrating and displaced from each other by 3/8c along the z-axis. There is 6 Nitrogen atoms and 6 Gallium, Indium or Aluminum atoms per unit cell in the Wurtzite structure. There is no inversion symmetry in this crystal, and polarity effects are observed along the z-axis. The point group of the wurtzite structure is C6.

I.3.2 The electrical properties

The band gap Eg is calculated by applying quadratic polynomial whose nonlinear coefficient is the bowing parameter b. as seen in the following formula [27]:

$$E_g = Eg_{InN}(x) + Eg_{GaN}(1-x) - 3.8x(1-x) \quad \text{I.2}$$

where (x) is the Indium content in InGaN, Eg_{InN} and Eg_{GaN} are band gap energies of InN and GaN.

The semiconductor band gap changes with temperature. The new value of the band gap is given by Varshni et al. [8].

$$E_g = E_{g0} - \frac{\alpha T^2}{T+\beta} \quad \text{I.3}$$

Where E_{g0} (T = 0), α and β are Varshni's thermal coefficients.

System	Material	E_{g0} (eV)	α (10^{-4} eV/K)	β (K)
III–V	w-AlN	6.242	7.2	500
	α-GaN	3.484	12.8	1190
	InN	1.915	2.45	624

Table I.4: E_{g0} and Varshni's thermal coefficients group III–V semiconductors.

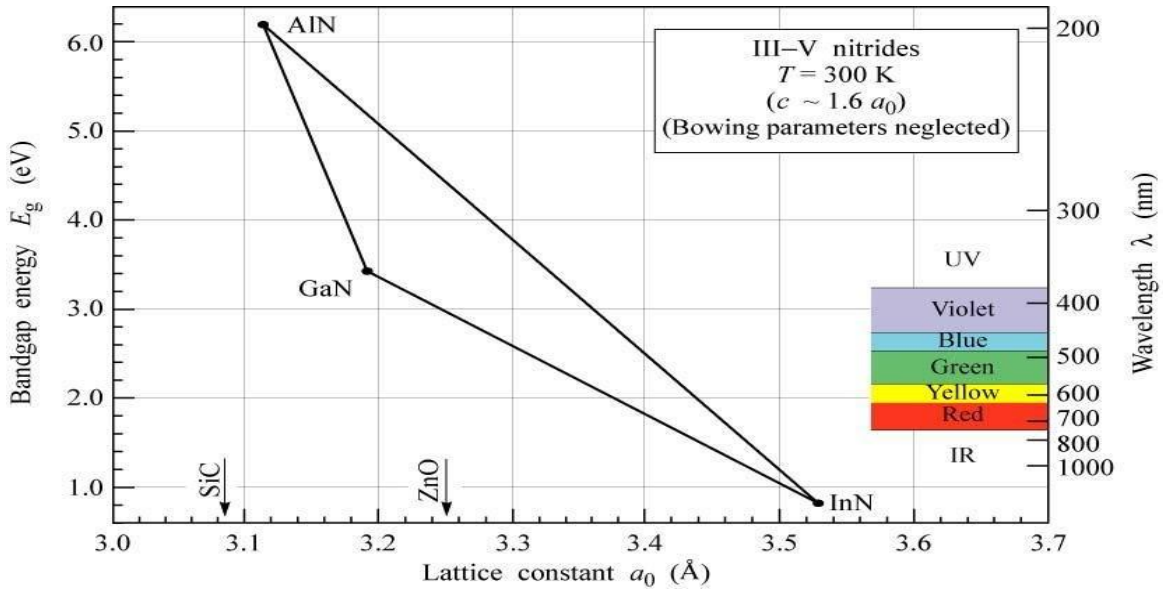

Figure I.4: Graph of the band gap energy vs. lattice constant for group III-nitrides [8].

I.3.3. The elastic properties

The polarization has a big influence on the GaN based devices, this is due to the non-cubic symmetry of GaN materials, and hence compressively strained active regions in InGaN LEDs, will induce both spontaneous and piezoelectric polarization charges. This will generate a strong internal electric field (IEF), generally on the MV/cm order, resulting in reduction of the overlap between electron and hole wave functions, efficiency droop and blue-shift in the wavelength at a high injection current [6].

Where the total polarization is the sum of the spontaneous and the piezoelectric polarization. The III-V nitrides materials parameters related to the polarization are based on the research of F. Bernardini, et al [28], the model used and the calculation of the spontaneous, piezoelectric and total polarization will be discussed in detail in the fourth chapter.

I.3.4. The optical properties

When the generated photons escape out of the device, the light travels from a medium with a higher refractive index to a medium with a lower refractive index, a total internal reflection occurs at the interface. Also some photons can be reabsorbed by the active region or trapped in the device. Hence the refractive index and the absorption process have very high impact on the extraction efficiency.

The refractive index

when involving light, the refractive index has a big impact on semitransparent or opaque materials. To treat the interaction of light with materials, it is necessary to consider the refractive index as a complex number. In this case, the complex refractive index N is written in the form:

$$N = n + ik \qquad \text{I.4}$$

where n is the refractive index and k is the absorption index. The real part of the complex refractive index, n, accounts for the interaction of light with the non-absorbing part of the medium, and the imaginary part of the complex refractive index k, represents the absorptive properties of the medium through which the light travels. The refractive index and absorption coefficient of GaN are important when designing the LEDs devices. The refractive index of GaN is about 2.85 for a wavelength of 362 and about 2.3 for a wavelength of 827 [29]. These refractive index values are large enough to induce difficulties in extracting photons, in particular total internal reflections.

The absorption process

Not all photons emitted internally can escape from the semiconductor due to the absorption. Since as a beam of light passes through a material it gradually loses intensity, due to the attenuation process. Caused by the interaction of light with a material by absorption. In cases where absorption is present, the absorption coefficient α_a is related to k by:

$$\alpha_a = \frac{4\pi k}{\lambda} \qquad \text{I.5}$$

When attenuation takes place in a homogeneous solid, the amount of light transmitted by a semitransparent plate of thickness x is given by the absorption rule:

$$I = I_0 e^{(-\alpha L)} \qquad \text{I.6}$$

Where I_0 and I are the intensities at the initial and final points of the light path, α is the absorption coefficient (α GaN = 150 cm^{-1}) and x is the distance travelled by each light ray.

I.3.5. The thermal properties

The thermal expansion coefficient and thermal conductivity are very important for LEDs device design. Where GaN are promising materials in optoelectronic devices industry due to the high thermal conductivity and thermal stabilities. Knowing that thermal expansion coefficient mismatch results in strain relaxation, cracking, and defect formation, where elimination of thermal mismatch between the substrate and epitaxial layers enhances the performance of the device by eliminating cracks, and the thermal conductivity help for heat dissipation of the device, in such a way that the good thermal conductivity, in combination with the vertical geometry of GaN based structure, allows the LEDs to operate at higher current densities and temperatures. This has to be taken in consideration when designing LEDs.

System	Material	αth (10^{-6}K−1)		K (W/cm K)
III–V	w-AlN	Aa	αc	3.19b
		3.042	2.227	
	α-GaN	5.0	4.5	1.95b
	InN	3.830	2.751	0.45d

Table I.5: Thermal expansion coefficient α_{th} and thermal conductivity K for III-Nitride at 300K [7].

I.4. Metal–Semiconductor Contacts

They are contact electrodes, which are used in the semiconductor devices and integrated circuits to serve as regions through which connections are made to an external power supply. The first type is the Schottky contact and the second type is the ohmic contact.

I.4.1. Schottky Contact

A Schottky barrier contact exhibits an asymmetrical current–voltage (I–V) characteristic when the polarity of a bias voltage applied to the metal–semiconductor contacts is changed.

I.4.2. Ohmic Contacts

For LEDs device applications, the ohmic contacts is the best choice, in order to have negligible voltage drop across a metal–semiconductor contact.

I.5. Doping in nitride materials

To boost the concentration of electrons or holes in the semiconductor devices, it is essential to introduce impurity atoms, which are acceptor for p-type and donor for n-type materials. In GaN based devices, Silicon and magnesium are typical impurities widely used for n-type and p-type semiconductors respectively, including LEDs and lasers. Generally, The activation energy of any doping impurities can be derived from the Bohr hydrogen model equations (III.14) which will be explained in the third chapter, the ionization energy is hence given by [3,4]:

$$E_i = \frac{-m_e^* q^4}{32(\pi\varepsilon_0\varepsilon_s)^2} \quad \text{I.7}$$

The donor activation energy of Mg is about 200 meV, and that of Si doped is about 20 meV [1-5].

I.5.1. Fermi level and quasi Fermi level

I.5.1.a Fermi level

The Fermi statistics are used in the derivation of distribution functions for carriers in a semiconductor [1-5].

The Fermi–Dirac (F-D) statistics are known as quantum statistics because their distribution functions based on quantum-mechanical principles.

Particles that obey the Fermi–Dirac (F-D) statistics have much higher density and stronger interaction among themselves than the classical particles.

The Fermi function is given by:

$$f(E) = \frac{1}{1+e^{(E-E_F)/K_BT}} \quad \text{I.8}$$

General expressions for the equilibrium densities of carriers in a semiconductor can be derived using the Fermi–Dirac (F-D) distribution function.

The Maxwell–Boltzmann (M-B) statistics are also known as the classical statistics, since they apply only to particles with weak interactions among themselves. Such as electrons and holes in semiconductor, which obey the Maxwell–Boltzmann (M-B) statistics. For undoped and lightly doped semiconductors, the Maxwell–Boltzmann (M-B) distribution function is used instead of the Fermi–Dirac (F-D) distribution function, it is given by:

$$f(E) = e^{(E-E_F)/K_BT} \quad \text{I.9}$$

An intrinsic semiconductor behaves like an insulator because the conduction band states are totally empty and the valence band states are completely filled. However, as the temperature increases, some of the electrons in the valence band states are excited and reaches the conduction band states by thermal energy, leaving behind an equal number of holes in the valence band.

I.5.1.b The Quasi Fermi level

A quasi Fermi level is caused by the application of an external voltage, which alter the populations of electrons in the conduction band and valence band. The displacement from equilibrium is such that the carrier populations can no longer be described by a single Fermi level, however it is possible to describe using concept of separate quasi-Fermi levels for each band, given by:

$$n(r) = N_c F_{1/2}\left(\frac{E_{Fn}(r)-E_c}{k_BT}\right) \quad \text{I.10}$$

$$p(r) = N_v F_{1/2}\left(\frac{E_{F_h} - E_{F_n}(r)}{k_B T}\right) \quad \text{I.11}$$

I.5.2.The density of states

The density of state N(E), gives the number of allowed states where an electron can be occupied per unit volume per unit energy given by the flowing equations:

$$N_c(E) = \frac{1}{2\pi^2}\left(\frac{m_n}{\hbar^2}\right)^{\frac{3}{2}}(E - E_C)^{\frac{1}{2}} \quad \text{I.12}$$

$$N_V(E) = \frac{1}{2\pi^2}\left(\frac{m_h}{\hbar^2}\right)^{\frac{3}{2}}(E_V - E)^{\frac{1}{2}} \quad \text{I.13}$$

I.5.3. The carrier concentration

The number of electrons existing in the conduction band energy levels is the integral of the product of the available electronic states total number and the occupation probability of a state at an energy E, which is given by [1-5,24]:

$$n = \int_{E_c}^{\infty} D_e(E) f_e(E) dE \quad \text{I.14}$$

Where $D_e(E)$ is the density of states and $f_e(E)$ is the probability of occupation :
Thus, the intrinsic carrier density can be expressed by:

$$n_i = N_c e^{\frac{E_i - E_c}{k_B T}} \quad \text{I.15}$$

$$p_i = N_v e^{\frac{E_v - E_i}{k_B T}} \quad \text{I.16}$$

$$n_i = n_0 = p_0$$

Where n_0 and p_0 denote the equilibrium electron and hole densities, respectively.
The relationship between the square of the intrinsic carrier density and the product of electron and hole densities which is called the law of mass action equation, used for the non-degenerate case where the doping levels is low, is given by:

$$n_0.p_0 = {n_i}^2 = N_c.N_v e^{-\frac{E_g}{k_B.T}} \quad \text{I.17}$$

From the last equation it is clear that the product $n_0.p_0$ depends on the temperature, band gap energy, and the effective masses of electrons and holes. This equation is used to calculate the minority carrier density in an extrinsic semiconductor when the majority carrier density is known given by:

$$p_0 = \frac{{n_i}^2}{n_0} \quad \text{I.18}$$

For an extrinsic n-type semiconductor.

Neutrality relationship is given by:

$$p - n + N_D^+ - N_A^- = 0 \qquad \text{I.19}$$

$$p - n + N_{\ D} - N_{\ A} = 0 \qquad \text{I.120}$$

The Fermi level is given by :

$$E_F - E_i = kTln(^{N_D}/_{n_i}) \qquad \text{I.19}$$

$$E_i - E_F = kTln(^{N_A}/_{n_i}) \qquad \text{I.20}$$

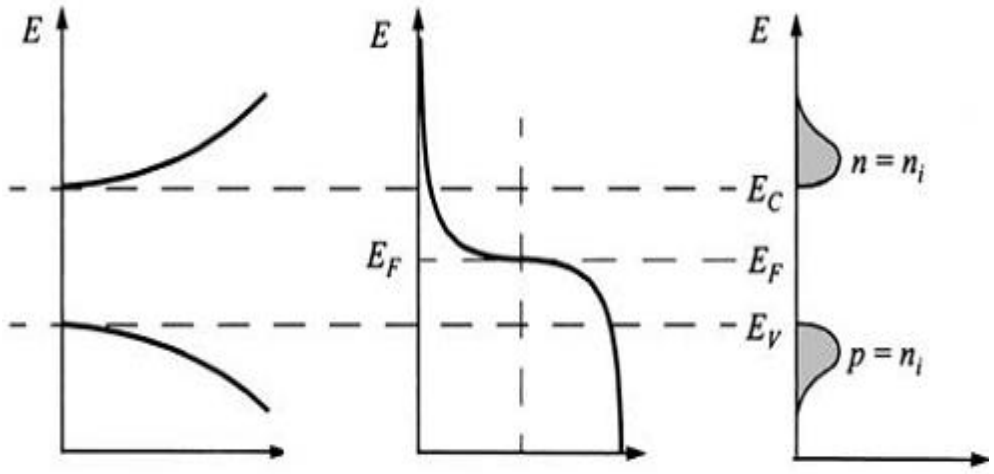

Figure I.5: Density of states(left), Fermi distribution (center)and carrier concentration(right)intrinsic equilibrium [24].

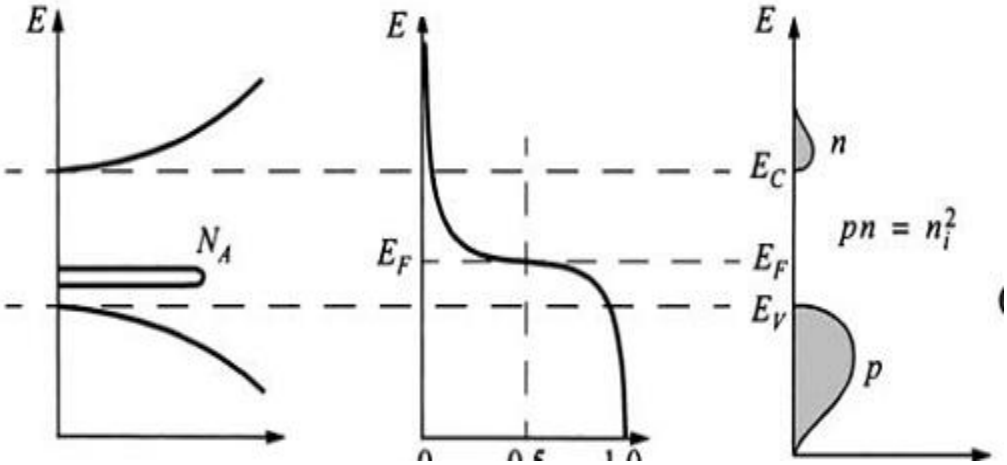

Figure I.6: Density of states(left), Fermi distribution (center) and carrier concentration(right) p-type semiconductors in thermal equilibrium [24].

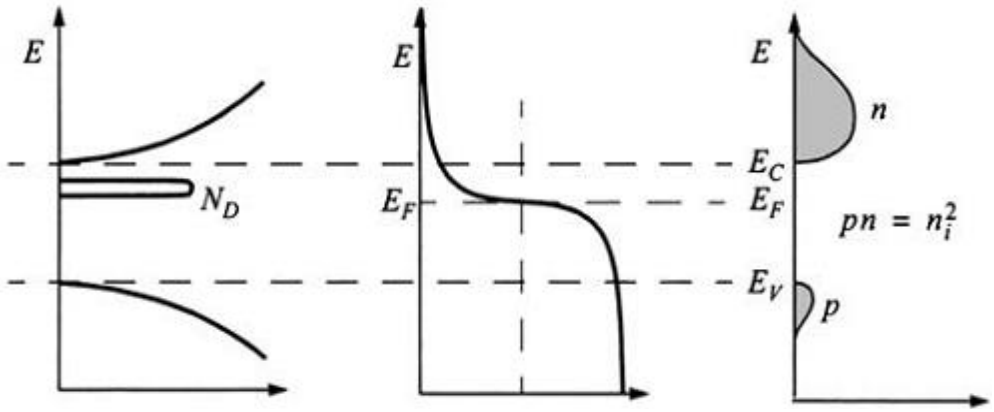

Figure I.7: Density of states(left), Fermi distribution (center) and carrier concentration(right) n-type semiconductors in thermal equilibrium quasi fermi [24].

I.6. Substrates

I.6.1. Sapphire substrates

Generally sapphire is used as a substrates for III–nitride LEDs [30-32], because it has many advantages such as:

- The transparency to UV and visible light.
- It reduces the parasitic light loss in the substrate.
- It is not inexpensive.

But, there are a some disadvantages which are:

- Thermal expansion coefficient between nitride materials and sapphire gives rise to a high density of threading dislocations and biaxial stress in epitaxial layers.
- A large mismatch in lattice constant (~15%).
- It has a poor thermal conductivity, limiting heat dissipation in LEDs.
- It is an insulator, hence the LEDs must have a lateral configuration.

I.6.2. SiC Substrates

SiC is utilized as substrate for InGaN-based LEDs [33-35].

The advantages of the SiC Substrates are:

- It can be easily doped to make a conductive substrate ,which allow the fabrication of LEDs with a vertical geometry.
- The fabrication is simple, because a Ni-based contact is formed on the backside of the substrate as the n-type electrode, and only one wire bond is required for top-emitting LEDs.
- It is highly thermally conductive, which will enhance heat dissipation from LED.
- The lattice mismatch between SiC and GaN is about 3.5%, which is very small as compared to that between sapphire and GaN, which is in the otder of 14%.

But, there are a some disadvantages which are:

- It has relatively high prices.
- It is sufficiently large to result in a large number of dislocation.
- It has micro structural defects in epilayers.
- The doped SiC is typically opaque at the wavelengths of visible light.
- It absorbs UV wavelengths, hence it is not suitable for developing deep-UV emitters.

I.6.3. Silicon substrates

A big effort has been done to grow III–nitride LEDs on Si substrates [36-38], because of it is low cost. This substrates has many advantages such as:

- His thermal stability under typical nitride growth conditions.
- A high crystalline quality and a smooth surface finish of the Si wafers, are available in large sizes.
- It allows easy die separation, simple wet-etch substrate removal.
- The potential to integrate LEDs with Si control electronics.
- LEDs grown on Si allows to form the n-type contact on the backside of the substrate and have a vertical structure, which enhances current spreading uniformity.

However, most reported LEDs on Si have many divagates such as:

- The enormous 17% lattice mismatch of GaN on Si.
- A high series resistance, due to the need of the AlN buffer.
- The greater thermal expansion coefficient of GaN as compared to that of Si gives rise to a tensile stress in epilayers. Cracking may occur upon cooling down from the growth temperature.
- This choice is less efficient than the sapphire or SiC substrates.
- Poor light extraction due to light absorption of silicon.
- High defect density due to the high thermal and lattice mismatch between Si and nitrides.

I.6.4. GaN and InGaN substrates

For nitrides LEDs grown on foreign substrates, there are two kind of mismatches the first is in lattice constant and second is the thermal expansion coefficient.

The use of GaN Substrates [39,40] has many advantage such as:

- A avoid high density of threading dislocations.
- Reduce residual biaxial stress in the epilayers.
- The growth procedure can be greatly simplified as the homoepitaxy process does not require additional steps.
- The defects and stress in the epilayers would be reduced, leading to improved performance.

- It can be used to fabricate Simple vertically structured LEDs.
- The good thermal conductivity, in combination with the vertical geometry of GaN, allows the LEDs to operate at higher current densities and temperatures.

In addition to the same advantages of the GaN Substrates, The use of InGaN Substrates [41-43] has other advantages such as:

- Less wavelength shift.
- Reduce the green gap.
- Enhance the IQE.
- Lattice mismatch reduction.

1.7. Conclusion

The properties that are studies give a clear pucture obout the adventeges of the III-Nitride semiconductor, especially in the optoelectronics.

Chapter II

Light Characteristics and Chromaticity

II.1. Introduction

Understanding the physical behavior of the light and its characteristics, will help the design of LEDs, especially the color mixing which is very important in the case of broad band spectrum and white light generation, in this chapter we will see how the color is represented by CIE method, we will speak about the color rendering, we will understand the relation between the light color and the black body temperature CCT, and explain the importance of the Color mixing for the LEDs.

II.2. The aspects characteristics of the light

There are several concepts referred to characterize the aspects of any light, which are Commission International de I'Eclairage (CIE), the correlated color temperature (CCT), and The color rendering index (CRI or Ra).

II.2.1. The representation of the color by CIE method

The Commission International de I'Eclairage CIE is a method used to describe the composition of any color in terms of three primarie colors, they are red, green, blue. It is generally used to describe LED characteristics [44-46]. where the tristimulus values X, Y, Z, can be added to produce real spectral colors. And three quantities (x, y, z) are the so called chromaticity coordinates, they are usually used to represent the color. But only two of the reference stimuli can define a color because the third quantity is calculate from the two others, where the CIE 1931 chromaticity diagram uses (x, y) coordinates to map out chromaticity coordinates as seen in Figure II.1 and provide a numerical representation of the color [47-49].

X, Y and Z tristimulus values are obtained by the following equations [8,47]:

$$X = \int_{380}^{780} \bar{x}(\lambda)P(\lambda)d\lambda \quad \text{II.1}$$

$$Y = \int_{380}^{780} \bar{y}(\lambda)P(\lambda)d\lambda \quad \text{II.2}$$

$$Z = \int_{380}^{780} \bar{z}(\lambda)P(\lambda)d\lambda \quad \text{II.3}$$

Where $P(\lambda)$, is the spectral power densities and $\bar{x}(\lambda)$, $\bar{y}(\lambda)$ and $\bar{z}(\lambda)$ are CIE color matching functions.

The chromaticity coordinates x , y and z are calculated from the tristimulus values according to[47]:

$$x = \frac{X}{X+Y+Z} \quad \text{II.4}$$

$$y = \frac{Y}{X+Y+Z} \quad \text{II.5}$$

$$z = \frac{Z}{X+Y+Z} = 1 - x - y \quad \text{II.6}$$

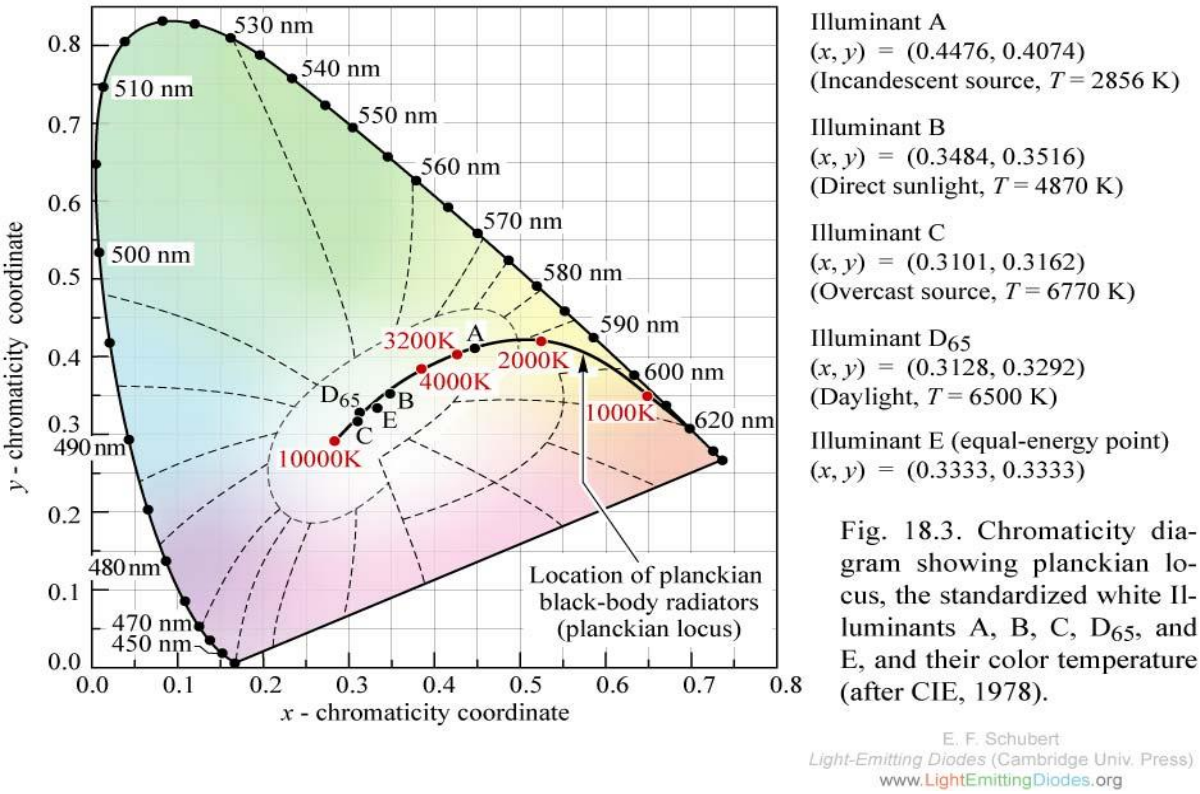

Figure II.1: The chromaticity diagram CIE1931, with Planckian locus standard illuminants [8,47].

II.2.2. Color rendering index (CRI)

The CIE defined the color rendering in the International Lighting Vocabulary as ‘‘Effect of an illuminant on the color appearance of objects by conscious or subconscious comparison with their color appearance under a reference illuminant’’.

The color rendering index (CRI) is a quantitative measurement of a white light source’s ability to reproduce the colors in comparison to a reference light source of the same correlated color temperature (CCT). The reference light source can be a Planckian radiator for color temperatures below 5000 K. The difference between the test source and the reference source of light is scaled and subtracted from 100. The score for each test color is defined as the special Color Rendering Index Ri. the CRI rated on a scale from 0 to 100, 100 is the maximum Ri score that indicates a perfect match [47].

The purpose of a color-rendering index is to find a correlate of the visual impression the observer has, when viewing the illuminated scene. This measurement is used as one of the important LED characteristics [50-52].

II.2.3. The correlated color temperature (CCT)

The correlated color temperature (CCT), is the temperature of a Planckian radiator having the chromaticity (x, y) nearest the chromaticity associated with the given spectral distribution on (CIE

1931 standard) diagram as seen in Figure II.1. As the temperature of the black body increases, the chromaticity location moves from the red wavelength range towards the center of the diagram. Meaning that at low temperatures, the radiation occurs mostly in the infrared. As the temperature increases, the maximum of the radiation shifts into the visible wavelength range. Typical temperatures in the white region of the chromaticity diagram range between 2500 and10000 K, where low CCT implies "warmer" light, and high color temperature appears to be a "colder" light, such descriptions is essential in the electrical lighting system especially for GaN LEDs [53-55]. Also shown in Figure II.1. are the locations of several standard illuminants. These include A, B, C, D65. Table II.2 give the list of some standard values daylight illuminants.

Illuminant	Nominal CCT(K)
CIE illuminant D50	5000
CIE illuminant D55	5500
CIE standard illuminant D65	6500

Table II.1: The CCT of CIE daylight illuminants [47].

The maximum intensity of radiation generated by a black body of temperature T occurs at a specific wavelength which is given by Wien's law Equ(III.1), which will be discussed in the next chapter.

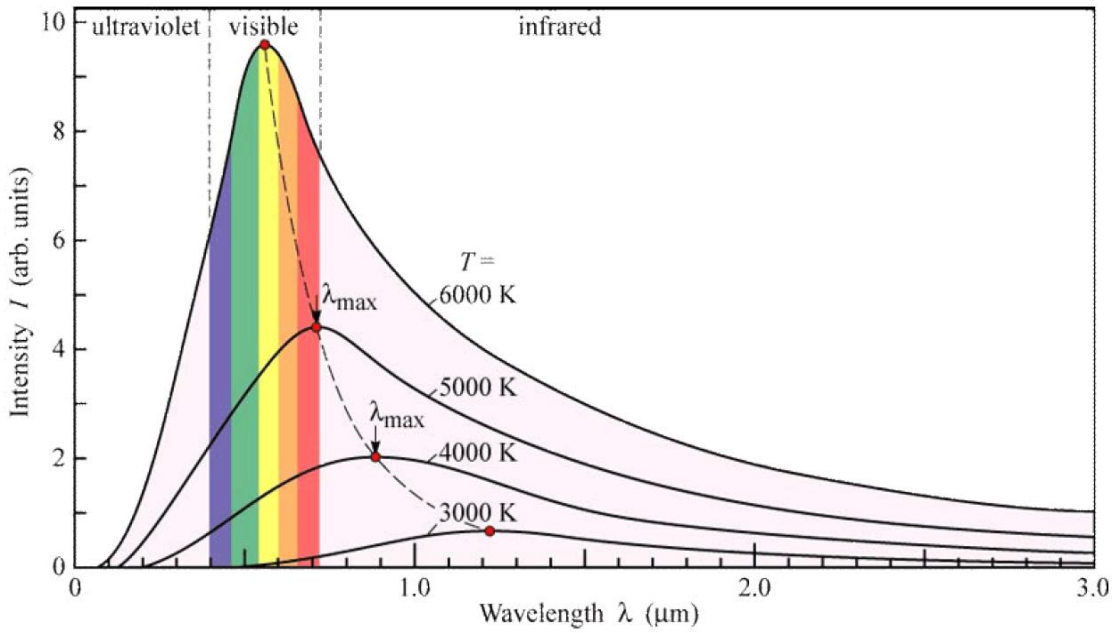

Figure II.2: The peak wavelength for different temperature of black body [8].

CCT (Tc)	Chromaticity coordinates	
	x	y
6400	0.313	0.337
5000	0.346	0.359
4040	0.380	0.380
3450	0.409	0.394
2940	0.440	0.403
2720	0.463	0.420

Table II.2: The CCT values of LED lamp and there chromaticity coordinates [47].

II.2.4. Color mixing

The combination or additive mixing of two or more light sources is employed in a number of applications. In solid state lighting displays, three different types of LEDs, usually emitting in the red, green, and blue spectrum are used. Those three colors are mixed so that the observer can experience a wide range of colors. Another useful application of color mixing is the generation of white light by complementary colors.

where X, Y and Z are the tristimulus values, they can be added to produce real spectral colors. They are obtained by the following equations [8]:

$$X = \int_{380}^{780} \bar{x}(\lambda)P_1(\lambda)d\lambda + \int_{380}^{780} \bar{x}(\lambda)P_2(\lambda)d\lambda + \int_{380}^{780} \bar{x}(\lambda)P_3(\lambda)d\lambda \approx \bar{x}(\lambda_1)\,P_1 + \bar{x}(\lambda_2)P_2 + \bar{x}(\lambda_3)P_3 \quad \text{II.7}$$

$$Y = \int_{380}^{780} \bar{y}(\lambda)P_1(\lambda)d\lambda + \int_{380}^{780} \bar{y}(\lambda)P_2(\lambda)d\lambda + \int_{380}^{780} \bar{y}(\lambda)P_3(\lambda)d\lambda \approx \bar{y}(\lambda_1)\,P_1 + \bar{y}(\lambda_2)P_2 + \bar{y}(\lambda_3)P_3 \quad \text{II.8}$$

$$Y = \int_{380}^{780} \bar{z}(\lambda)P_1(\lambda)d\lambda + \int_{380}^{780} \bar{z}(\lambda)P_2(\lambda)d\lambda + \int_{380}^{780} \bar{z}(\lambda)P_3(\lambda)d\lambda \approx \bar{z}(\lambda_1)\,P_1 + \bar{z}(\lambda_2)P_2 + \bar{z}(\lambda_3)P_3 \quad \text{II.9}$$

Where $P_1(\lambda)$, $P_2(\lambda), P_3(\lambda)$ are spectral power densities and $\bar{x}(\lambda)$, $\bar{y}(\lambda)$ and $\bar{z}(\lambda)$ are CIE color matching functions given by the Table II.3. The spectral power density is obtained by the following equations [8]:

$$P = \int_{380}^{780} P(\lambda)d\lambda. \quad \text{II.10}$$

Where $P(\lambda)$ is the power spectral density.

Here, the color is represented by the three chromaticity coordinates quantities (x, y and z) given by the Table II.3.

The new chromaticity coordinates and the new light are generated by a mixed of three colors, which are given by:

$$x = \frac{\bar{x}(\lambda_1)P_1+\bar{x}(\lambda_2)P_2+\bar{x}(\lambda_3)P_3}{\bar{x}(\lambda_1)P_1+\bar{x}(\lambda_2)P_2+\bar{x}(\lambda_3)P_3+\bar{y}(\lambda_1)P_1+\bar{y}(\lambda_2)P_2+\bar{y}(\lambda_3)P_3+\bar{z}(\lambda_1)P_1+\bar{z}(\lambda_2)P_2+\bar{z}(\lambda_3)P_3} \quad \text{II.11}$$

$$y = \frac{\bar{y}(\lambda_1)P_1+\bar{y}(\lambda_2)P_2+\bar{y}(\lambda_3)P_3}{\bar{x}(\lambda_1)P_1+\bar{x}(\lambda_2)P_2+\bar{x}(\lambda_3)P_3+\bar{y}(\lambda_1)P_1+\bar{y}(\lambda_2)P_2+\bar{y}(\lambda_3)P_3+\bar{z}(\lambda_1)P_1+\bar{z}(\lambda_2)P_2+\bar{z}(\lambda_3)P_3} \quad \text{II.12}$$

$$z = \frac{\bar{z}(\lambda_1)P_1+\bar{z}(\lambda_2)P_2+\bar{z}(\lambda_3)P_3}{\bar{x}(\lambda_1)P_1+\bar{x}(\lambda_2)P_2+\bar{x}(\lambda_3)P_3+\bar{y}(\lambda_1)P_1+\bar{y}(\lambda_2)P_2+\bar{y}(\lambda_3)P_3+\bar{z}(\lambda_1)P_1+\bar{z}(\lambda_2)P_2+\bar{z}(\lambda_3)P_3} \quad \text{II.13}$$

Wavelenght λ [nm]	CIE color Matching functions			Chromaticity coordinates		
	$\bar{x}$	$\bar{y}$	$\bar{z}$	x	y	z
410	0.0435	0.0012	0.2074	0.1726	0.0048	0.8226
420	0.13438	0.004	0.6456	0.17141	0.0051	0.82349
561	0.6112209	0.9926005	0.0036232	0.38024	0.61750	0.00226
562	0.6279758	0.9897426	0.0030706	0.38738	0.61054	0.00208

Table II.3: CIE color Matching functions and Chromaticity coordinates [47].

In the case of two colors mixing. The chromaticity coordinates x and y of the new generated color are computed simplifying the two equation (II.14) and (II.15) we obtain:

$$x = \frac{\bar{x}(\lambda_1)P_1+\bar{x}(\lambda_2)P_2}{\bar{x}(\lambda_1)P_1+\bar{x}(\lambda_2)P_2+\bar{y}(\lambda_1)P_1+\bar{y}(\lambda_2)P_2+\bar{z}(\lambda_1)P_1+\bar{z}(\lambda_2)P_2} = \frac{\bar{x}(\lambda_1)+\bar{x}(\lambda_2)\frac{P_2}{P_1}}{\bar{x}(\lambda_1)+\bar{y}(\lambda_1)+\bar{z}(\lambda_1)+(\bar{x}(\lambda_2)+\bar{y}(\lambda_2)+\bar{z}(\lambda_2))\frac{P_2}{P_1}}. \quad \text{II.14}$$

$$y = \frac{\bar{y}(\lambda_1)P_1+\bar{y}(\lambda_2)P_2}{\bar{x}(\lambda_1)P_1+\bar{x}(\lambda_2)P_2+\bar{y}(\lambda_1)P_1+\bar{y}(\lambda_2)P_2+\bar{z}(\lambda_1)P_1+\bar{z}(\lambda_2)P_2} = \frac{\bar{y}(\lambda_1)+\bar{y}(\lambda_2)\frac{P_2}{P_1}}{\bar{x}(\lambda_1)+\bar{y}(\lambda_1)+\bar{z}(\lambda_1)+(\bar{x}(\lambda_2)+\bar{y}(\lambda_2)+\bar{z}(\lambda_2))\frac{P_2}{P_1}}. \quad \text{II.15}$$

Where $\bar{x}(\lambda)$, $\bar{y}(\lambda)$ and $\bar{z}(\lambda)$ are the CIE color matching functions given by the Table II.3.

P_1 and P_2 are the optical power of two colors.

The power ratio is defined as $\frac{P_2}{P_1}$, named as Li factor.

Thus, the chromaticity coordinate of two mixed color is a linear combination of the individual chromaticity coordinates weighted by the Li factors.

Table.II.4. gives the needed complementary Wavelengths λ_1 and λ_2 , and the required power ratio to generate the white color with respect to CIE Illuminant D65 [8].

complementary Wavelengths		power ratio
λ_1 [nm]	λ_2 [nm]	$P(\lambda_2)/P(\lambda_1)$
410	561.3	0.356
420	561.7	0.891
430	562.2	1.42
440	562.9	1.79
450	564	1.79
460	565.9	1.53

Table II.4: complementary Wavelengths λ1 and λ2 and the required power ratio [8,47].

The luminescent power is calculated using the following equation (3) [31]:

$$P = \frac{h \times c}{\lambda} \times \int R_{RAD} \times dA \qquad \text{II.16}$$

where λ is the emission wavelength, and R_{RAD} is the radiative emission rate.

Chapter III

Light Emitting Diodes

III.1. Introduction

The semiconductors have two types of band gaps, they are indirect and direct, the later is generally use in the LDs and LEDs manufacturing, this technology, has allowed a great achievement of energy saving. Furthermore, the white light LEDs have a big importance in modern display industry, such as high efficiency light bulbs and display panels, as they consume very small power to produce light. However, there had been no practical technology to manufacture white LED until 1993, when Nichia Corporation and Shuji Nakamura developed the blue LED technology [1,5]. Because the white light generation required three primary colors (red, green, and blue), this achievement made full color displays and white LED possible, and enabled many others optoelectronic applications.

This chapter describes the different theories and laws of quantum and semiconductor physics, the used semiconductors in LED devices, and presents the different Light emitting diode structure, in addition it explains the generation of mixed color and white light using many techniques such as Phosphor converted and dichromatic sources, finally the three kind of recombination's that happen in the LED structures, the different quantum efficiencies, and the aspects characteristics of white LEDs are presented.

III.2. Physical quantum mechanics theory

At the end of the 19 century, the limit to explain many physical problems by the classical mechanic has been reached, especially, in the atomic scale, hence new concepts come out, it is the quantum mechanics, which was able to explain many phenomena in the atomic levels [1-5], such as the black body radiation studied by Wien's, wave particles duality proposed by De Broglie and photo-electron interactions explained by Einstein, all this leads to the invention of new technology especially in electronic and optoelectronic domain.

III.2.1. Wien's Law

By studying the body radiation of many objects at different temperatures, Wilhelm Wien noticed that the wavelength corresponding to the maximum of radiation was inversely proportional to the temperature of the black body. From where the famous law of Wien:

$$\lambda_{max} = \frac{\sigma_w}{T} \qquad \text{III.1}$$

Where σ_w is a constant equal to 0,298 cm·K.

III.2.2. Planck postulation

At 1901, Max Planck provided a detailed explanation of the observed blackbody spectrum by introducing the hypothesis that the atoms vibrating at a frequency ν in a material could only radiate

or absorb energy in quantized packages proportional to the frequency, he postulated that this energy is given bay:

$$E_n = h\nu = \hbar\omega \quad n = 0,1,2 \ldots \qquad \text{III.2}$$

where n is an integer used to express the quantization, h = 6.628× 10^{-34}J/s is Planck constant and ħ = h/2π is the reduced Planck's constant.

III.2.3. The discovery of Hertz

The photoelectric effect is the emission of electrons when a light is shined on matter. Visible light produces this emission on the surface of several bodies. Ultraviolet produces it in most substances. The light brings energy to all the bodies that absorb it, where a part of this energy is used to eject electrons with a kinetic energy is given by:

$$E_c = \frac{1}{2}mv^2 \qquad \text{III.3}$$

III.2.4. Einstein assumption

In 1905, Einstein assumed that radiation behaved in the photoelectric effect like a beam of particles. Each particle of light which is called photon has energy E proportional to the frequency of the monochromatic radiation that accompanies it:

$$E = h\nu \qquad \text{III.4}$$

where E is the energy, ν frequency constant. When a substance absorb an incident photon, all of the energy $h\nu$ is transferred to an electron in the material. when this energy is greater than the threshold value $h\nu_0$, the electron overcomes the energy barrier and leaves the material with the energy:

$$\frac{1}{2}mv^2 = h(\nu - \nu_0) \qquad \text{III.5}$$

$h\nu_0$ is called extraction work. It is in the range of few eV. In addition to energy, another important quantity is the momentum. It is a vector with three components given by:

$$\vec{p} = \mathrm{m}\vec{v}. \qquad \text{III.6}$$

a quantity of movement is attributed to the photon:

$$p = \frac{h}{\lambda} = \frac{hc}{\nu} \qquad \text{III.7}$$

The relation $p = \frac{hc}{\nu}$, joined to $E = h\nu$, made it possible to perfectly explain the compton effect, which is the effect of the diffusion of photons by electrons.

III.2.5. Bohr postulation

Bohr postulated that the angular momentum is expressed by:

$$L_n = m_0 v r_n = n\hbar \quad \text{III.8}$$

Where n=1, 2, 3 ...,

The Coulomb attractive force must balance the centripetal force on the electron to be stable in the orbits. Hence we have:

$$\frac{m_0 v^2}{r_n} = \frac{q^2}{4\pi\varepsilon_0 r_n^2} \quad \text{III.9}$$

From the two previous equations we obtain :

$$r_n = \frac{4\pi\varepsilon_0 (n\hbar)^2}{m_0 q^2} \quad \text{III.10}$$

Knowing that the kinetic energy is given by:

$$\text{K.E} = \frac{1}{2} m_0 v^2 = \frac{1}{2}\frac{q^2}{4\pi\varepsilon_0 r_n} \quad \text{III.11}$$

and the potential energy is given by:

$$\text{P.E.} = -\frac{q^2}{4\pi\varepsilon_0 r_n} \quad \text{III.12}$$

Hence the total electron energy is given by:

$$E_n = \text{P.E.} + \text{K.E.} = -\frac{1}{2}\frac{q^2}{4\pi\varepsilon_0 r_n} \quad \text{III.13}$$

Substituting r_n given by I.14 into I.15 yields:

$$E_n = -\frac{m_0 q^4}{2(4\pi\varepsilon_0 r_n)^2} = \frac{-13.6}{n^2}(\text{eV}) \quad \text{III.14}$$

the last equation shows that the ionization energy of the first Bohr orbit with n = 1 is E_1 =−13.6 eV. This gives clear picture of the allowed energy transitions.

III.2.6. The De Broglie hypothesis

In 1925 De Broglie proposed that since the photon exhibited particle-like properties, particles should also exhibit wave like properties. He hypothesized that the wavelength characteristic of a given particle with momentum p can be calculated from $p = h/\lambda$, where λ is the wavelength of the electromagnetic radiation. Based on De Broglie's wave–particle duality theory, the momentum of a particle is given by:

$$p = m_0 v = \hbar k \quad \text{III.15}$$

III.2.7. Schrödinger equation

Schrodinger, in 1926. provided a formulation called wave mechanic, which incorporated the principles of quanta introduced by Planck, and the wave-particle duality principle introduced by de Broglie. Based on the wave-particle duality principle. the motion of electrons will be described in a crystal by wave theory. This wave theory is given by Schrodinger's wave equation.

$$\nabla^2\Psi(x) + \frac{2m_0}{\hbar^2}[E(x) - U(x)]\Psi(x) = 0 \qquad \text{III.16}$$

where, $\hbar$ is the reduced Planck Constant where $\hbar = h/2\pi$, m_0 is the mass of an electron, $\psi(r, t)$ is the wave function, V(r, t) is the potential energy as a function of position, E is the energy.

III.2.8. Bloch theorem

Bloch theorem relates the value of the wave function in the unit cell of periodic potential $U(x)$ to an equivalent point in any other unit cell, this will simplify Schrödinger equation solution and when a particle moves in a periodic potential its wave functions can be expressed in a form known as Bloch functions:

$$U(x + a) = U(x) \qquad \text{III.17}$$

$$\Psi(x + a) = e^{ikx}\Psi(x) \qquad \text{III.18}$$

III.3. The used semiconductors in LED devices

Round Henry Joseph noticed that light was emitted from a SiC crystallite. The first light-emitting diode (LED) had been born. But the emission process was not well understood. Lossev reported detailed investigations of the luminescence phenomenon observed with SiC semiconductor. He noticed that luminescence occurred in some diodes when they are biased. He concluded that the light was not generated by incandescence but by electroluminescence. The development of the quantum theory of solids was important for understanding the theory and the properties of light-emission in semiconductors. Where many semiconductor materials has been used such as [7,9]:

- GaAs, AlGaInP and AlGaAs.
- ZnS and ZnO.
- GaP and GaAsP.
- InGaN and AlGaN.

Material	Energy band gap (eV)	Wavelength (µm)	Color of LEDs
GaN	3.3	0.375	UV, blue
InGaN	0.67–3.3	0.375–1.85	Blue, green, red
AlGaN	3.3–6.2	0.2–0.375	UV, blue
SiC	2.86	0.435	Blue
ZnSe	2.70	0.46	Blue
GaP	1.98	0.63	Green, red
AlGaInP	1.35–1.98	0.63–0.92	Yellow, orange, amber, red
AlGaAs	1.43–2.19	0.57–0.83	Orange, red
GaAsP	1.41–1.95	0.63–0.88	Yellow, orange, red
GaAs	1.43	0.84	IR emitter
InGaAs	0.34–1.43	1.3	IR

Table III.1: Energy band gap, wavelength, and color for some semiconductor [7].

III.4. The different Light emitting diode structure

III.4.1. Homo-junction LED

A p-n junction diode is obtained by doping the semiconductor with impurity atoms, which are acceptor for p-type and donor for n-type materials. It can be a p-n homojunction diode which is formed by the same semiconductor. It plays an important role for manufacturing a wide variety of optoelectronic devices such as light emitting diodes. The LED can have a homojunction structure. If it is forward biased, the electrons are injected or diffused from n-side to p-side and holes in the opposite way. At the junction or near the junction, the electrons and holes can recombine and emit photons.

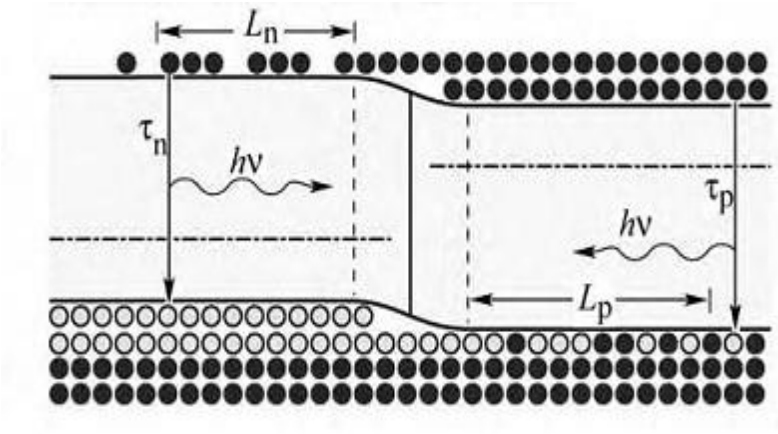

Figure III.1: Band structure of the Homo-junction LED [8].

III.4.2. Hetero-junction LED

If the p-n junction is formed using two semiconductor materials having different band gap, joined together, p-n heterojunction diode is obtained. It plays an important role as the basic device structure for fabricating a wide variety of optoelectronic devices such as light emitting diodes (LEDs).

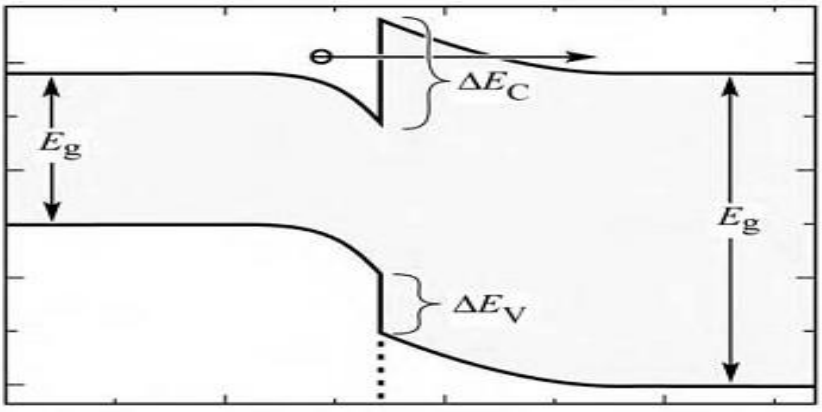

Figure III.2: Band structure of the Hetero-junction LED [8].

III.4.3. Multi-heterojunction LED

The multi-heterojunction, is obtained when a thin layer of semiconductor with a smaller bandgap is sandwiched between two wider bandgap. When the electrons and holes are injected across the p-n junction, they are confined within the well, the chance for recombination and emitting photons is higher compared to previous p-n junction LEDs.

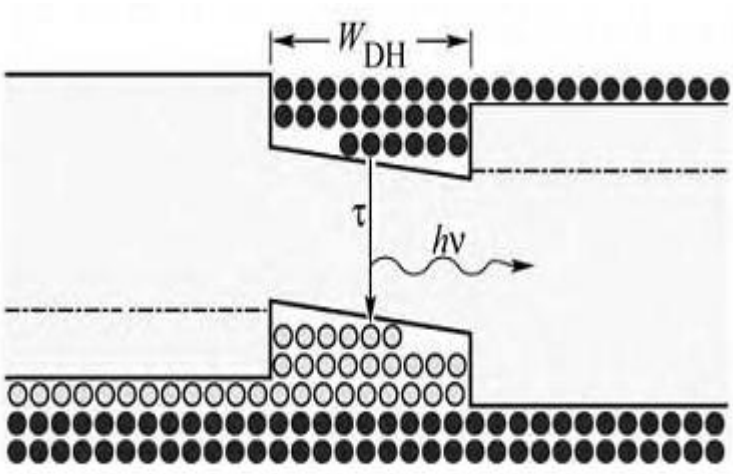

Figure III.3: Band structure of the Multi-heterojunction LED [8].

III.4.4. Quantum well structure LED

The single and the multiple quantum well (SQW, MQW) have the same multi-heterojunction structure, except that the width of the well is in the De Broglie wave length order, MQW can confine higher amount of carriers and results high optical output power.

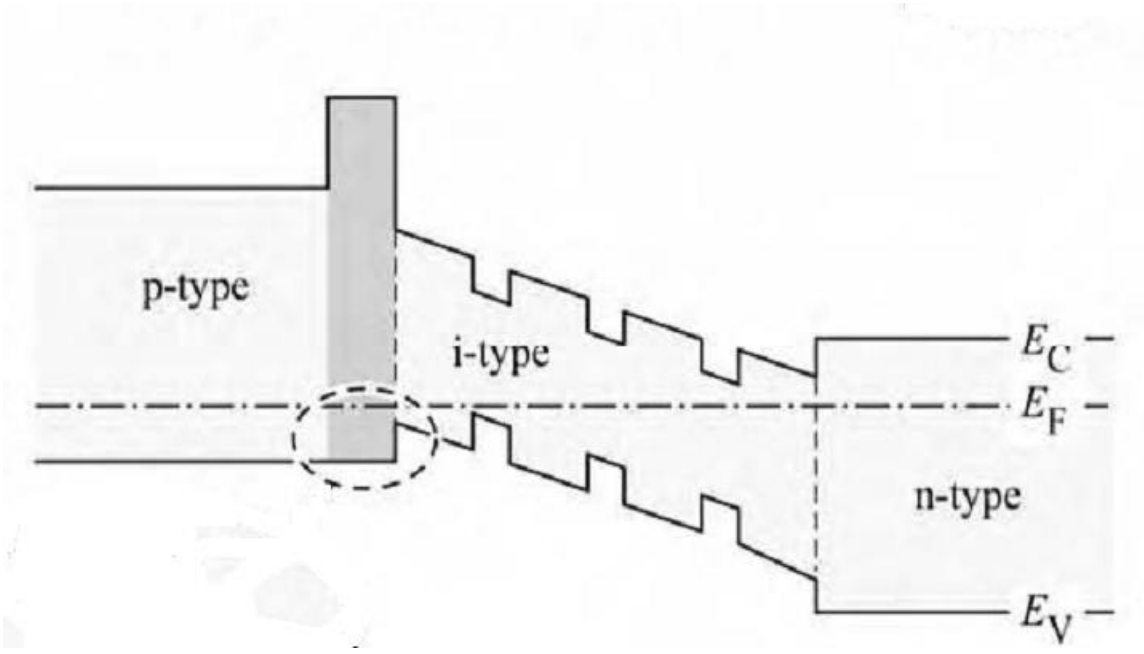

Figure III.4: Band structure of the MQW LED [8].

III.5. Band-to-band Recombination and Spectral Width

The recombination of electron and hole produces a photon with energy $h\nu$ nearly equal to the band gap given by the equation(III.4). Using the joint dispersion relation, the joint density of states can be calculated taking in consideration the new mass value given by:

$$\frac{1}{m_r^*} = \frac{1}{m_e^*} + \frac{1}{m_h^*} \qquad \text{III.20}$$

and one obtains

$$\rho(E) = \frac{1}{2\pi^2}\left(\frac{2m_r^*}{\hbar^2}\right)^{\frac{3}{2}}(E - E_C)^{\frac{1}{2}} \qquad \text{III.21}$$

The distribution of carriers in the allowed bands is given by the probability of emission.

$$f_B(E) = e^{(-E)/K_B T} \qquad \text{III.22}$$

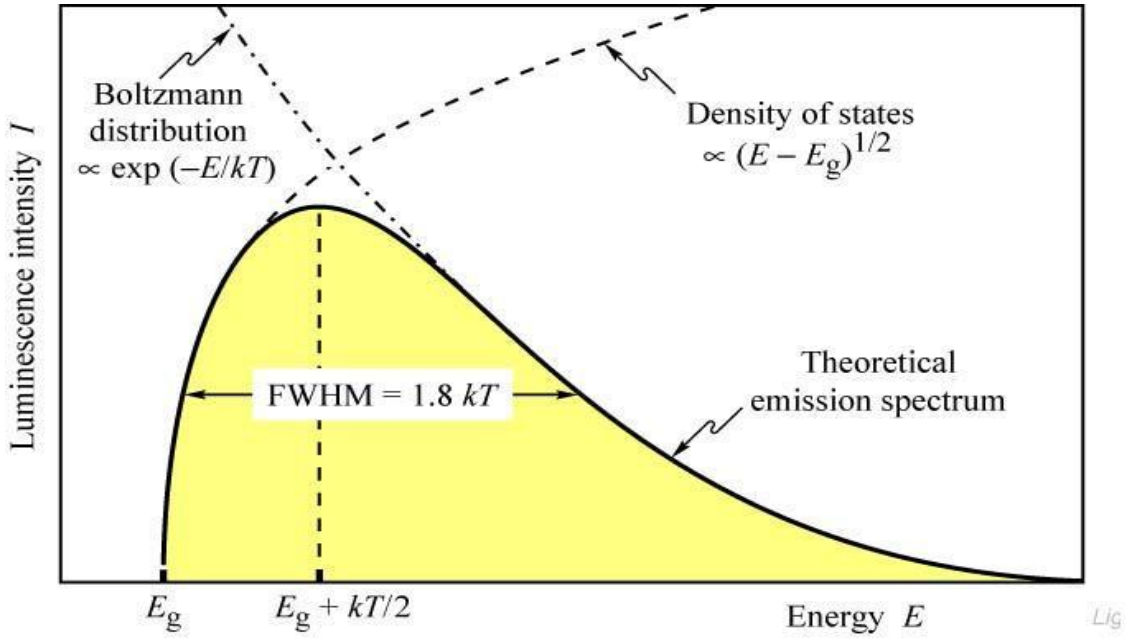

Figure III.5: The effect of the probability of emission and the optical joint density of state on the wavelength shape [29].

The emission intensity $I(E)$ is proportional to the following expression:

$$I(E)\, \alpha \sqrt{(E - E_C)}\, e^{(-E)/K_B T} \qquad \text{III.23}$$

Because the largest electron concentration in the conduction band is at kT/2 above E_C, similarly the most probable energy for a hole in the valence band has an energy kT/2 below E_V [29]. The photon energy is approximately given by:

$$h\nu = Eg + kT \qquad \text{III.24}$$

Under forward bias of the LED, electrons injected from n-side recombine with holes injected from p-side, where the recombination is taking place in the active layer. For practical purposes we

can ignore the kT term and get equation (III.25), where the wavelength value of the photons emitted in each quantum well is obtained by the following equation:

$$\lambda = \frac{h.c}{Eg} \quad \text{III.25}$$

where:

h (Planck 's constant)= 6.625 x 10^{-34} J-sec and c = 3x 10^{8} m/sec.

The spectral width is given by the full width at half maximum (FWHM) intensity. The light spectrum of an LED shows a peak at the wavelength λ, there is a spread of wavelengths Δλ associated with a spread of energy ΔE:

$$\Delta E = 1.8kT \quad \text{III.26}$$

$$\Delta\lambda = {}^{1.8kT\lambda^2}/_{hc} \quad \text{III.27}$$

The spectral width on either side of the wavelength peak thus has a dependence on λ^2 and the spectral width is given by 2Δλ. The FWHM becomes larger as the wavelength is increased from visible to infrared.

III.6. LEDs' characteristics

Knowing the characteristics of the LED and their related parameters, will help to optimize the functionality of the device, the most important characteristics are investigated in the following session.

1. The luminous efficiency is the total luminous flux divided by the total electric power consumed by the LED.

2. Quantum yield involved is referred to the absolute quantum yield, which is the ratio between the number of emitted photons and the number of absorbed photons, where P is the optical power emitted into free space.

3. The internal quantum efficiency (IQE) is the number of photons generated inside the LED per second divided by the number of electrons injected into the LED per second.

The recombination rate is given by [29]:

$$R = \frac{\Delta n}{\tau} \quad \text{III.28}$$

Where Δn is the excess carrier concentration and τ is the excess carrier life time.

$$\frac{1}{\tau} = \frac{1}{\tau_r} + \frac{1}{\tau_{nr}} \quad \text{III.29}$$

Where τ_r is the radiative recombination life time and τ_{nr} is the non radiative life time

The internal quantum efficiency is given by:

$$\eta_i = \frac{\tau}{\tau_r} \quad \text{III.30}$$

Which is the ratio of the radiative transitions to the total number of transitions.

The photon flux is given by:

$$\Phi = \eta_i \frac{i}{e} \quad \text{III.31}$$

The energy of the photon is given by:

$$P_E = h\nu \quad \text{III.32}$$

Hence the generated optical power is given by:

$$P_{gen} = \eta_i \frac{i}{e} h\nu \quad \text{III.33}$$

The internal quantum efficiency is defined as [29]:

$$\eta_{int} = \frac{P_{int}/_{h\nu}}{I/_e} \quad \text{III .34}$$

where P_{int} is the optical power emitted from the active region and I is the injection current.

4. Extraction Efficiency It is the number of photons emitted in free space per second divided by the number of photons emitted from the active region per second.

Increasing the extraction efficiency is very important for the LEDs. Generally a part of the photons generated by the higher band gap active layer will be absorbed by the lower band gap active layer. This will decrease the EQE, knowing that the absorption coefficient is given by the following equation [8]:

$$\alpha = \alpha_0 \sqrt{(E - E_g)/E} \quad \text{III.35}$$

Where α is the absorption coefficient, α_0 is the absorption coefficient at $h.\nu = 2E_g$, E is the photon energy and E_g is the band gap. Limiting the absorption effect will increase the extraction efficiency $\eta_{extraction}$. Also the use of reflectors to redirect additional parts of generated photons upward is one great solution. Hence, more light will be extracted [32,56,57].

The light extraction efficiency is defined as:

$$\eta_{extraction} = \frac{P/_{h\nu}}{P_{int}/_{h\nu}} \quad \text{III.36}$$

5. The external quantum efficiency (EQE) $\eta_{external}$ of the LED is calculated as follows [27]:

$$\eta_{external} = \eta_{int} \times \eta_{extraction} \quad \text{III.37}$$

Where $\eta_{extraction}$ is the extraction efficiency.

$$\eta_{external} = \frac{P/_{h\nu}}{I/_e} = \eta_{int} \times \eta_{extraction} \quad \text{III.38}$$

$$P_{OUT} = \eta_{external} \frac{1.24}{\lambda} i \quad \text{III.39}$$

6.Wall-Plug Efficiency is the power conversion ratio of the electrical power and the light output Pout:

$$\eta_w = \frac{P_{OUT}}{I\,V} = \frac{\hbar w}{e\,V}\eta_{ext} \qquad \text{III.40}$$

7. The reflection coefficient is given by [32,56,57]:

$$r = \frac{n_1\cos(\theta_1) - n_2\cos(\theta_2)}{n_1\cos(\theta_1) + n_2\cos(\theta_2)} \qquad \text{III.41}$$

8.The reflectivity is given by:

$$\mathrm{R} = |r|^2 = \left(\frac{n_1 - n_1}{n_1 + n_1}\right)^2 \qquad \text{III.42}$$

Some LED losses:

- Reabsorption loss.
- Reflection loss.
- Total reflection loss.

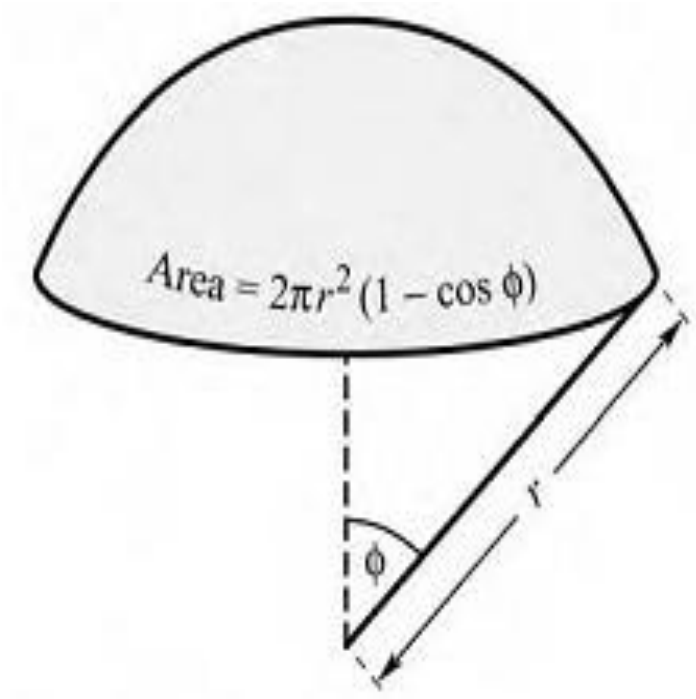

Figure III.6: The escape cone and the critical angle[8].

III.7. Multi color and White LEDs

The multi color and white light LEDs are very important because they are used in general purpose illumination and display devices , this solid state technology was possible after the realization of the InGaN blue LEDs in 1994 [10].

III.7.1 LED structures for Multi color and white light LED

III.7.1.1 Multiple quantum well structure

Many MQW structure was used to generate multi color and white light such as stacking two QW layers that emit in the blue and green, or three layers emitting in the blue, green, and red [11-15].

III.7.1.2 Horizontally Staked quantum well structure

A phosphor-free white light-emitting diode LED was fabricated with laterally distributed blue and green InGaN/GaN multiple quantum wells MQWs grown by a selective area growth method [17].

III.7.1.3. Vertically arranged quantum well structure

A Vertically arranged quantum well structure having blue-green color tunable monolithic LED with multi-junction structure. This is achieved by growing a blue LED on a conventional green LED [15].

III.7.2 Multi color and white light generation methods

The Multi color and white light is obtained by many technique such as:

- The used phosphor with Blue or UV LED.
- Combination of RGB LEDs.
- Organic LEDs (OLEDs).

III.7.2.1. Phosphor converted LEDs

The first white LEDs lamp was fabricated by the combination of a blue LED chip and YAG : Ce yellow-emitting phosphor, which is the most common method in lighting and display areas [16]. However, this technique has many advantages such as:

- Low cost and small space.
- Can generate a cool white with a color temperature of 5500 K and CRI of 70.
- Can generate a warm white with a color temperature of 3200 K and CRI of 90.

But suffers from some many drawbacks such as:

- A poor color rendering index (CRI).
- Low stability of color temperature.
- The change of the lighting color with the drive voltage.
- The phosphor coating thickness.

All of this will make the production of stable LEDs very difficult.

To optimize the color rendering properties of white and multicolor emitting LEDs, another techniques are used such that the red green blue (RGB) emitting color phosphors excited by n-UV LEDs. Where the color obtained by n-UV LEDs only depends on the phosphors. Therefore phosphors play a decisive role.

Also another approach called the RGGB, the red and blue primary semiconductor sources are used in conjunction with a green phosphor pumped by blue. The broad green phosphor replaces the green and yellow LEDs in the four-LED approach.

In the RRGGB approach, the blue primary semiconductor source is used to pump the green and red phosphors.

III.7.2.2 Generation of multi color and white light by multi chromatic sources

Generation by dichromatic sources

One way to generate light with different colors is the use of two narrow emission bands, called complementary wavelengths. Two complementary colors, can generate a mix of color and by changing the power ratio, will result in tristimulus values that are perceived as different colors especially white light.

Generation using Three-Chip LEDs

The three primary colors, red, green, and blue with identical intensities perceived by the eye, can be mixed together to generate mix of color and white light. Three LEDs with those colors can be used in this technique, this can cover the overall regions of the chromaticity diagram see Figure II.1.

Generation using Four-Chip LEDs

We can obtain higher color rendering index with four LEDs, this is good choice for color-tunable and white-light generation where the wavelengths of four LEDs are required.

Chapter IV
TCAD Device Simulation Tools

IV.1. Introduction

For efficient design of semiconductor devices and process, technology computer-aided design (TCAD) tools are commonly used in this industry, such as APSYS from Crosslight, ATLAS from SILVACO and tiberCAD from tiberlab. In this chapter we will cite the different simulators and the different used models and parameters, also the Commands Order of ATLAS simulator which used in our design [23,58].

There are many simulator used for this purpose such as:

- Synopsys: Sentaurus Dvice
  Taurus Medici
- Silvaco: ATLAS
  Victory Dvice
  Athena
- Crosslight: APSYS
  LASTIP
- TiberCAD

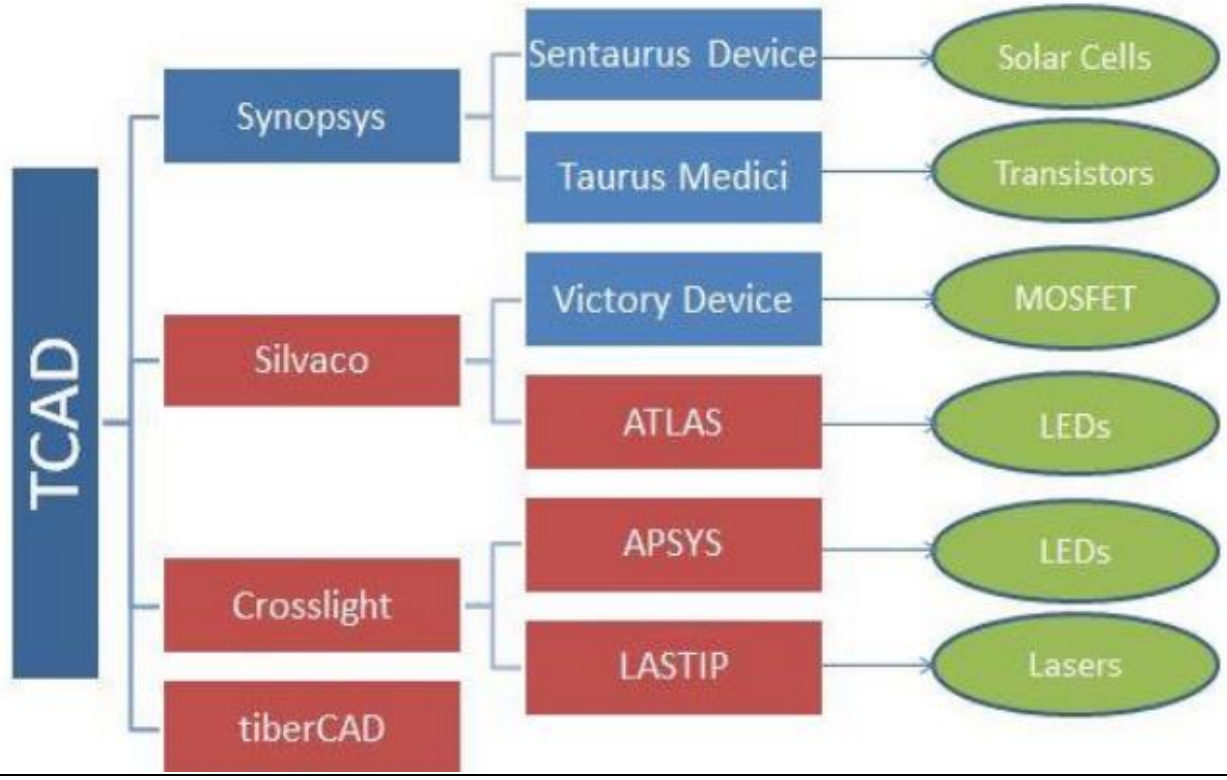

Figure IV.1: Major TCAD Device Simulation Tools.

IV.2. Models and parameters

The semiconductor devices simulators have several adequate physical models for each studied case, in this section we will focus on the models related to LED devices, especially those used for III-V nitrides materials. The simulation software solves many equations of semiconductor physics.

IV.2.1 Poisson's equation

Poisson's Equation relates variations in electrostatic potential to local charge densities, the equation is written as:

$$div(\varepsilon \nabla \Psi) = \rho \qquad \text{IV.1}$$

IV.2.2. Drift-Diffusion Transport Model

The drift–diffusion model is used to compute the flow of electrons and holes. The drift current is generated by an electric field $\vec{E}$, and it is proportional to the conductivity of electrons and holes. The diffusion current is driven by the concentration gradient of electrons ∇_n and holes ∇_p. It is proportional to the diffusion coefficient D_n and D_p, respectively. For uniform semiconductors, the total current density of electrons and holes is written as:

$$\vec{j} = qn\mu_n \vec{E} + qD_n \nabla_n \qquad \text{IV.2.a}$$

$$\vec{j} = qn\mu_p \vec{E} + qD_p \nabla_p \qquad \text{IV.2.b}$$

IV.2.3. The continuity equations

It describes how the hole and electron densities change due to transport, recombination, and generation processes:

$$\frac{\partial n}{\partial t} = \frac{1}{\mathrm{q}} div J_n + G_n - R_n \qquad \text{IV.3.a}$$

$$\frac{\partial p}{\partial t} = \frac{1}{\mathrm{q}} div J_p + G_p - R_p \qquad \text{IV.3.b}$$

IV.2.4. Farahmand Modified Caughey Thomas model

It is used to obtain the composition and temperature dependent low field mobility [31], given by:

$$\mu_0(T,N) = \mu_{min}\left(\frac{T}{300}\right)^{\beta_1} + \frac{(\mu_{max}-\mu_{min})\left(\frac{T}{300}\right)^{\beta_2}}{1+\left[\frac{\mathrm{N}}{\mathrm{N_{ref}}\left(\frac{\mathrm{T}}{300}\right)^{\beta_3}}\right]^{\alpha\left(\frac{\mathrm{T}}{300}\right)^{\beta_4}}} \qquad \text{IV.4}$$

IV.2.5. Polarization model

Polarization modeling is critical for GaN based devices. The polarization in wurtzite materials is characterized by two components, spontaneous polarization (P_{SP}), and piezoelectric polarization (*Ppz*), where the strain value is used to calculate the (*Ppz*), finally the total polarization will be obtained.

The strain

The lattice constant of the ternary nitride alloys can be calculated using Vergarde's law:

$$a_{InGanN} = a_{InN}(x) + c_{GaN}(1-x). \quad \text{IV.5}$$

The calculation of the strain due to lattice mismatch is obtained by:

$$\varepsilon = 2\frac{a-a_0}{a_0} \quad \text{IV.6}$$

where a and a_0 are the lattice constants of the epilayer, and substrate respectively.

The piezoelectric polarization

The piezoelectric polarization (Ppz) happen when applying stress to the structure, it is calculated by:

$$P_{PE} = \varepsilon\left(e_{31} - e_{33}\frac{C_{13}}{C_{33}}\right) \quad \text{IV.7}$$

Spontaneous polarization

The spontaneous polarization (*Psp*) which is an intrinsic property of III-nitride materials, due to the asymmetry in hexagonal wurtzite structure can be expressed as:

$$P_{SP} = P_{SPInN}(x) + P_{SPGaN}(1-x) \quad \text{IV.8}$$

Therefore, the total polarization, Pt_t, is given by:

$$P_t = P_{PE} + P_{SP} \quad \text{IV.9}$$

Wurtzite materials	AlN	GaN	InN
P_{SP}	-0.09	-0.034	-0.042
e_{31}	-0.53	-0.34	-0.41
e_{33}	1.5	0.67	0.81
C_{13}	127	100	94
C_{33}	382	392	200

Table IV.1: Spontaneous and piezoelectric polarization, and lattice constants [28].

IV.2.6. The nitride density of states masses and the effective density of states

The nitride density of states masses is a very important parameter in our simulation where the following formulas are used for this purpose [58]:

$$m_e\,(In_x\,Ga_{1-x}N) = 0.12x - 0.2(1-x) \qquad \text{IV.10.a}$$

$$m_h\,(In_x\,Ga_{1-x}N) = 0.17x - 1.0(1-x) \qquad \text{IV.10.b}$$

We used the obtained values of density states masses to calculate the effective density of states for electrons and holes using the flowing equations:

$$N_c = 2\left(\frac{2\pi m_e m_0 KT}{h^2}\right)^{\frac{3}{2}} \qquad \text{IV.11.a}$$

$$N_V = 2\left(\frac{2\pi m_h m_0 KT}{h^2}\right)^{\frac{3}{2}} \qquad \text{IV.11.b}$$

IV.2.7. The electron affinity and the permittivity

The electron affinity is obtained by applying affinity rule [58] we have:

$$\chi = 4.1 + 0.7(Eg_{GaN} - Eg_{InGaN}) \qquad \text{IV.12}$$

The permittivity as function of composition fraction *x*, is given by following formula:

$$\varepsilon\left(In_xGa_{(1-x)}N\right) = 15.3x + 8.9(1-x) \qquad \text{IV.13}$$

IV.2.8. Optical Radiative Recombination

One important physical mechanism we have to consider for recombination are photon transition. This mechanism occurs primarily in one step and is therefore a direct recombination mechanism. For radiative recombination, an electron loses energy when it moves from the conduction band to the valence band. This effect, is important for semiconductors whose specific band structure allows direct transitions. The recombination rate is given by the following model:

$$R = Bnp \qquad \text{IV.14}$$

where n and p are the carrier concentrations and B is the radiative recombination coefficient.

Refrances	radiative recombination coefficients$[cm^3s^{-1}]$
Mhengini[59]	1×10^{-11}
David grundmann[60]	7×10^{-11}
laubsch[61]	0.12×10^{-11}

Table IV.2: Radiative recombination coefficients.

IV.2.9. Shockley-Read-Hall (SRH) Recombination model

When there is a trap in the forbidden gap, phonon transitions will happen. This is a two step process, the theory that explain this phenomenon was derived by three scientist they are Shockley and Read and Hall [27]. This recombination model is given by the following equation:

$$R_{SRH} = \frac{np - n_i^2}{\tau_{n0}(p + p_t) + \tau_{p0}(n + n_t)} \quad \text{IV.15}$$

where n and p are the carrier concentrations of a homogeneously doped semiconductor, τ_{n0} and τ_{p0} are the electron and hole lifetimes.

Refrances	Shockley-Read-Hall (SRH) recombination coefficients$[s^{-1}]$
Menghini[59]	2.3×10^7
David grundmann[60]	2×10^7
laubsch[61]	0.25×10^7
Zhong[62]	1×10^7

Table IV.3: Shockley-Read-Hall (SRH)recombination coefficients .

IV.2.10. Auger Recombination model

Auger recombination occurs through a three particle, where the excess energy is transferred to an electron within the valence or conduction band [27].

Auger Recombination is commonly modeled using the expression [27]:

$$R_{Auger} = C_p n p^2 \quad \text{IV.16}$$

$$R_{Auger} = C_n n^2 p \quad \text{IV.17}$$

$$R_{Auger} = C_n(n^2 p - n_i^2 n) + C_p(p^2 n - n_i^2 p) \quad \text{IV.18}$$

Where C_n and C_p are Auger coefficients.

Refrances	Auger recombination coefficients $[cm^6 s^{-1}]$
Menghini[59]	1×10^{-30}
David grundmann[60]	1×10^{-29}
Laubsch[61]	3.5×10^{-31}

Table IV.4: Auger recombination coefficients.

IV.2.11. The internal quantum efficiency(IQE) using ABC model

The internal quantum efficiency(IQE) is given by the ABC model [19]:

$$\eta_{int} = \frac{R_{raditive}}{R_{total}} = \frac{B.n^2}{A.n + B.n^2 + C.n^3}. \quad \text{IV.19}$$

Where: η_{int} is the internal quantum efficiency, n is the carrier density, and the term A, B and C are Shockley-Read-Hall (SRH), radiative and Auger recombination coefficients, respectively.

IV.2.12. The refractive index model:

The refractive index is given by Adachi's model, and is expressed by Equation [58]:

$$n_r(w) = \sqrt{A\left(\frac{hw}{E_g}\right)^{-2}\left\{2 - \sqrt{1 + \frac{hw}{E_g}} - \sqrt{1 - \frac{hw}{E_g}}\right\} + B} \quad \text{IV.20}$$

For $Al_x Ga_{1-x}N$, the compositional dependence of the A and B parameters are given by the expressions the following Equations:

$$A(x) = 9.827 - 8.216x - 31.59x^2 \quad \text{IV.21}$$

$$B(x) = 2.736 + 0.842x - 6.293x^2 \quad \text{IV.22}$$

For $In_x Ga_{1-x}N$, the compositional dependence of the A and B parameters are given by the expressions the following Equations:

$$A(x) = 9.827 + 9.827x - 53.57x \quad \text{IV.23}$$

$$B(x) = 2.736 - 2.736x - 9.19x \quad \text{IV.24}$$

IV.3. Atlas Simulator software

In this thesis ATLAS simulator has been used, where his LED simulator provides general capabilities for simulation of light emitting diode (LED) devices.

The LED simulator supports the use of many semiconductor materials [58] such as:

- zincblende (e.g., AlGaAs/GaAs, InGaAsP/InP).
- wurtzite (e.g., GaN/AlGaN/InGaN).
- organic/polymer material systems.

It can also account polarization and strain effects on both emission spectra and piezoelectric polarization [58].In addition, many characteristics can be obtained, such as the LED efficiency, the emission power versus current, the wavelength and the spectra of the emission, and the extraction of electrical characteristics.

The specification of the LED devices, the selection and the physical models including the optical models, and also the extraction of device characteristics, all of that are described as follow:

For LED devices, when III-nitride Wurtzite materials are used, various models are involved like WZ.KP model which is derived from K.P method [63] and used to analyze spectral characteristics, such as emission wavelength and emission spectra, QWELL model is used for spontaneous recombination, three bulk recombination mechanisms should be involved when simulating LED devices, which are Shockley-Read-Hall (SRH), Auger, and radiative recombination, these mechanisms are enabled by specifying SRH, AUGER, and OPTR models respectively, on the MODEL statement associated with the active regions of the LED device, for the specification of the rate constant for the radiative recombination model, the COPT parameter has to be enabled, the value of this constant can be calibrate using more physical radiative models. The competition between radiative and non-raditive recombination mechanisms will cause LED efficiency degradation, this allow to analyze this efficiency degradation.

Polarization model is critical for GaN based devices, it is used to calculate the total polarization which is the sum of the spontaneous and the piezoelectric polarization, the III-V nitrides materials parameters related to the polarization are based on the research of F. Bernardini, et al [28], the values of the different coefficients related to the polarization are listed in Table III.1. To include the effects of polarization on a region, the POLARIZATION parameter has to be specified on the corresponding REGION statement, this will only include spontaneous polarization. To include piezoelectric polarization, the CALC.STRAIN parameter has to be specified. Thus the simulator will automatically calculate strain from the lattice mismatch, then calculate the piezoelectric polarization and apply it to the region.

Data extraction LED: The extraction of luminous intensity is done when the LED parameter is specified on any REGION statement, the luminous intensity emitted is computed and written to the log file. Then led.log is loaded into TonyPlot visualization tool, and the characteristics can be plotted, such as luminous intensity versus current, where the luminous intensity is obtained by integrating the luminous spectrum. This will gives capabilities for viewing and analyzing simulator output. In addition the plotted graphs can be compared using overlays feature.

Extracting emission spectra: From the SOLVE statement multiple spectrum can be saved by files. The spectral intensity can obtained as a function of energy and wavelength integrated over all wells specified as LEDs. LMIN and LMAX specify the minimum and maximum values of wavelength in microns. The minimum and maximum values of energy is specified by EMIN and EMAX and given in eV. The probe is used to measure wavelength for LED devices. This will extract the wavelength from the peak of the spectral response over a specified range.

DeckBuild is the graphical user interface (GUI) for Silvaco's TCAD programs. it has numerous simulator specifics and general debugger style tools, such as powerful extract

statements, GUI based process input, line by line runtime execution and intuitive input syntactical error messages.

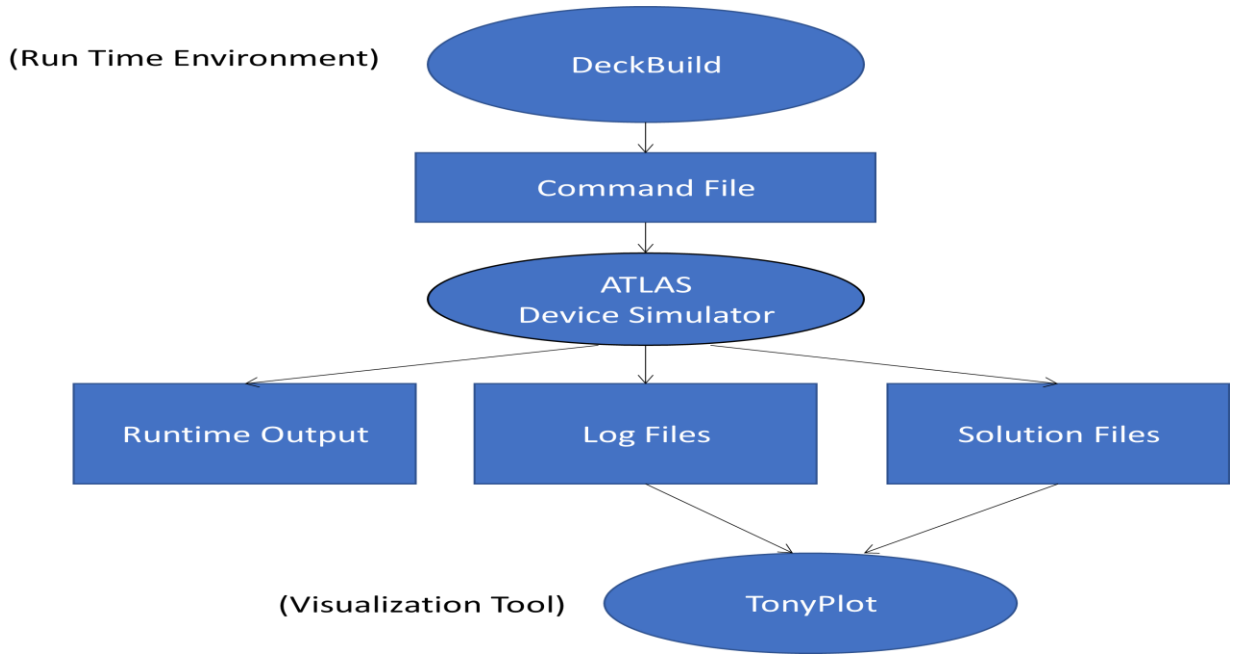

Figure IV.2: Run time environment.

IV.4. The Order of Atlas Commands

There are five groups of statements that must occur in the correct order (Table IV.5). The most used commands are described below:

a. **MESH** defines a mesh with the simulated structure.
b. **REGION** defines each region of the structure and indicate the used material.
c. **ELECTRODE** allows to define the position of an electrode and the used material.
d. **DOPING** allows to define a type, a concentration and a profile of doping for a given region of the structure.
e. **CONTACT** specifies the contact type. In LEDs the default contact is ohmic.
f. **MATERIAL** makes it possible to define specific parameters associated with each material such as the forbidden band, the permittivity, the mobility of carriers. In ATLAS, the default settings for several materials are already implemented.
g. **INTERFACE** allows to define the parameters of the interface of two regions.
h. **DEFECTS** activates the band gap defects model.
i. **MODELS** specifies the physical models used.
j. **METHOD** allows to choose the numerical methods used to solve the equations and also to choose the parameters related to these algorithms.
k. **LOG** allows to record all electrical characteristics calculated by ATLAS in a ".log" type file. All data generated by the SOLVE command is stored in this file.

l. **LOAD** loads previous solutions.

m. **SOLVE** allows to order ATLAS to find a solution.

n. **SAVE** saves the structure and the internal quantities for any point in a ".str" file.

o. **EXTRACT** allows to extract numerical values from ".log" files.

p. **TONYPLOT** makes it possible to use the visualization tool.

Group	Statements
Structure Specification	MESH
	REGION
	ELECTRODE
	DOPING
Material Models Specification	MATERIAL
	MODELS
	CONTACT
	INTERFACE
Numerical Method Selection	METHOD
Solution Specification	LOG
	SOLVE
	LOAD
	SAVE
Results Analysis	EXTRACT
	Tonyplot

Table IV.5: Atlas Command Groups with the Primary Statements in each Group.

Chapter V Design and Numerical Simulation of LED Structures

V.1. Introduction

One of the methods utilized in solid state lighting is the combination of two or more complementary wavelengths generated from LEDs, having typically red, green, blue and violet colors. This will create a mixture, where the observer can preseive it as a wide range of colors including the white light, due to the tristimulus sensitivity of the eyes. In addition the high luminous efficiency are always desirable for LED, where the dichromatic aproach to generate many colors of the spectrum and white light, is the best as compared to the other choices. In this technique two apropriate mixed spectrum are perceived as the wanted color light. Moreover the white light can be obtained by two wavelengths of complementary colors. All the following simulated devices is based on this technical aproach.

In this chapter the folowing studies are presented:

- Comparative study between violet and green InGaN-based SQW LEDs grown on GaN substrates.
- Design and simulation of dual wavelength LED with two QWs.
- Design and simulation of color tunable vertically stacked QW LED with double cathode single anode.
- Design and simulation of color tunable laterally arranged quantum well LED with double anode single cathode.

V.2. Comparative study of violet and green InGaN-based SQW LEDs using Silvaco TCAD tool

Solid-state lighting technology is replacing conventional incandescent and fluorescent lamps, where III-nitride Wurtzite based light emitting diodes LEDs [1] is generally used for this purpose. In the other hand the violet and the green LEDs are widely used in the generation of white and multi- color lights.

In many reported works [14], InGaN LED structure using GaN material as substrate shows a promising results when designing long wavelength devices, where different spectra with a peak emission ranging from 410 to 590 nm are obtained, which can generate violet, blue, green, yellow and amber colors. Previous studies have introduced various structures and methods to obtain different range of colors light LEDs, where conventional LED are involved, in particular, three LED chips each emitting red, green, and violet light, or two LED chips each emitting green, and violet light, in the two methods the LEDs are arranged laterally, thus requiring a very dense circuitry for driving the individual color emission [8], many other structure are also designed for the same purpose. The main issue of this simulation work is a Comparative study between violet and green InGaN-based SQW LEDs grown on GaN substrates. in this work GaN, InGaN and AlGaN

materials, and GaN substrate are used. The studied structures are needed when designing different colors emissions and white light LEDs.

V.2.1. Parameters and Simulation Models

The used device simulator in this work is The ATLAS software, where The continuity and the transport equations are utilized to describe the way that the electron and hole densities evolve as a result of transport, generation, and recombination processes. The models used for III-nitride Wurtzite materials, are WZ.KP model which is derived from K.P method, and the QWELL model. The radiative, Shockley-Read-Hall (SRH), and Auger recombination, are involved when simulating LED devices, the used coefficients are in the accepted values as given in Table. V.1, Farahmand Modified Caughey Thomas model is used to obtain the composition and temperature dependent low field mobility [58], which is given by the Equation (IV.4). Polarization model is necessary for GaN based devices, where the III-V nitrides materials parameters related to the polarization are based on the research of F. Bernardini, et al[28], and they are given by Table IV.1. The spontaneous polarization can be expressed by the Equation (IV.8).The piezoelectric polarization can be calculated by the Equation (IV.7).The band gap Eg is calculated by the formula (I.2). The band gap energies of InN and GaN, have values listed in Table.V.1 . The emitted Wavelength is obtained by Equation (III.4). The electron affinity is obtained by the rule (IV.12). where the ALIGN parameter is used [31]. The GaN substrate is used in those structures, the theoretical polarization charge was assumed between 30% and 50% [18], The total series resistance of the anode and the cathode contacts is supposed to be ideal.

Parameter	value
Eg_{GaN}	3.4 eV
Eg_{InN}	1.8 eV
The bowing parameter	3.8 eV
The operating temperature	300 K
The electron affinity χ	$4.1 + 0.7(Eg_{GaN} - Eg_{InGaN})$
The used polarization charge scale	Between 30% to 50%
Auger recombination coefficients(C)	Between $1.0 \times 10^{-30} cm^6 s^{-1}$ To $1.0 \times 10^{-31} cm^6 s^{-1}$
Radiative recombination coefficient(B)	$1.0 \times 10^{-11} cm^3$
Shockley-Read-Hall(SRH) recombination coefficients(A)	$1.0 \times 10^7\ s^{-1}$
Activation energy of Mg doper	200 meV
Activation energy of Si doper	20 meV

Table.V.1: The used parameters in the two LEDs and their values.

V.2.2. Device Structure

The proposed blue LED structure consists of GaN substrate, followed by 2 µm n-GaN layer with doping density, $1 \times 10^{19} cm^{-3}$, and a 6 nm thick GaN barrier, the active region is 4 nm thick $In_{0.12}Ga_{0.88}N$ single quantum well (SQWs) followed by 6 nm thick GaN quantum barrier, followed by 0.02 µm thick p-$Al_{0.15}Ga_{0.85}N$ electron blocking layer with doping density, $1 \times 10^{18} cm^{-3}$, followed by 0.28 µm thick p-GaN layer with doping density, $1 \times 10^{19} cm^{-3}$, the green LED structure has the same layer structure except that the indium content in the SQW is 45%, the Figure V.1. illustrate the structure of the two devices.

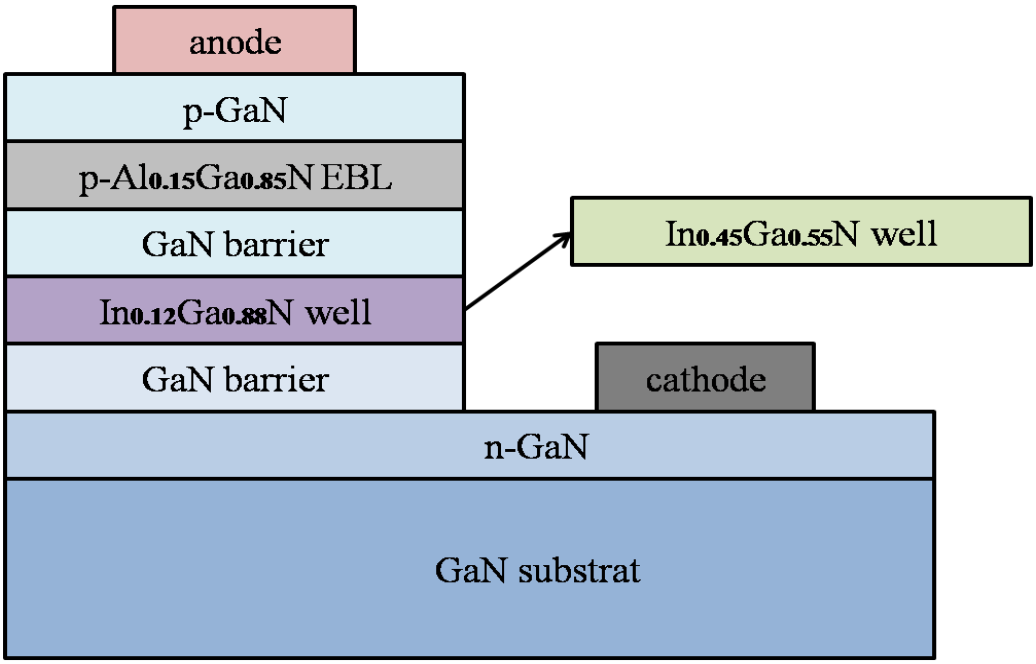

Figure V.1: Violet and green SQW LEDs structure.

V.2.3. Results and Discussion

When the violet SQW LED is forward biased by 3.6V, a violet spectra is generated having photoluminescence (PL) peaks centered near 410 as seen in Figure V.2.a, in the other hand when the green SQW LED is forward biased by 3.6V, a green spectra is generated having PL peaks centered near 561 as seen in Figure V.2.b.

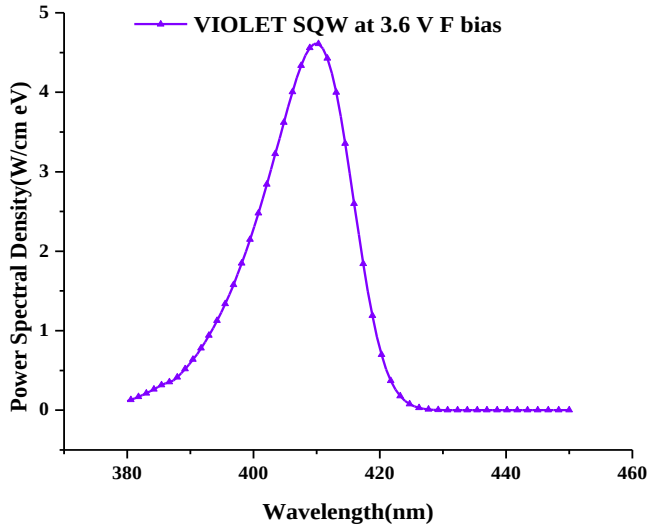

(a)

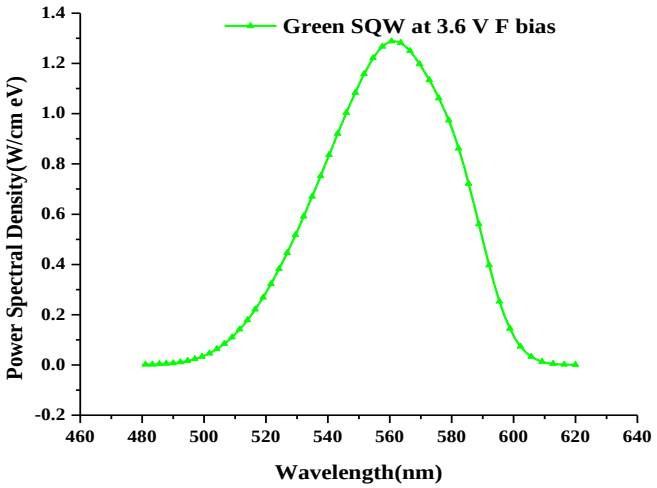

(b)

Figure V.2: Power spectral density: (a) the violet SQW, and (b) the green SQW.

If we compare between The two LEDs graphs in Figure V.3 we observe that the increase of indium element content in the SQW decreases LED turn-on voltage which is in good agreement with other research works [15,64], since the threshold voltage can be expressed as function of the band gap energy of these used materials, by the approximated equation [3,76]:

$$V_{th} \approx V_D \approx \frac{E_g}{e}. \qquad \text{V.1}$$

Where V_{th} is the threshold voltage, V_D is the diffusion voltage, energy.

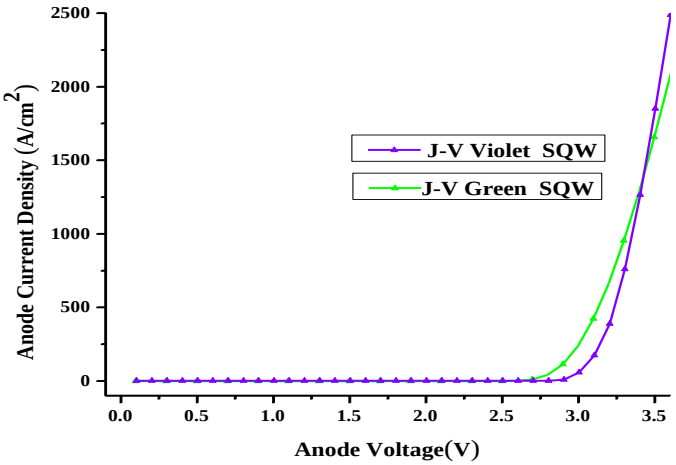

Figure V.3: The J/V characteristics of the violet and green SQWs LEDs.

The polarization charge concentration in the green LED is greater than that of the violet LED as illustrated in Figure V.4, this is due to the higher lattice mismatch between the SQW and the GaN barrier in the green LED, see equation (IV.7), this leads to higher total polarization see equation (IV.9).

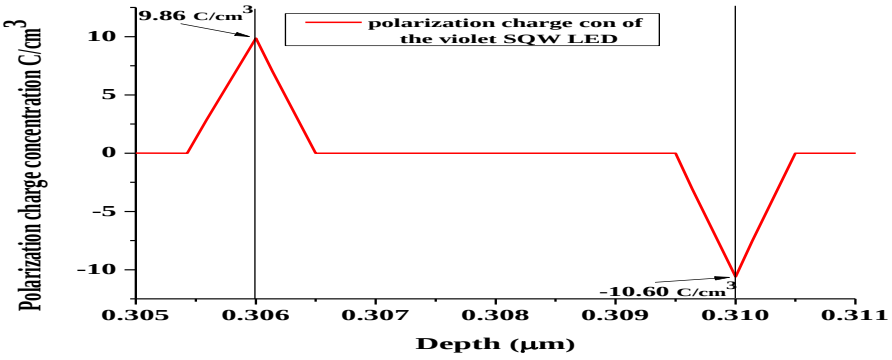

(a)

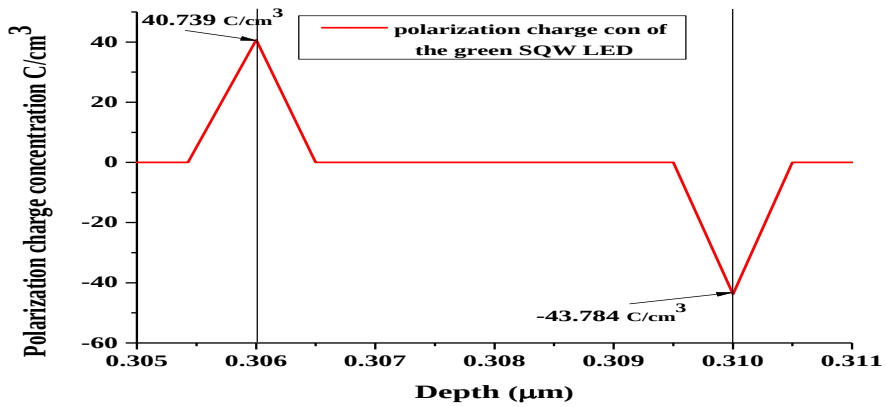

(b)

Figure V.4: Polarization charge concentration: (a) the violet SQW, and (b) the green SQW.

This will increase the quantum confined Stark Effect (QCSE) and cause a change in the conduction and valance band profile [65,66] as shown in Figure V.5.

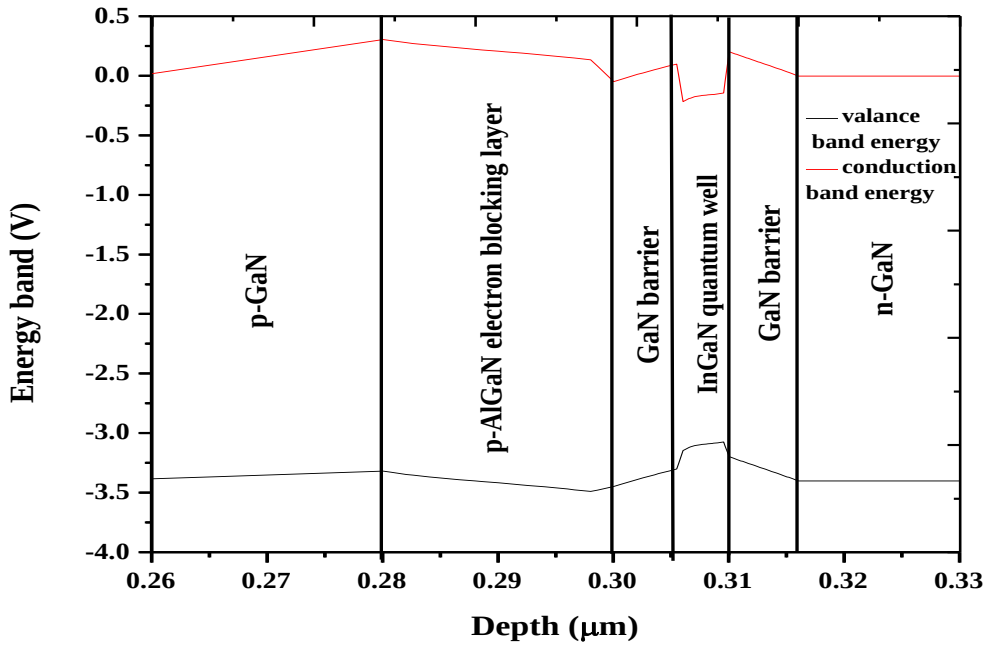

(a)

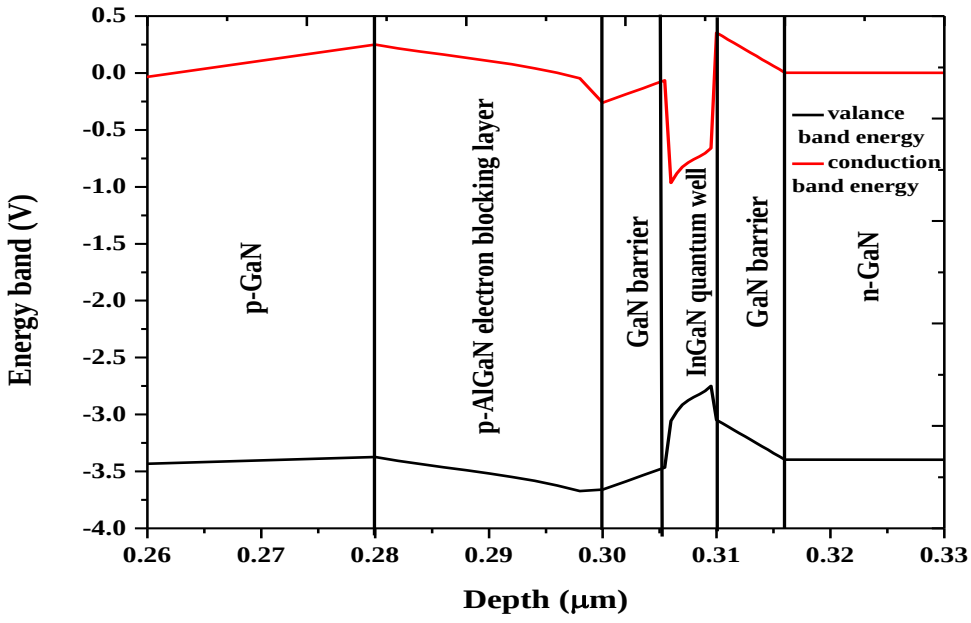

(b)

Figure V.5: The conduction and the valance band of (a) the violet SQW, and (b) the green SQW at 3.5 V F bias.

The change in conduction and valance band profile, reduces the overlap between electron and hole wave functions [65,66] as shown Figure 6. This will cause an additional internal quantum efficiency droop. The quantum confined Stark Effect (QCSE) becomes more significant for the

green SQW as compared to that of the violet one, due to the increased of the lattice mismatch between the green SQW and the GaN barrier as displayed in Figure 5.b.

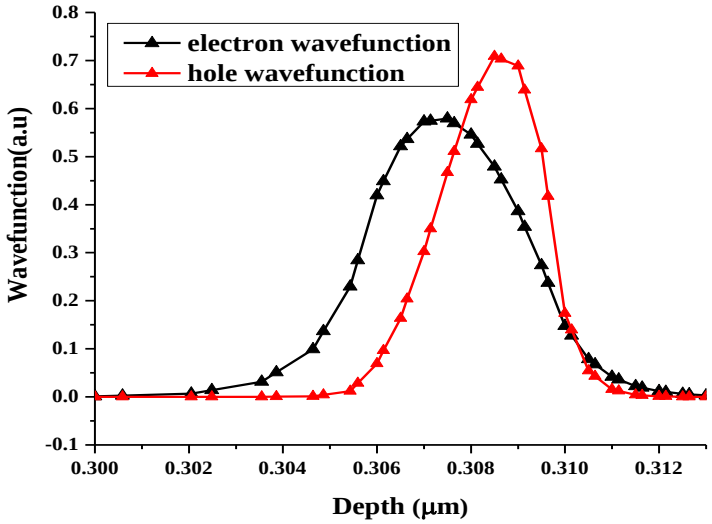

(a)

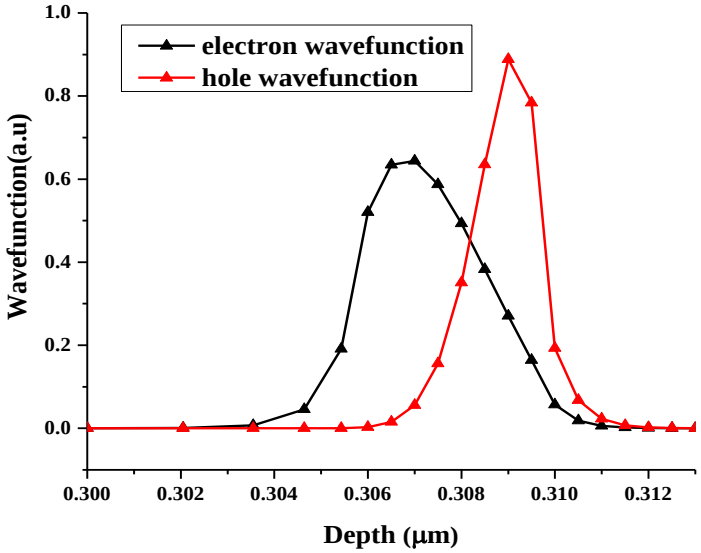

(b)

Figure V.6: The wave functions of (a) the violet, and (b) the green SQW.

The total recombination rate in the violet SQW reaches 3.706 10^{28}carriers per cm^3s, and the Auger recombination rate reachs 6.881 10^{26} carriers per cm^3s, but the total recombination rate in the green SQW reaches 4.9 10^{28}carriers per cm^3s and the Auger recombination rate reachs 3.1 10^{28} carriers per cm^3s, wich is very high rate , this will reduce IQE of the green SQW LED as ullistrated in Figure V.7.

(a)

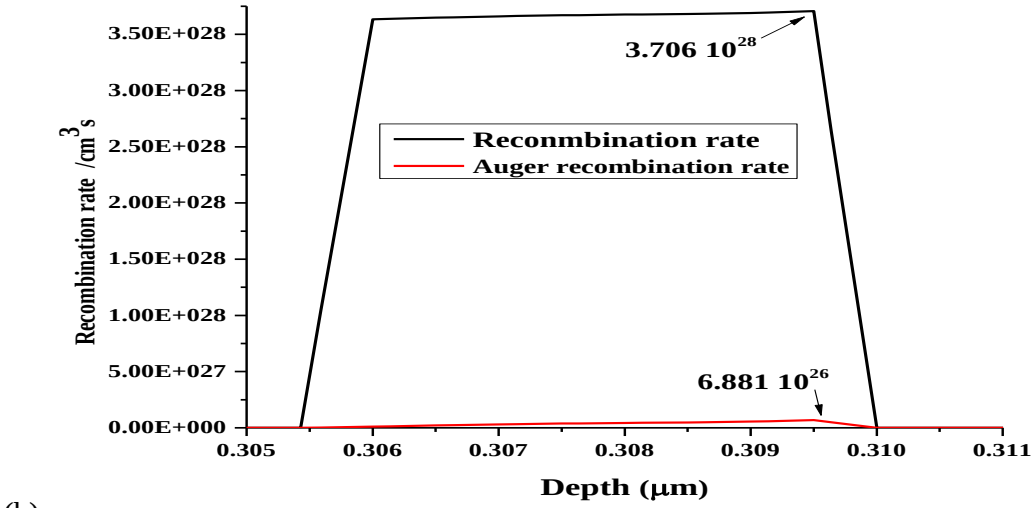

(b)

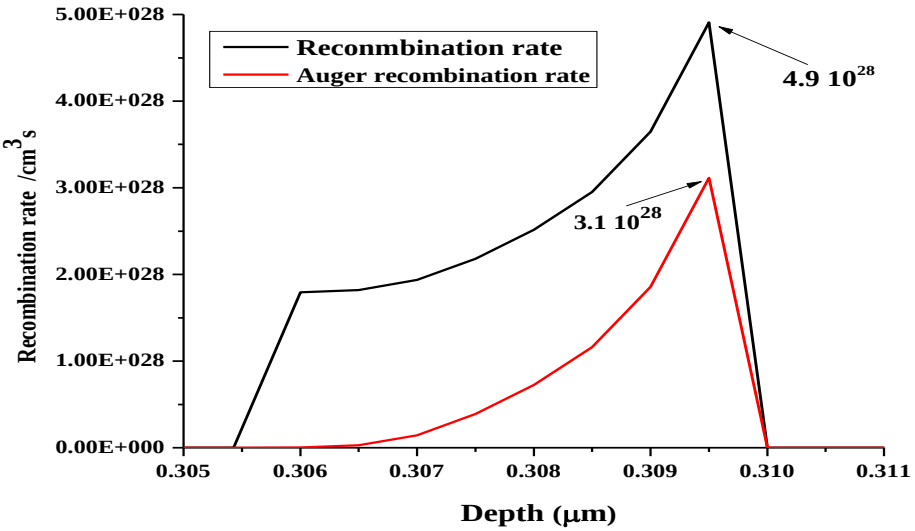

Figure V.7: Total and Auger recombination rate of (a)the violet, and (b) the green SQW LED.

The Figure 8. shows the obtained internal quantum efficiency (IQE) versus anode current density, it is clear that there is a reduction in the (IQE) at high current density where the Auger recombination is one of the major cause of the efficiency droop [59,60,61,62,67,68].

In addition the violet LED shows better IQE as compared to the IQE of the green LED, where the decreasing material quality and increasing quantum confined Stark effect (QCSE) due to the high polarization fields have a big impact on the IQE [65,66], the two factors reduces LED efficiency when increasing indium content. The first one leads to increased nonradiative recombination, and the second one reduces the overlap between electron and hole wave functions as presented in Figure V.8.

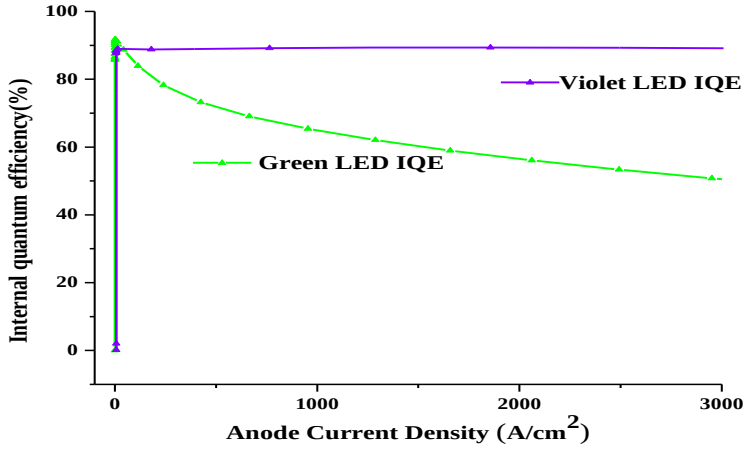

Figure V.8: The IQE of the two LEDs structures.

By changing the polarization scale factor in the simulator from 0.3 to 0.5 in the violet LED, its IQE is slightly reduced, but this change has high influence on the reduction of the IQE of the green LED as shown in Figure 9.

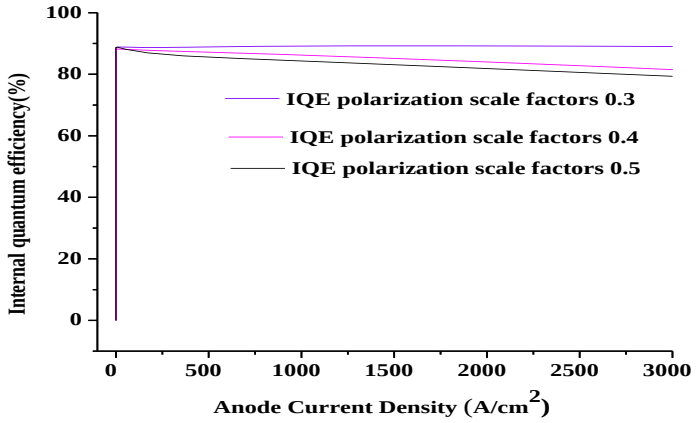

(a)

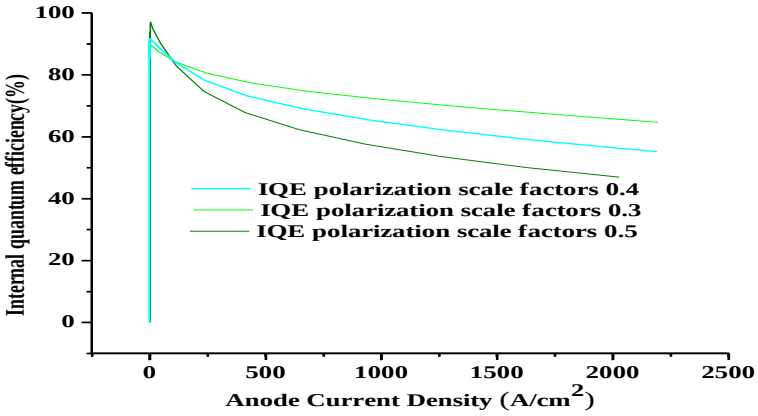

(b)

Figure V.9: The IQE of (a) the violet, and (b) the green SQW LED for some polarization scale factor.

By changing the Auger recombination coefficient from 1×10^{-30} to 1×10^{-32} in the simulator for both the violet and the green LED, we can conclude that this effect has high influence on the two LEDs structure as illustrated in Figure 10.

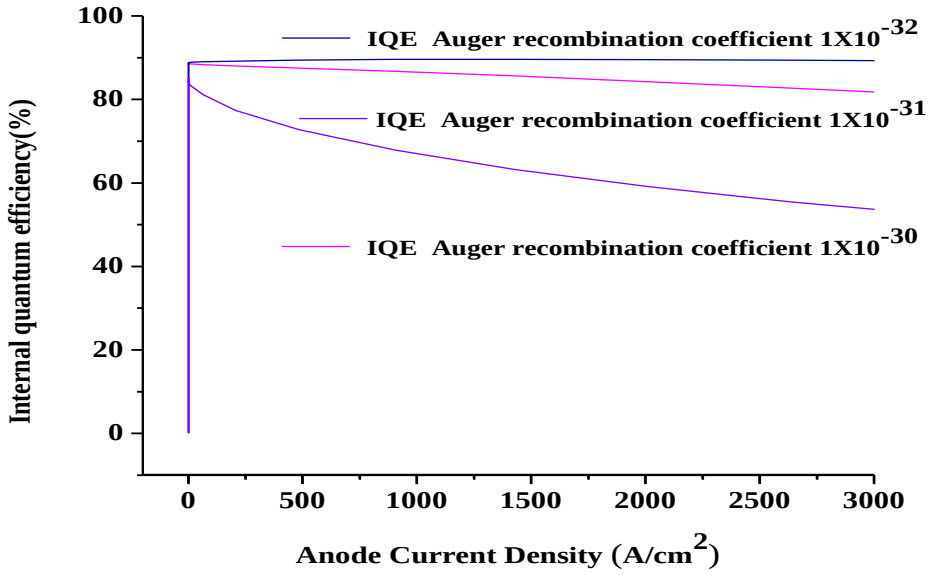

(a)

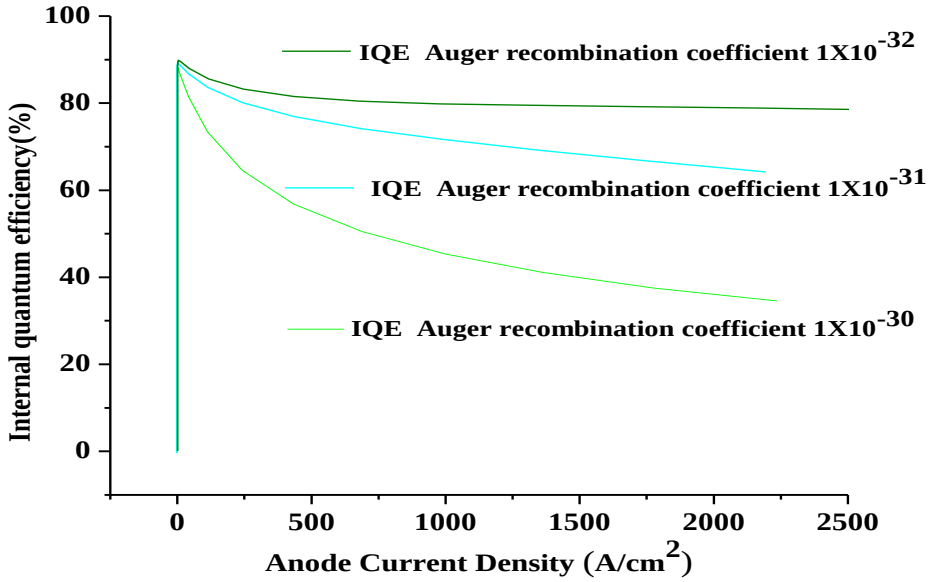

(b)

Figure V.10: The IQE of (a) the violet, and (b) the green SQW LED for some Auger recombination coefficient.

For the violet SQW the peak wavelengths are 412, and 410 nm at 3.4V forward biased , and 3.6V forward biased, respectively as shown in Figure V.11.

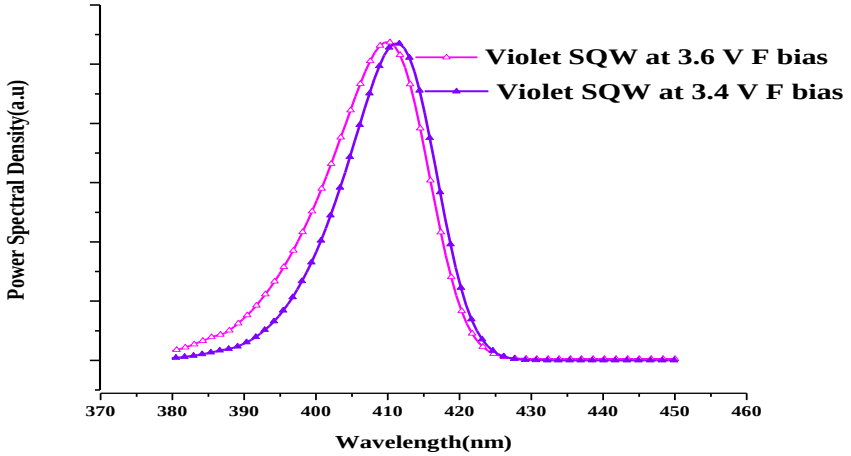

Figure V.11: Blue shift in the power spectral density of the violet SQW.

For the green SQW the peak wavelengths are 562, and 555 nm at 3.6V forward biased, and 4.5V forward biased, respectively as illustrated in Figure V.12.

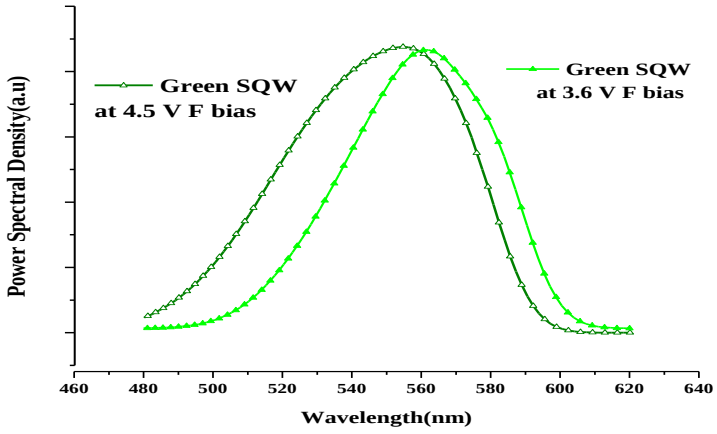

Figure V.12: Blue shift in the power spectral density of the green SQW.

As the current density increases from 100 to 2000 A/cm^2, there will be a reduction of (QCSE) this leads to a blue shift in the peak position wavelength of both LEDs. Many published experimental works came out with the same conclusion , in addition the violet peak wavelength shows a neglected blue-shift less than 4 nm, while the green peak wavelength exhibits a blue-shift of 10nm the obtained results agree with many previous works, where they observed that when the In content is higher the blue shift will be higher [69-72], see Figures V.13. In the other hand, The full-width half maximum (FWHM) of the violet and green wavelengths, were in the range [12-22 nm] and [52-64 nm], as seen in Figures V.13, respectively, this results agree with other studies[69-72], this has to be taken into consideration to obtain the needed color rendering when designing white light LEDs.

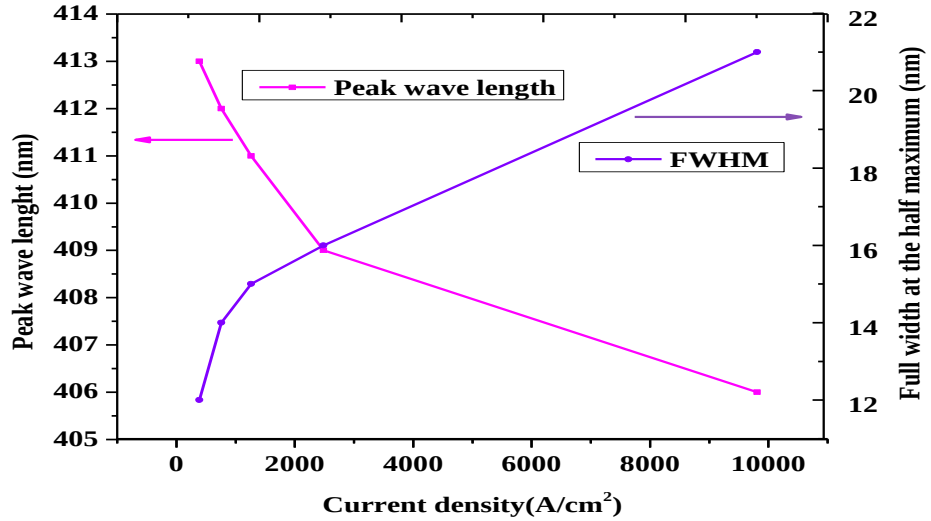

(a)

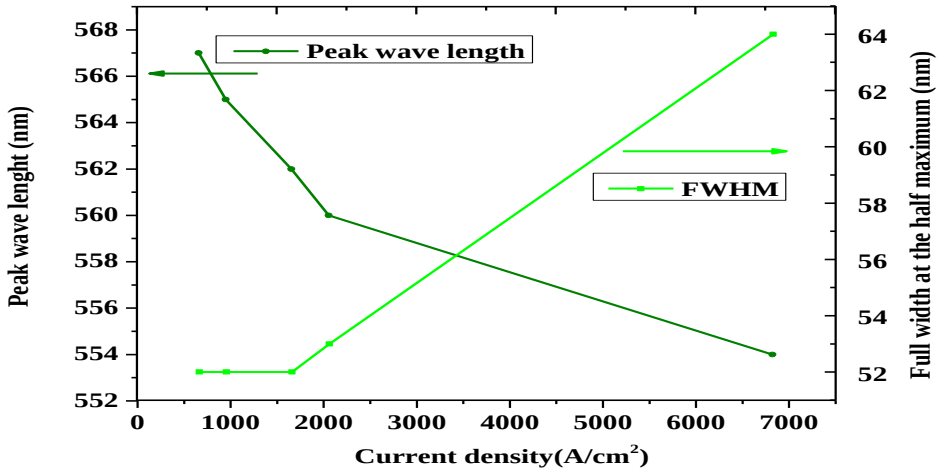

(b)

Figure V.13: Blue shift & The full-width half maximum of the power spectral density (a) the violet SQW (b) the green SQW.

V.2.4. Recapitulation

In summary, violet and green SQW LEDs are designed, the violet device can emit wavelengths close to 410 nm and the green device can emit wavelengths close to 561 nm. The simulated structures shows a blue shift of the both LEDs, but that of the green LED is higher than that of the violet LED. In addition the violet LED shows better IQE as compared to the IQE of the green LED, the reduction in IQE is caused by two effects, the first one is the decrease in material quality, this leads to increase of Auger nonradiative recombination [68], and the second one is the increase of the quantum confined Stark effect (QCSE) due to the high polarization fields which reduces the overlap between electron and hole wave functions [65,66,67].

V.3. Design and Simulation of Dual wavelength LED with two QWs

As a challenge to the phosphor based LEDs [1,9], the phosphor-free LEDs have been proposed. Generally, this type of LEDs is obtained by stacking InGaN/GaN quantum wells (QWs) having different indium compositions which generate different emission wavelength. They are grown sequentially [11,12]. A range of colors and white light is expected from the mixing of different generated spectrum. In this work, we simulated a structure with two QW active regions that can generate a dual emission wavelengths in the violet and green regions.

V.3.1. Parameters and Simulation Models

The same models have been utilized as the previous structures, all the used parameters are the same as the previous structure except the polarization charge scale and Auger recombination coefficients(C) which are listed in Table.V.2.

Parameters	values
The used polarization charge scale	40%
Auger recombination coefficients(C)	$1.0 \times 10^{-31} cm^6 s^{-1}$

Table.V.2: The used parameters in the two LEDs and their values.

V.3.2. Device Structure

The proposed LED structure consists of GaN substrate, followed by 2 µm n-GaN layer with doping density, $1 \times 10^{19} cm^{-3}$, and a 7 nm thick GaN barrier , then an active region with 3 nm thick $In_{0.12}Ga_{0.88}N$ followed by 7 nm thick GaN quantum barrier, followed by a second active region with 3 nm thick $In_{0.43}Ga_{0.57}N$ followed by 7 nm thick GaN quantum barrier, followed by 0.02 µm thick p-$Al_{0.15}Ga_{0.85}N$ electron blocking layer with doping density, $1 \times 10^{18} cm^{-3}$, followed by 0.28 µm thick p-GaN layer with doping density, $1 \times 10^{19} cm^{-3}$, the Figure V. 14. illustrate the structure of the device.

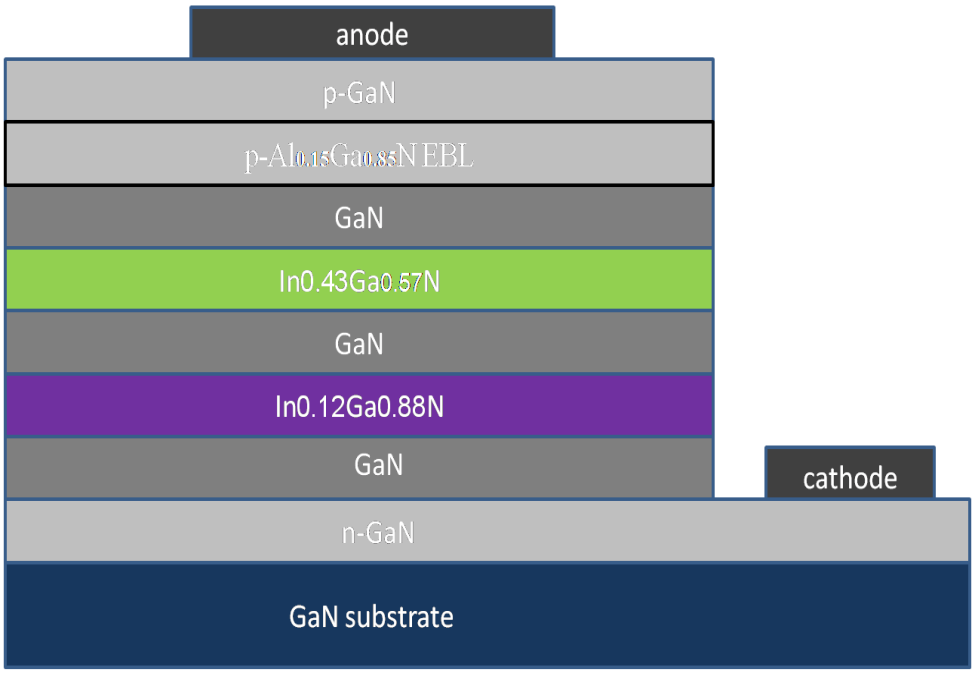

Figure V. 14: Stacked MQW having green and violet active layers structure.

V.3.4. Results and Discussion

When the structure is forward biased by 5.5V, violet spectra is generated having PL peaks centered near 420 nm and a green spectra is generated having PL peaks centered near 560 nm as presented in Figure V.15.

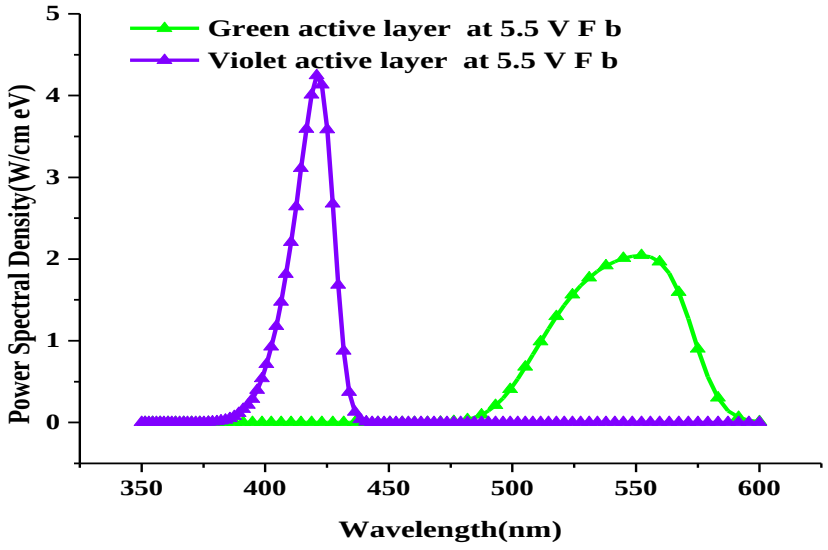

Figure V.15: Violet and green PSD of the two stacked quantum wells forward biased at 5.5 V.

The blue shift of the green SQW (35 nm) is bigger than of the violet SQW (7 nm) as seen in Figures V.16 .a and V.16 .b. In fact, many published experimental works showed that there is a dependence of the peak electroluminescence (EL) emission wavelength on the drive current. This

leads to blue shift, and that as the In content is high, the blue shift will be high [69-72, 74,77]. This problem has to be taken into consideration to obtain the needed color rendering when designing white light LEDs.

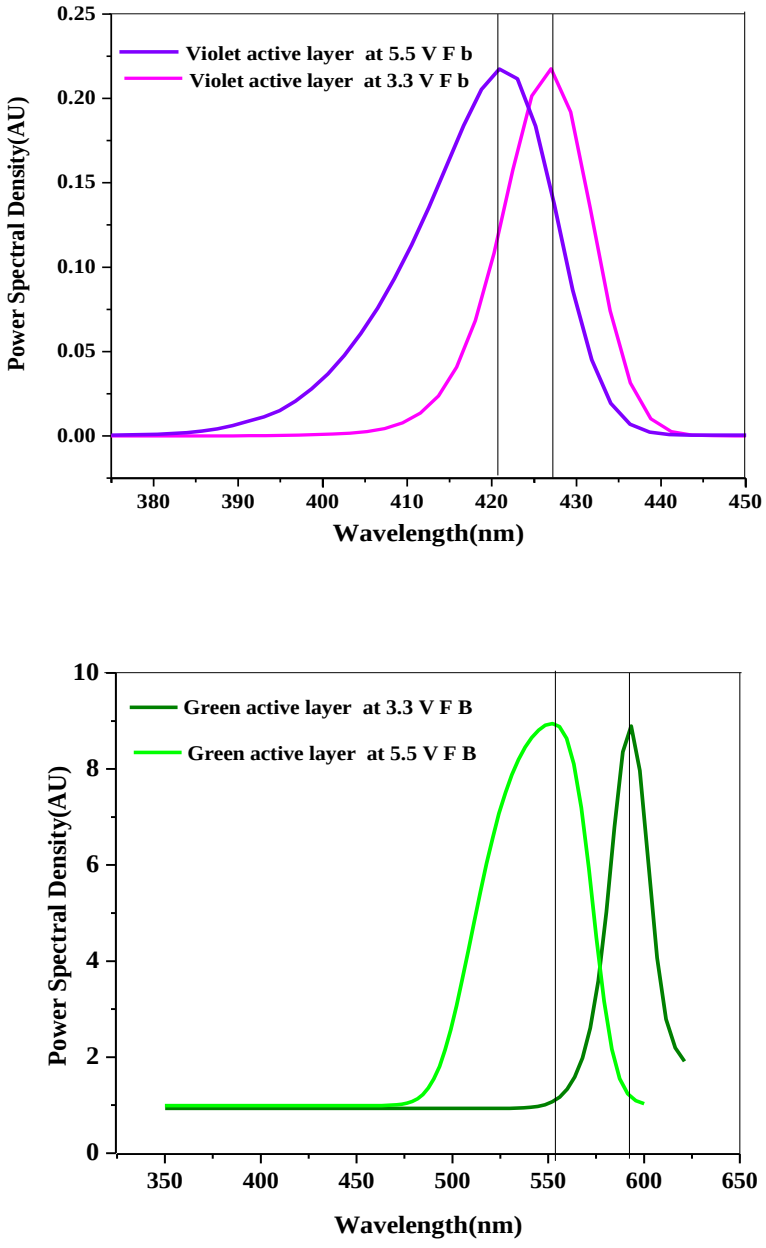

Figure V.16: : Blue shift in the Power spectrum of the device as a function of the injection current density (a) The violet active layer, (b) The green active layer.

The J/V graphs turn-on voltage is near 3V as seen in Figure V.17. Which is in good agreement with other research works [15,41].

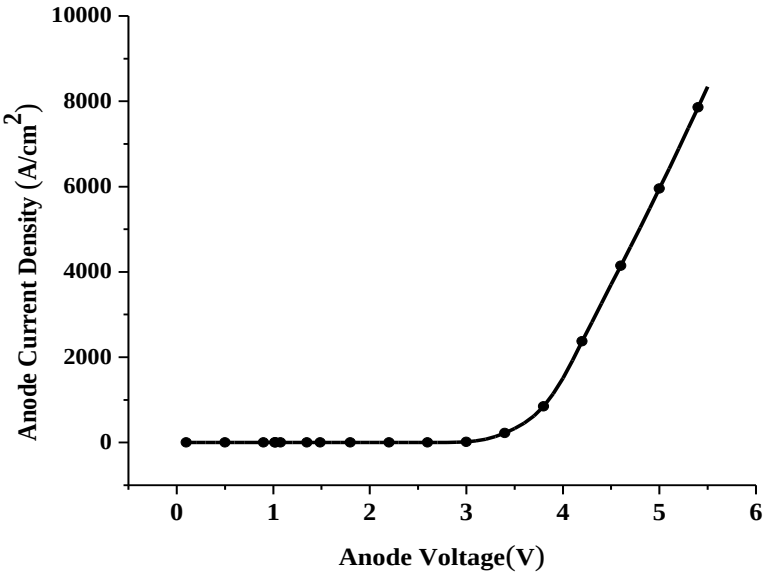

Figure V.17: The current-density versus anode voltage characteristics.

The lattice mismatch between the QWs and the GaN barriers structure produces a quantum confined Stark Effect (QCSE) in the conduction and the valance band [38,39,40], as shown in Figure V.18. The change in conduction and valance band profile, reduces the overlap between electron and hole wave functions [65,66]. This will cause an additional internal quantum efficiency drop. The quantum confined Stark Effect (QCSE) becomes more significant for the green active layer as compared to that of the violet one, due to the increased of the lattice mismatch between the green active layer and the two barriers.

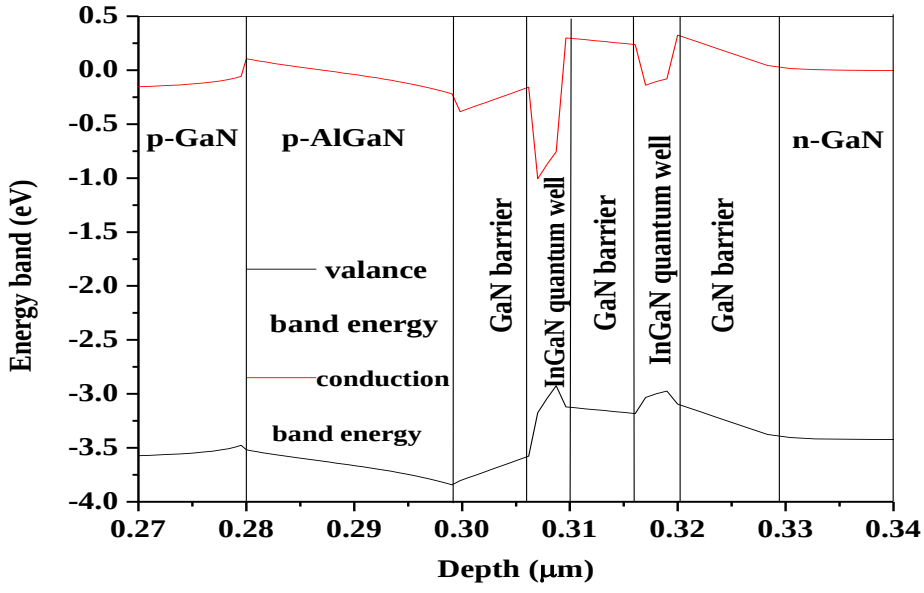

Figure V.18: The conduction and the valance band of the violet SQW at 3.5 VF bias.

The distribution of the electrons and holes over the entire active regions is illustrated in Figure V.19, where the carriers concentration in the green QW and in the violet QW is about $5.6 \times 10^{19} cm^{-3}$ and $1 \times 10^{19} cm^{-3}$ respectively, it is clear that the MQW structure suffer from inhomogeneous carriers distribution which is reported in many references [18].

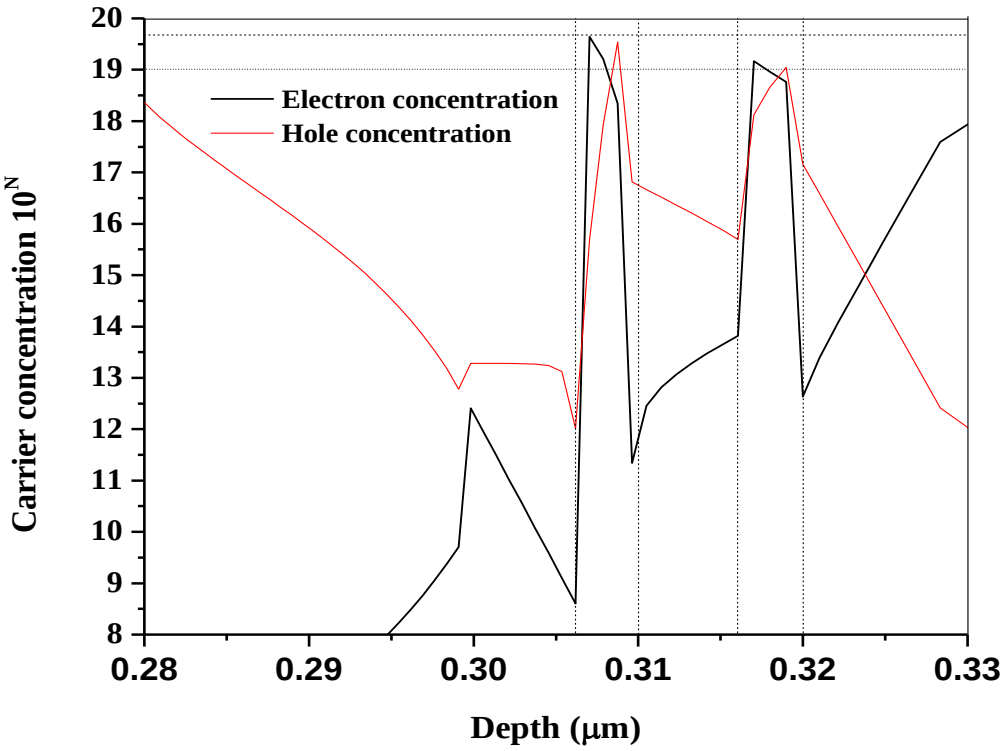

Figure V.19: The distribution of electrons and holes concentration for the violet and the green QW at an applied voltage of 3.5.

Because holes have a high effective mass and very low mobility, the green active layer takes the advantage of being the closest QW to the p-type region[73], which enhance his radiative recombination . Even thought, the violet active layer shows better radiative rate as compared to that of the green QW, due to the high polarization fields, and the increased of the nonradiative recombination in the green active layer, until a higher current injection is reached, this causes a saturation in the violet QW, in this situation the green QW shows better radiative recombination as seen in Figure V.20.

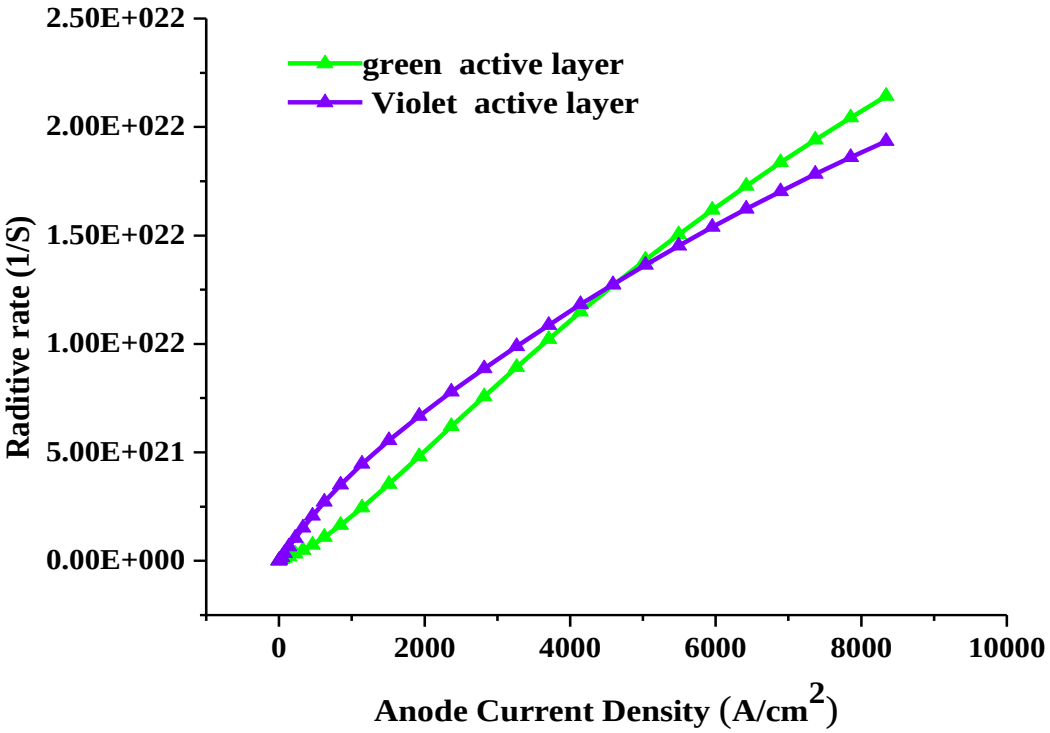

Figure V.20: The radiative rate versus anode current-density.

V.3.4. Recapitulation

In summary, MQW LED structure that generate violet and green light is designed. The violet active layer can emit wavelengths close to 420 nm and the green active layer can emit wavelengths close to 561 nm, a mixture of violet blue light will be generated, the structure can generate white light. The structure shows a blue shift of the both colors in the two active layers due to the increased current, this will affect the color rendering and the stability of light. Moreover the device suffer from inhomogeneous hole distribution, also a part of the photon generated by the higher band gap active layer will be absorbed by the lower band gap active layer this affect the performance of the device.

V.4. Design of color tunable vertically stacked QW LED with 1 anode, 2 cathode

In this studies design and simulation of tunable LED structure has been done, to obtain a phosphor free LED, and to overcome the non-uniform distribution of holes in the MQW active layers, moreover to realize an independent color control, the designed violet-green color tunable monolithic LED have a multi-junction structure with 1 anode, 2 cathode. It has three operation modes which are the green mode, violet mode, and mixture mode**,** and at a certain mixture ratio the white light is obtained, without the need of phosphor converter. In this study, the optical and electrical properties of the device will be discussed.

V.4.1. Parameters and Simulation Models

The used parameters and models are the same as the previous structures.

V.4.2. Device Structure

The proposed LED structure consists of GaN substrate, followed by 2 µm n-GaN layer with doping density, $1 \times 10^{19} cm^{-3}$, and a 6 nm thick GaN barrier, then an active region with 4 nm thick $In_{0.45}Ga_{0.55}N$ followed by 6 nm thick GaN quantum barrier, followed by 0.28 µm thick p-GaN layer with doping density, $1 \times 10^{19} cm^{-3}$, then a 6 nm thick GaN barrier followed by a second active region with 4 nm thick $In_{0.12}Ga_{0.88}N$ followed by 6 nm thick GaN quantum barrier, followed by 2 µm n-GaN layer with doping density, $1 \times 10^{19} cm^{-3}$, the Figure V.21. illustrate the structure of the device. In this structure the violet active layer is on the top of the violet active layer to reduce the effect absorption.

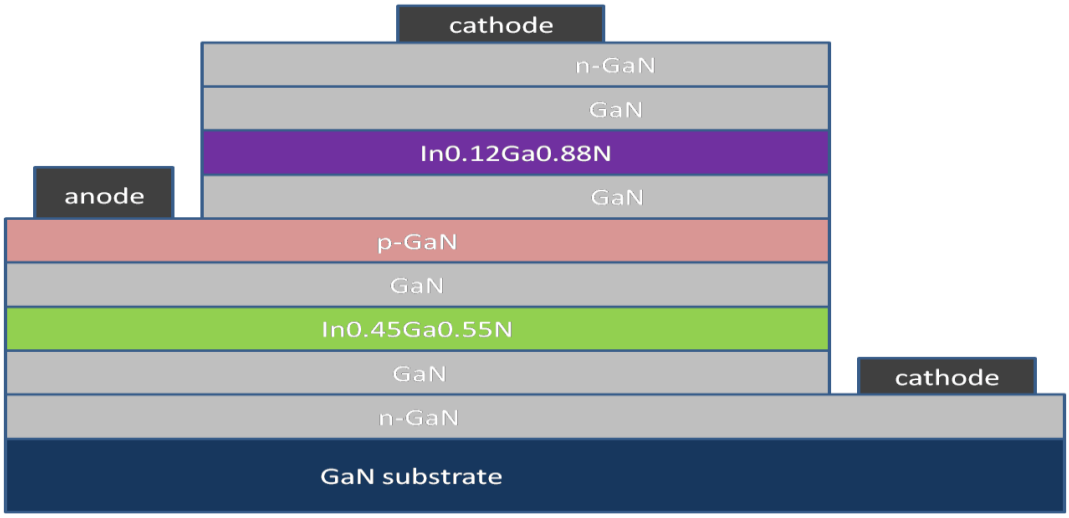

Figure V.21: Color tunable vertically stacked QW LED with 1 anode, 2 cathode.

V.4.3. Results and Discussion

When the two SQWs are forward biased with the same voltage, both violet and green spectra are generated, with Photoluminescence (PL) peaks centered near 410 and 561 nm, respectively. The obtained result is shown in Figure V.22.

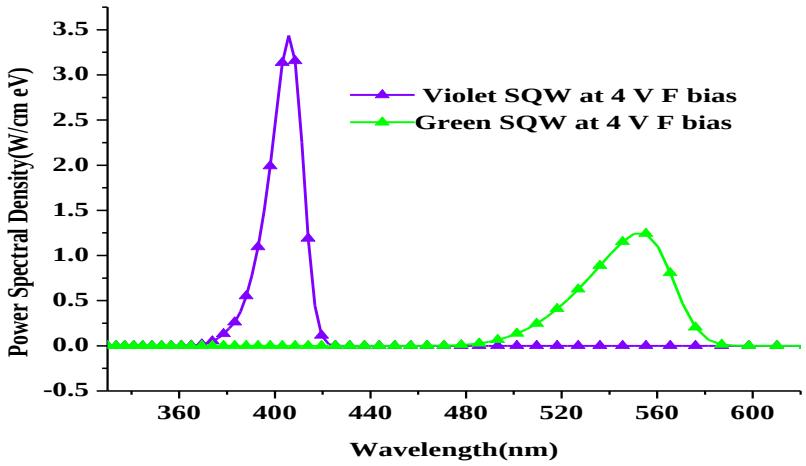

Figure V.22: Violet & green PSD of the two stacked quantum wells 4V FBs.

The LED device can operate by applying forward biasing voltage between the cathode and the anode contacts of only one active layer. This will generate just violet or green spectrum as displayed in Figure 23.

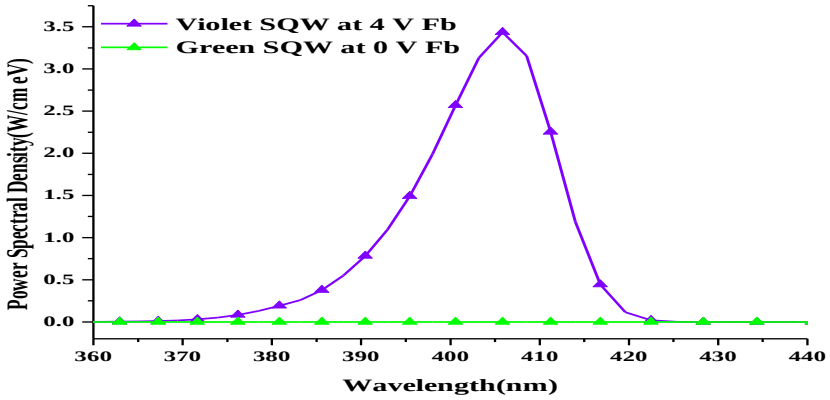

(a)

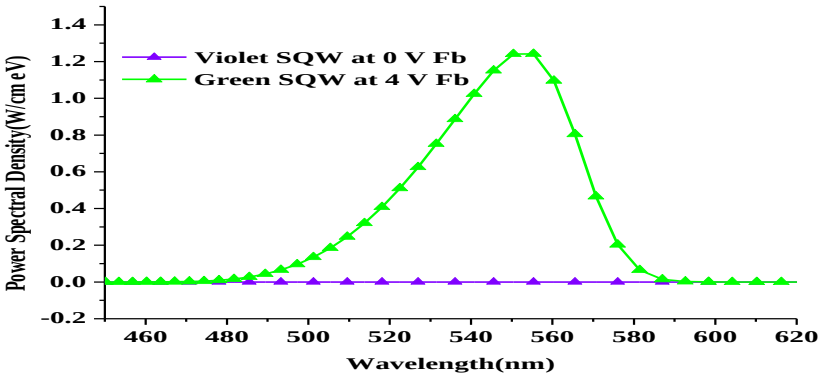

(b)

Figure V.23: Power spectrum obtained by biasing one QW (a) the violet QW, (b) the green QW.

Also, the LED device can be independently controlled by powering the two cathode contacts and the common anode with two different voltages. Here, a broad of EL spectra will be emitted, which are a mixture of violet (410nm) and green (561nm), where the white light can be generated as illustrated Figure V.24.

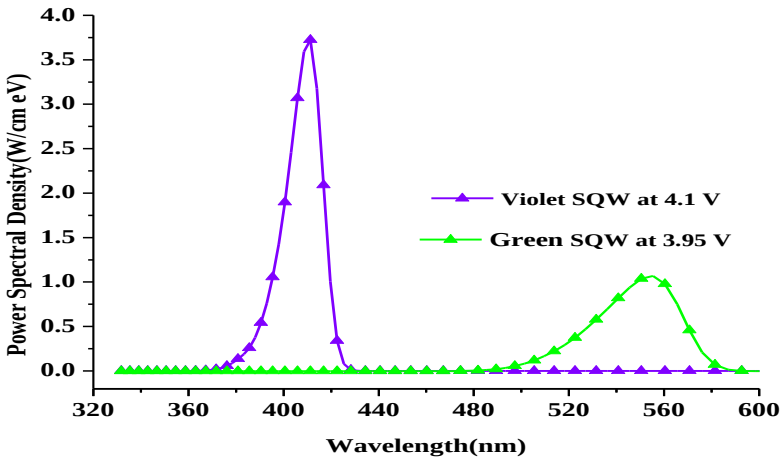

Figure V.24: Violet and green PSD of the two stacked quantum wells with specified FB.

The optical power (P) is calculated by the integration of the area under the power spectral density curve. The TONYPLOT graphics program of SILVACO simulator is used for this purpose as shown in Figure 25. The optical power of the green SQW is 0.191W/cm, and that of the violet SQW is 0.53 W/cm. The power ratio $\frac{P_2}{P_1} \approx 0.356$ is obtained, the result are satisfying the listed values of Table V.3. After the calculation the chromaticity coordinates, $x = 0.317$ and $y = 0.43$ are obtained, the results are in the region of white light as illustrated in the CIE 1931 xy chromaticity diagram of Figure II.1, close to the Illuminant C (x =0.310, y = 0.460).

The complementary wavelengths		The power ratio
λ_1 [nm]	λ_2 [nm]	P_2/P_1
410	561.3	0.356

Table V.3: The complementary wavelengths λ_1 & λ_2, and the power ratio to obtain white light.

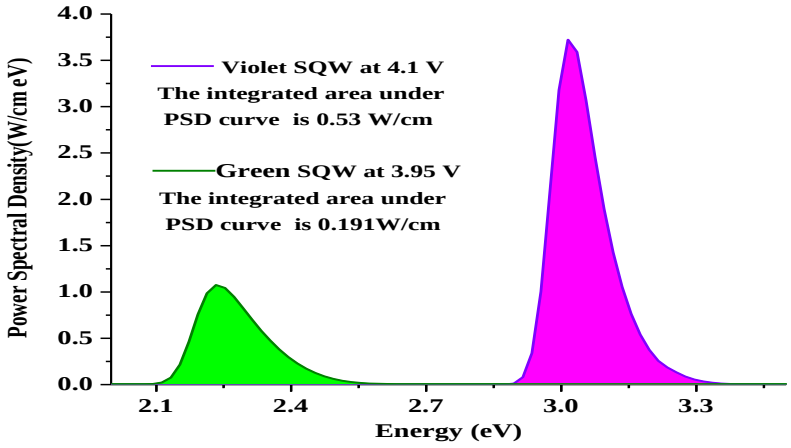

Figure V.25: The optical power calculation by the area integration under the PSD curve.

The current-density versus bias voltage (J-V) is shown in Figure V.26. A threshold voltage of the structure near 3V is observed, which is in a good agreement with previous experimental works [68, 71]. Since all the studied structures are InGaN based, where the threshold voltage can be expressed as function of the band gap energy of these used materials see the equation (V.1).

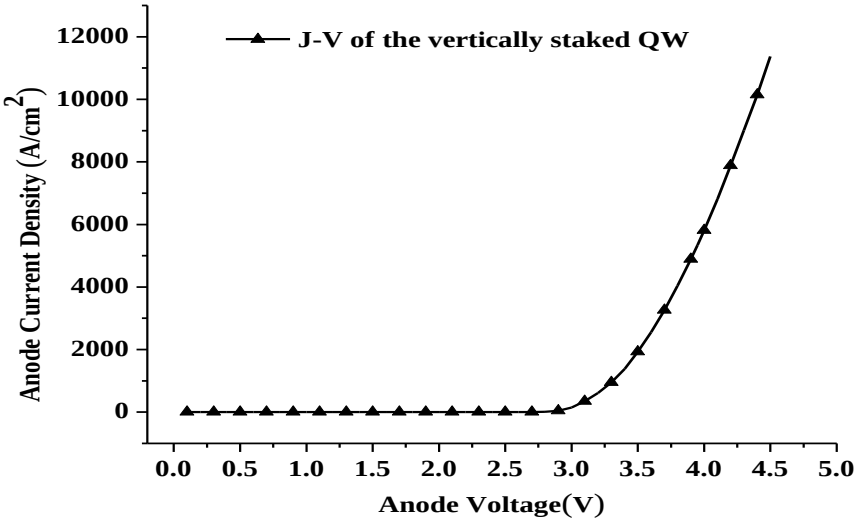

Figure V.26: The current-density versus anode voltage characteristics.

The blue active layer shows better radiative rate as compared to the radiative rate of the green active layer, due to the decrease in the material quality and the increase of the quantum confined Stark effect (QCSE) [65,66,67], as presented in Figure V.27.

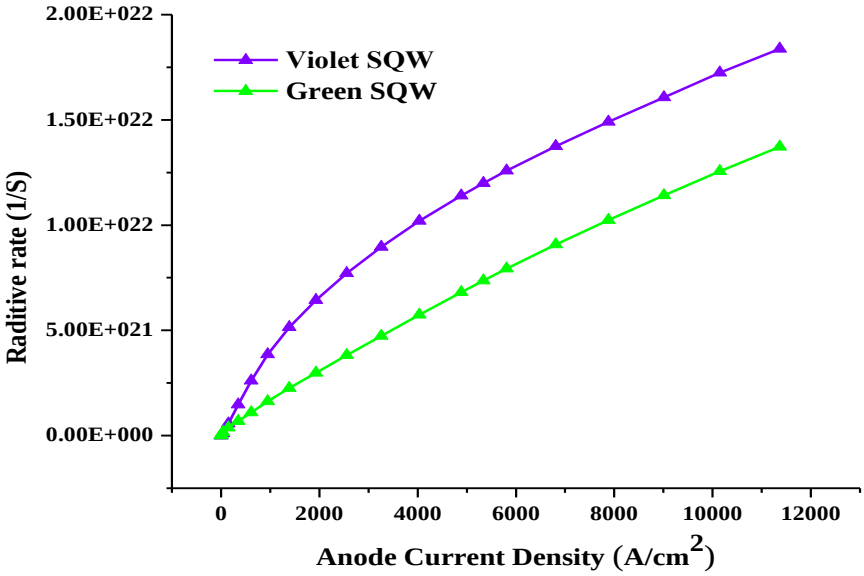

Figure V.27: The radiative rate versus anode current-density.

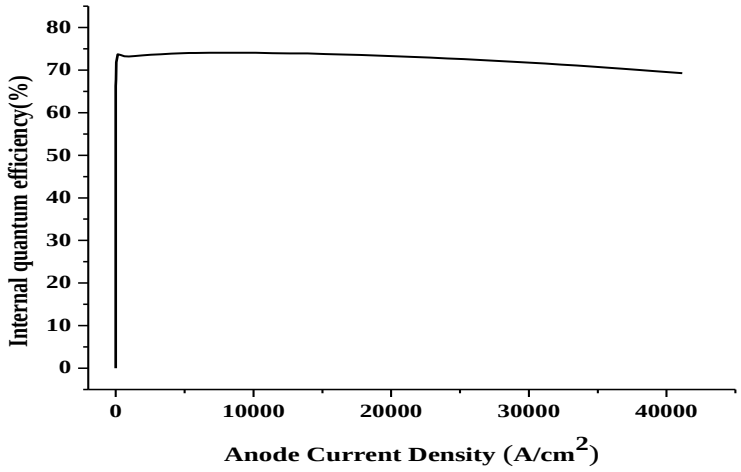

Figure V.28: The IQE of the LED structure.

Figure V.28 shows the obtained internal quantum efficiency (IQE) versus anode's current density.

The lattice mismatch between the QWs and the GaN barriers structure produces a quantum confined Stark Effect (QCSE) in the conduction and the valance band as shown in Figure 28. The change in conduction and valance band profile, reduces the overlap between electron and hole wave functions [65,66,67]. This will cause an additional internal quantum efficiency drop. The quantum confined Stark Effect (QCSE) becomes more significant for the green active layer as compared to that of the violet one, due to the increased of the lattice mismatch between the green active layer and the barrier as seen in Figure V.29.

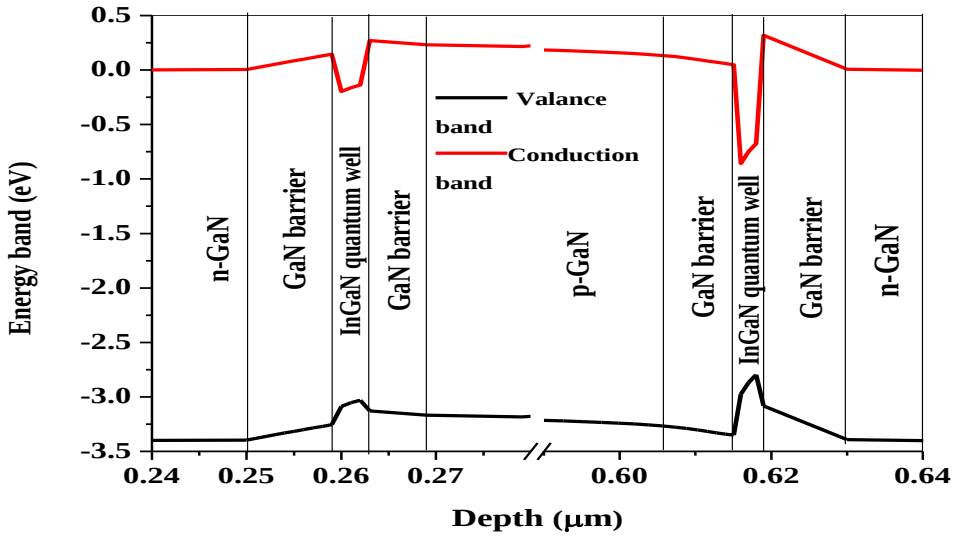

Figure V.29: The conduction and valance band of the green & the violet QW at 3.5V.

Generally, the closest QW to the p-type region mostly contributes to the radiative recombination in the InGaN MQW LEDs [73], because the holes have a high effective mass and very low mobility. which results in non-uniform distribution of holes in the MQW region. One approach is to put the p-type region in the middle between the two QW active regions to improve carrier spreading and ensuring uniform carrier distribution across the active regions, Figure V.30 shows the concentration of the carriers in the two active regions, which is $5 \times 10^{19} cm^{-3}$ in the green QW and $4 \times 10^{19} cm^{-3}$ in the violet QW, it is clear that this structure dos not suffer from inhomogeneous carriers distribution.

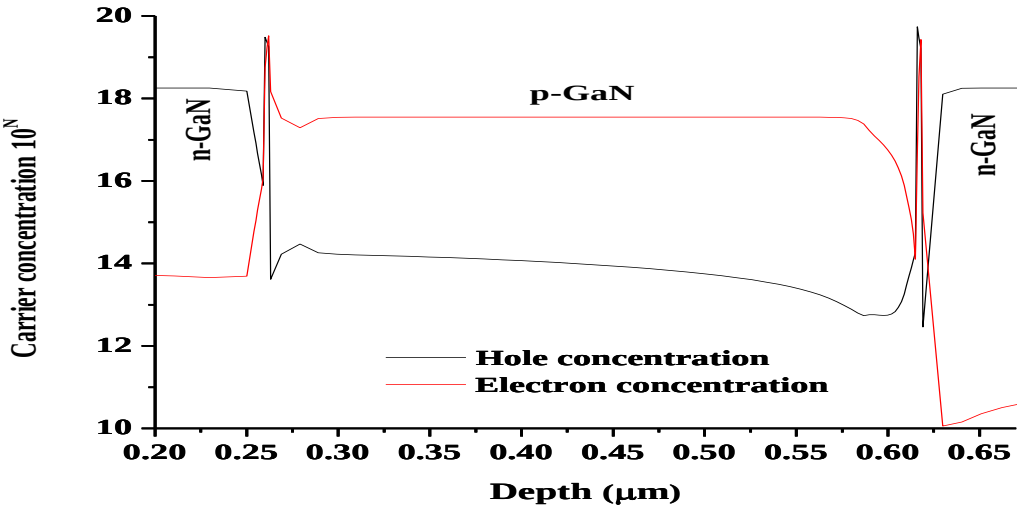

Figure V.30: The carrier concentration in the LED structure.

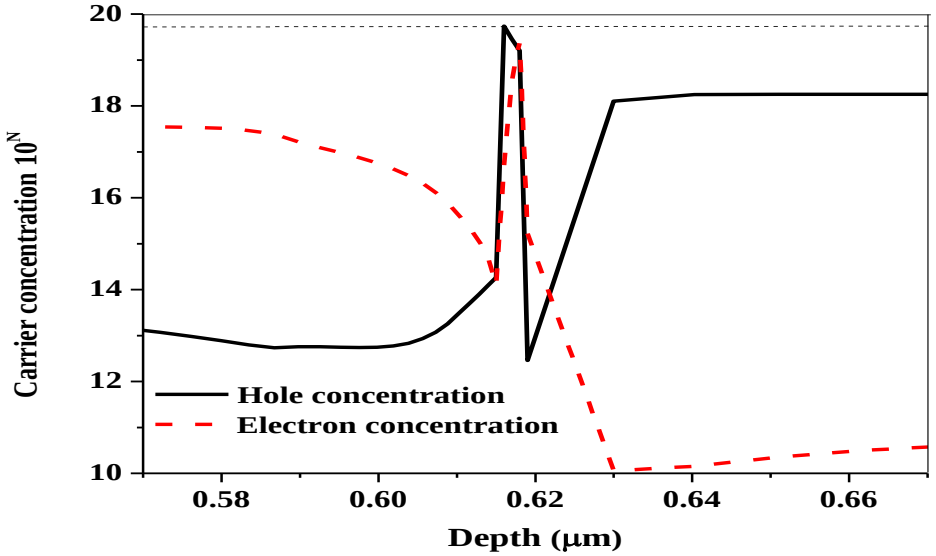

(a)

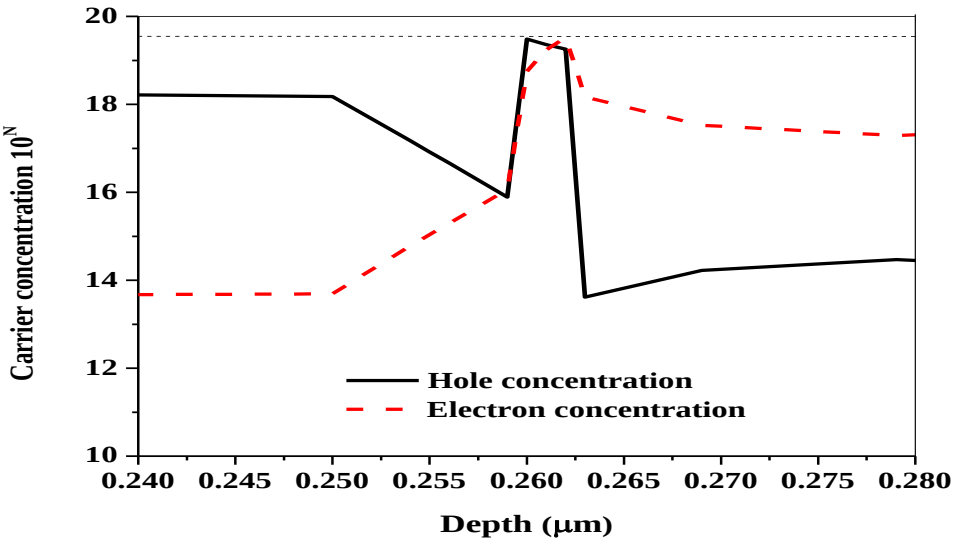

(b)

Figure V.31: The carrier concentration in (a) the green QW and (b) the violet.

V.4.4. Recapitulation

In this study, we demonstrate LED structure with multi-junction. The device is controllable with various biasing voltages to result in an independently adjustable violet and green emissions. The device can generate single emissions of violet (410nm) and green (561nm), or a violet-green mix emissions depending on the injected current and at certain mixture ratio the white light is obtained. The device structure is capable of realizing a high performance display device since it insure uniform carrier spreading across the active regions, in addition it is phosphor free, hence the structure is promising for many future solid stat lighting applications.

V.5. Design and numerical simulation of color tunable laterally arranged quantum well light emitting diode with double anode single cathode

The proposed work is a simulation and design of violet-green color tunable monolithic LED, we will perform a deep discussion about the obtained Results such as the power spectrum, The optical power calculation, CIE 1931 xy chromaticity diagram, the current-density versus anode voltage characteristics, the output light power versus the anode current, the IQE of the LED structure, the conduction and the valance band, the Blue shift in the Power spectrum.

The structure has three electrodes, this will give the opportunity of varying the color, which is a mixture of violet and green spectra. and at certain mixture ratio the white light is obtained with chromaticity coordinate (x=0.3113, y=0.3973). The lateral arrangement of the two (SQW) reduces the negative effect of photon absorption, and overcomes the non-uniform distribution of holes in the MQW region, which will give good external quantum efficiency (EQE).

The LED structure has been numerically investigated using ATLAS simulator, which is powerful tool for understanding, and designing electronic devices. It predicts many physical properties in different operating conditions without actual fabrication. This makes the optimization easier. Hence, saving time, money and energy [18].

V.5.1. Parameters and Simulation Models

All the used models in the previous simulation works are involved. In this simulation, GaN substrate has been used to avoid large number of disadvantages that are caused by highly lattice-mismatched sapphire substrate, especially when designing green LEDs. The acceptor activation energy of Mg doped is considered as 200 meV, and the donor activation energy of Si doped is 20 meV. Shockley-Read-Hall (SRH), radiative and Auger recombination coefficients are kept constant at $1.0 \times 10^{7} s^{-1}$, $1.0 \times 10^{-11} cm^{3}$ and $1.0 \times 10^{-31} cm^{6} s^{-1}$, respectively, which are in the accepted value ranges [59-62]. The polarization charge is assumed to be 40% of the theoretical value [18]. For simplicity, the anode and the cathode contacts are supposed to be ideal Ohmic, and the operating temperature is 300K.

V.5.2. Device Structure

The proposed device has a left side SQW, and a right side SQW with two anodes and one common cathode. The structure consist of GaN substrate, followed by 2 µm thick n-GaN layer (n doping = 1×10^{19}), and 6 nm thick GaN barrier. The left side active region is 3 nm thick $In_{0.15}Ga_{0.85}N$ single quantum well (SQW) followed by 6 nm thick GaN quantum barrier, followed by 0.02 µm thick p-AlGaN electron blocking layer (p doping=1×10^{18}), followed by 0.28µm thick p-GaN layer (p doping = 1×10^{19}). The right side active region has the same layers structure except that the indium content in the SQW is 46%. Figure .V. 32 illustrates the structure of the proposed device.

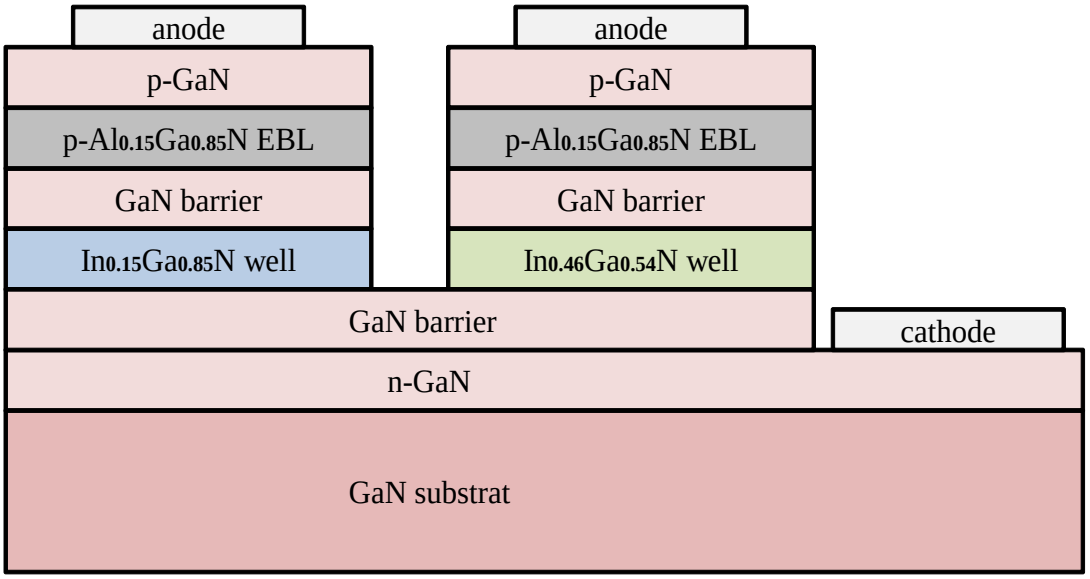

Figure V.32: Two laterally arranged SQWs LED proposed structure.

V.5.3. Results and Discussion

The proposed LED device can operate in three modes:

In the first mode, the two SQWs are forward biased with the same voltage, both violet and green spectra are generated, with Photoluminescence (PL) peaks centered near 420 and 561 nm, respectively. The obtained mixed color is shown in Figure. V. 33.

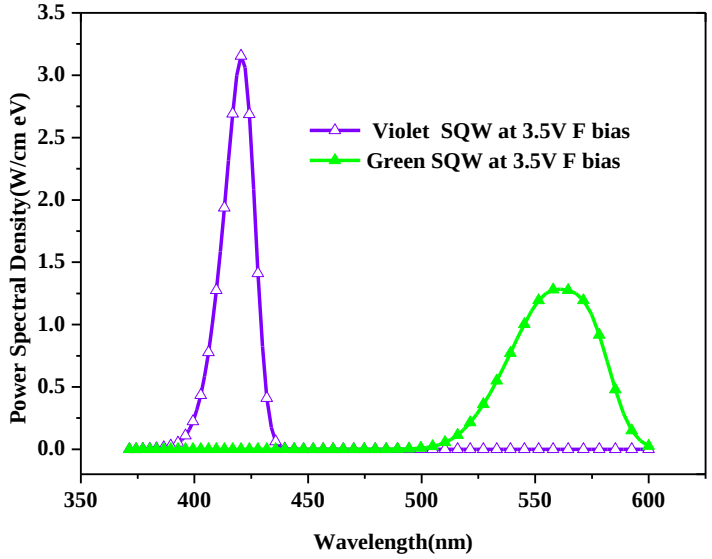

Figure V.33: Violet and green Power spectrum of the two single quantum wells.

In the second mode, the LED device will operate by forward biasing only one anode contact of the LED device, and the other anode is grounded with the common cathode. This will generate just violet or green spectrum as seen in Figure V.34 .

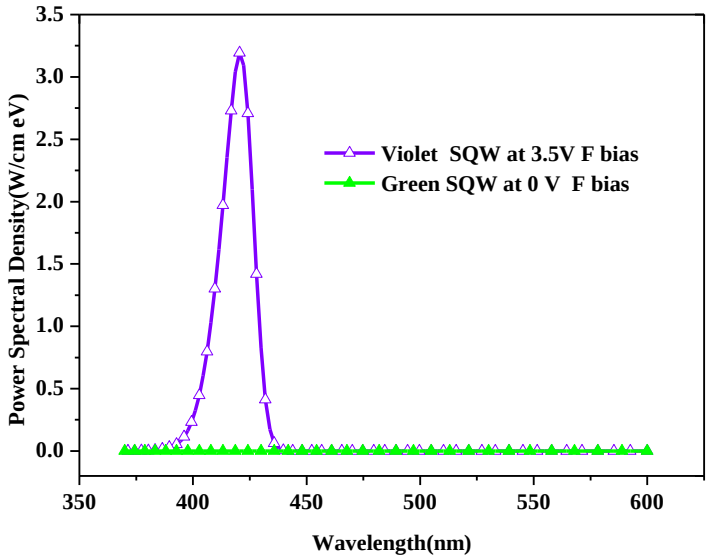

(a)

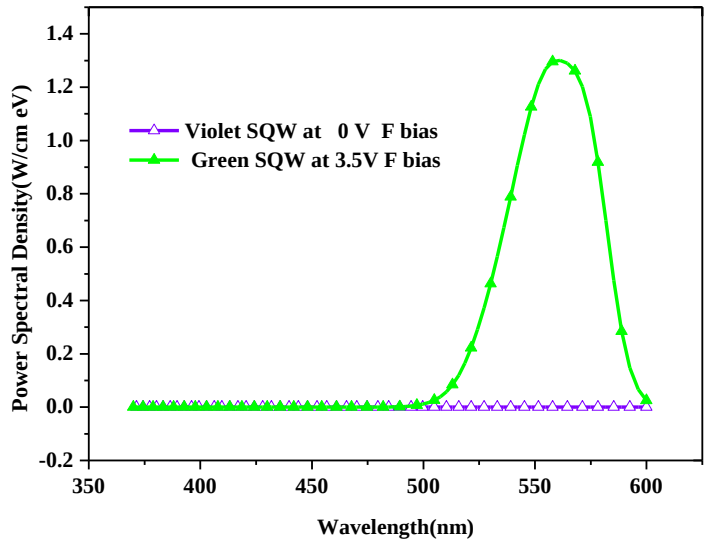

(b)

Figure V.34: Power spectrum obtained by biasing only one QW (a) the violet QW, (b) the green QW.

In the third mode, the LED device can be independently controlled by powering the two anode contacts with two different voltages. Here, a broad of EL spectra will be emitted, which are a mixture of violet and green, where the white light can be generated.

This involves the CIE193 (Commission International de l'Eclairage) system [53, 54,55]. It is used to describe the composition of any color in terms of primaries colors, where X, Y and Z are the tristimulus values, and can be added to produce real spectral colors. Here, the color is represented by the three chromaticity coordinates quantities (x, y and z) given by the Table II.3.

In the case of two colors mixing. The chromaticity coordinates x and y of the new generated color are computed using the two equation (II.14) and (II.15) we obtain :

Where $\bar{x}(\lambda)$, $\bar{y}(\lambda)$ and $\bar{z}(\lambda)$ are the CIE color matching functions given by the Table II.3.

P_1 and P_2 are the optical power of two colors having wavelengths λ_1 and λ_2, respectively.

Where $P(\lambda)$ is the power spectral density given by equation (II.10).

The power ratio is defined as $\frac{P_2}{P_1}$.

Table V.4 gives the needed complementary wavelengths λ_1 and λ_2, and the required power ratio to generate the white color with respect to CIE Illuminant D65 [3], where P_1 and P_2 are the optical powers of the two emitted wavelengths.

The complementary wavelengths		The power ratio
λ_1 [nm]	λ_2 [nm]	P_2/P_1
420	561.7	0.891

Table V.4: The complementary wavelengths λ1 and λ2, and the required power ratio to obtain white light.

Figure.V.35 shows violet and green power spectral density of the two SQWs independently biased with two different voltages. Here, two spectra having peak wavelength at 420 nm and 562 nm are obtained.

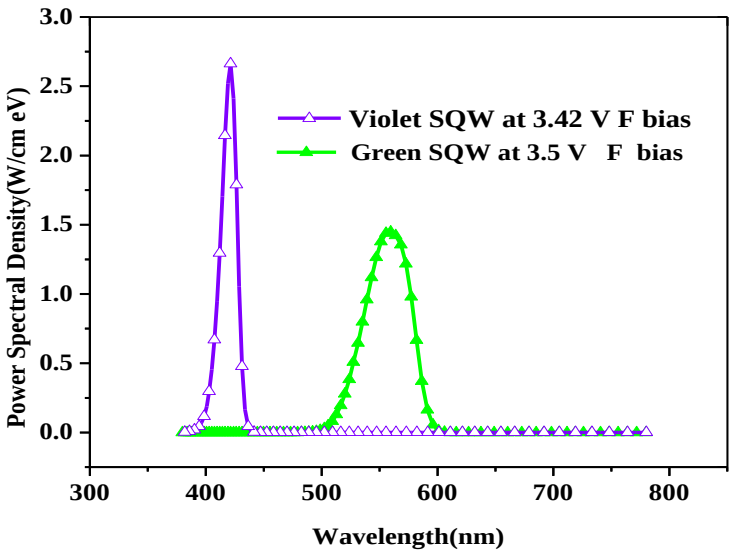

Figure V.35: Violet and green Power spectrum of the two SQWs with different Fvb.

The optical power P is calculated by the integration of the area under the power spectral density curve. The TONYPLOT graphics program of SILVACO simulator is used for this purpose as shown in Figure. V.36. The optical power of the green SQW is 0.3562 W/cm, and that of the violet SQW is 0.4005 W/cm. The power ratio $\frac{P_2}{P_1} \approx 0.89$ is obtained. After the calculation the chromaticity coordinates $x = 0.3113$ and $y = 0.3973$ are obtained. Thus results are near the values

xD65 = 0.3138 and yD65 = 0.3310 as presented in CIE 1931 xy chromaticity diagram of Figure V.37.

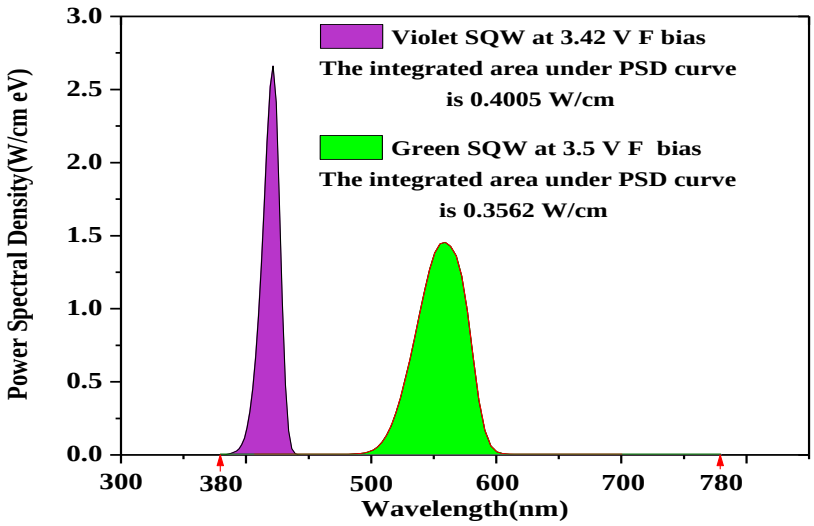

Figure V.36: The optical power calculation by the area integration under the PSD curve.

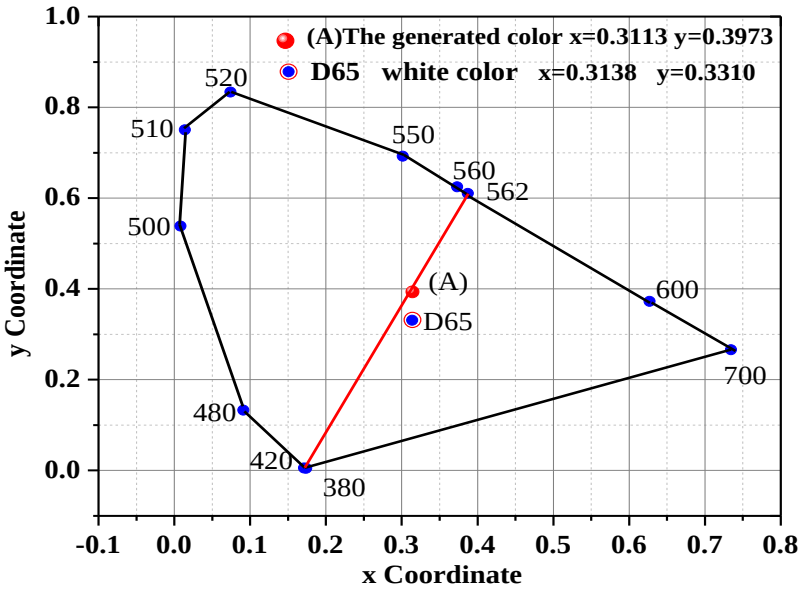

Figure V.37: CIE 1931 xy chromaticity diagram.

The current-density versus bias voltage (J-V) is shown in Figure. V.38. A threshold voltage of the structure is near 3V is observed, which is in a good agreement with previous experimental works [68, 71]. Since all the studied structures are InGaN based, where the threshold voltage can be expressed as function of the band gap energy of these used materials, by the approximated equation (V.1).

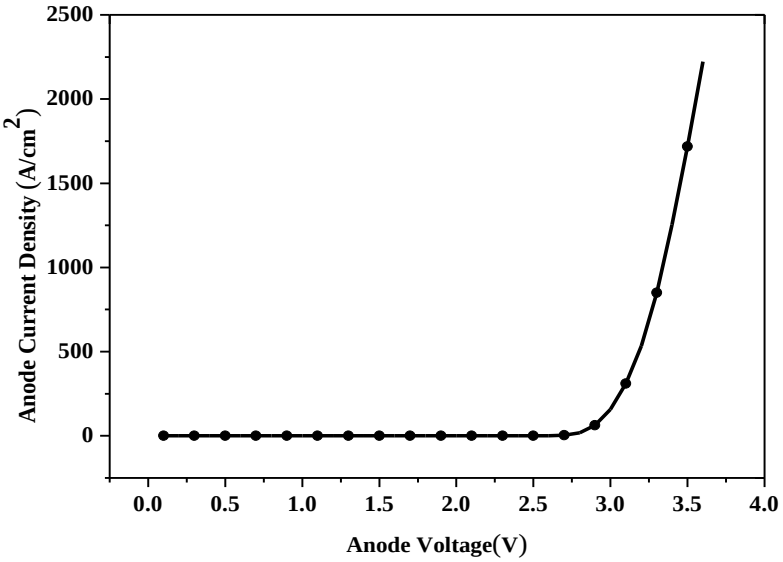

Figure V.38: The current-density versus anode voltage characteristics.

In ATLAS simulator the optical power is calculated by integrating the luminous spectrum, where the SPONTANEOUS parameter is used in the MODELS statement [27]. The optical power versus anode voltage is shown in Figure V.39.

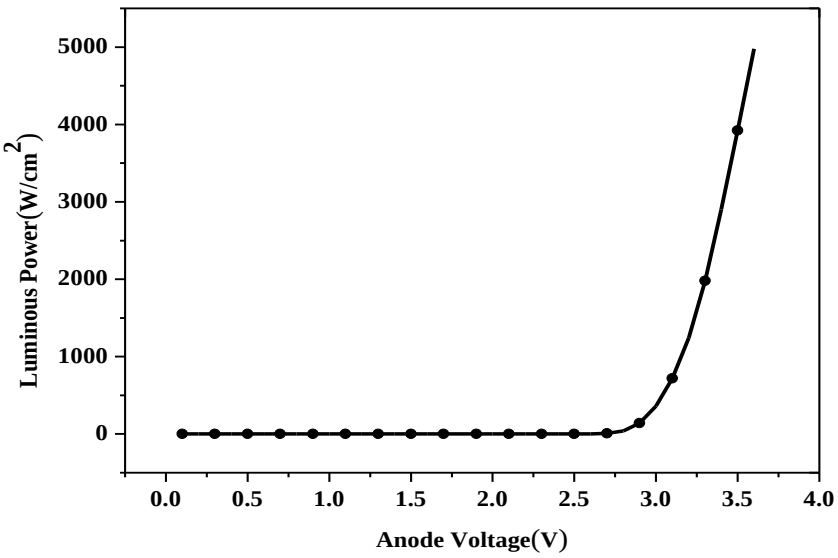

Figure V.39 The output light power versus anode voltage.

When the anode voltage reaches the threshold voltage, the current and the luminous power strongly increases as seen in Figure V.38 and Figure V.39, they show the same behavior due to the relation between them given by [55]:

$$P_{int}/h.\nu = \eta_{int}.I/e. \qquad \text{V.2}$$

Where P_{int} is the optical power emitted from the active region, η_{int} is the internal quantum efficiency, I is the injection anode current, and v is the frequency of optical radiation. Figure V. 40 shows luminous power versus anode current of the LED structure.

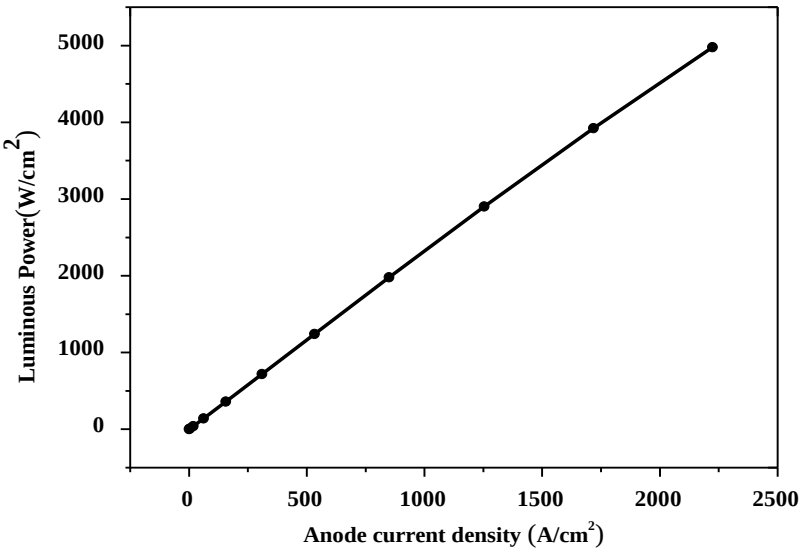

Figure V.40: The output light power versus the anode current.

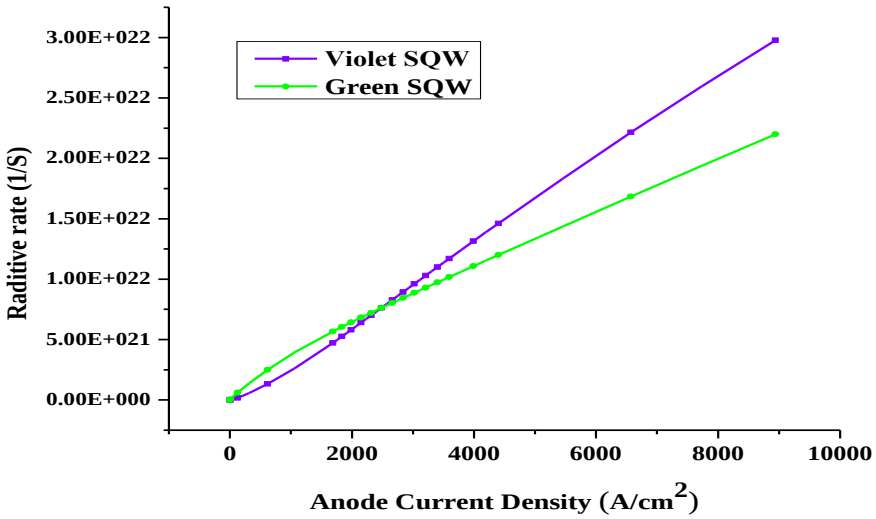

Figure V.41: The radiative rate versus anode current-density.

Since the turn-on voltage of the green SQW is smaller as compared to that of the violet SQW, his radiative rate is the highest until the violet SQW reaches his turn-on voltage, then the violet active layer shows better radiative rate, due to the decrease in the material quality and the increase of the quantum confined Stark effect (QCSE) of the green SQW as compared to that of the violet SQW [65,66,67], as presented in Figure V.41.

If we compare between the current-density versus anode voltage (J-V curves) characteristics of the violet and the green SQW, we see that the increase of indium element content in the SQW decreases LED turn-on voltage. As illustrated in Figure V.42. That is in a good agreement with other research works [16, 64,75,76].

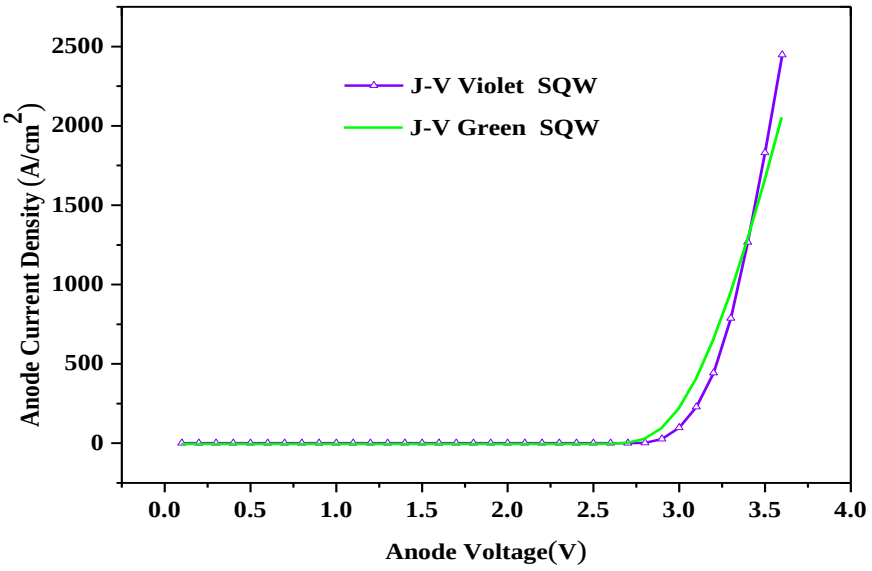

Figure V.42 : The current-density versus anode voltage of the violet and green SQWs.

The internal quantum efficiency (IQE) is obtained by the equation (IV.19).

Figure V.43 shows the obtained internal quantum efficiency (IQE) versus anode's current density. It is clear that there is a reduction in the (IQE) at high current density, where the Auger recombination is one of the major causes of the efficiency droop [62,66,67]. In addition the quantum confined Stark effect (QCSE) will also lower the IQE, because it has a negative impact on the wave function overlap [55,65,67,77].

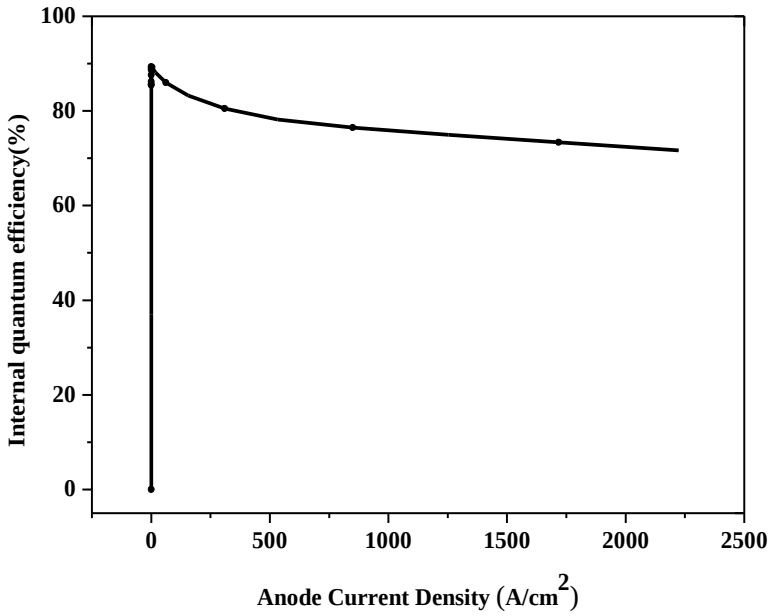

Figure V.43: The IQE of the LED structure.

The external quantum efficiency (EQE) $\eta_{external}$ of the LED is calculated as follows [22]:

$$\eta_{external} = \eta_{int} \times \eta_{extraction}. \quad \text{V.3}$$

Where $\eta_{extraction}$ is the extraction efficiency.

Increasing the extraction efficiency is very important for the LEDs' characteristics. In the case of the vertically stacked dual-wave length MQW structure, which has two or more active layers with a different band gaps, a part of the photons generated by the higher band gap active layer will be absorbed by the lower band gap active layer. This will decrease the EQE, knowing that the absorption coefficient is given by the equation (III.35).

However, in the case of laterally arranged SQW, the absorption effect will be limited, since the generated photons do not make multiple passes through the active layers with lower band gap energy. This will increase the extraction efficiency $\eta_{extraction}$. Moreover, reflectors can be used to redirect additional parts of generated photons upward. Hence, more light will be extracted [65].

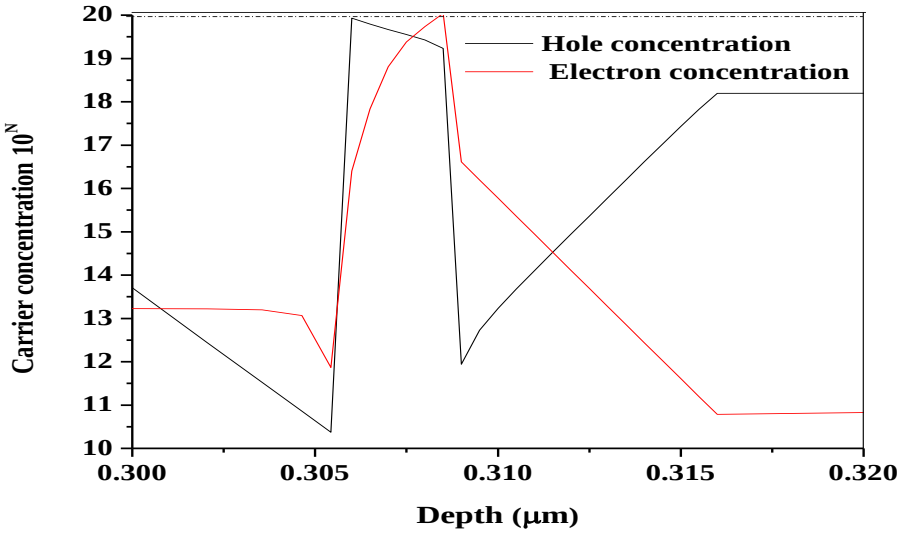

(a)

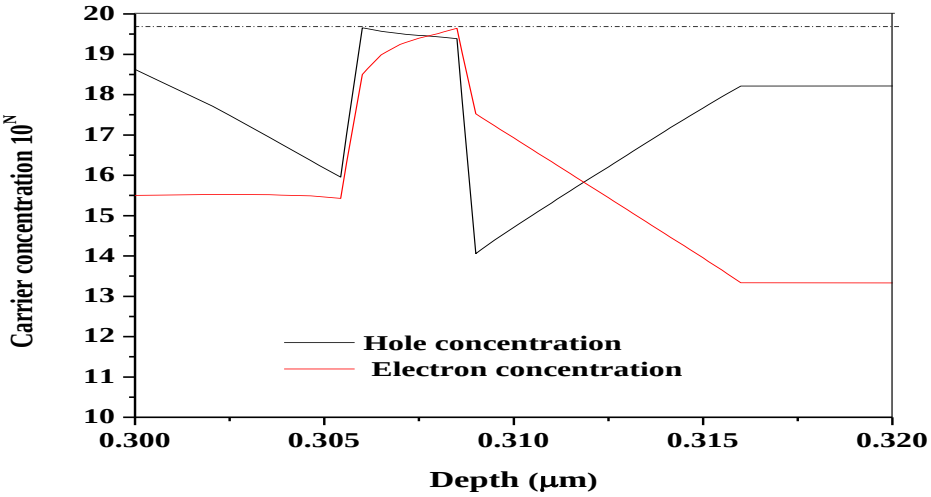

(b)

Figure V.44: The carrier concentration in (a) the green SQW and (b) the violet SQW.

Figure V.44 shows the concentration of the carriers in the two active regions, which is $8 \times 10^{19} cm^{-3}$ in the green QW and $6 \times 10^{19} cm^{-3}$ in the violet QW, it is clear that the inhomogeneous carriers distribution is reduced, because the charge carriers are injected in parallel and simultaneously, into both SQWs.

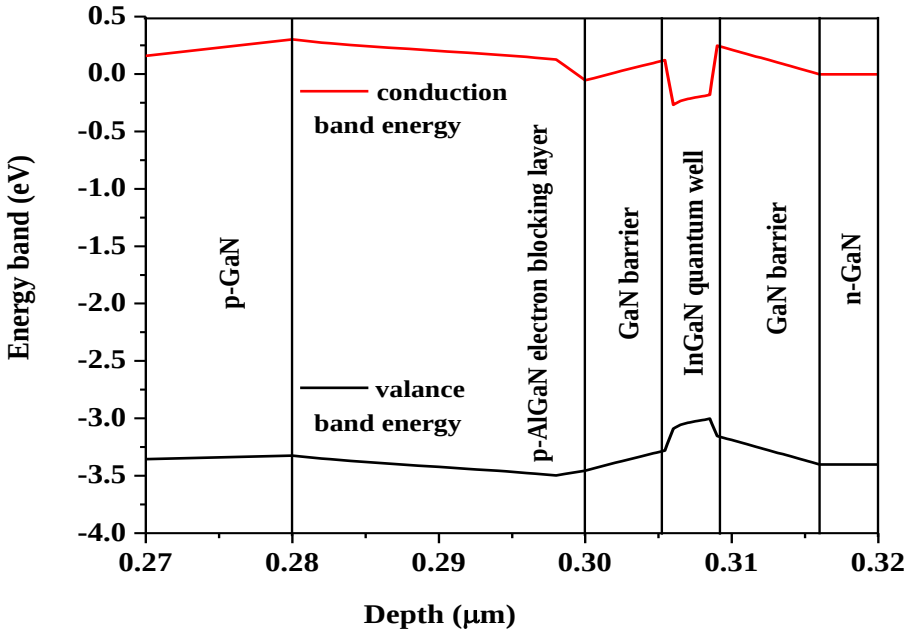

(a)

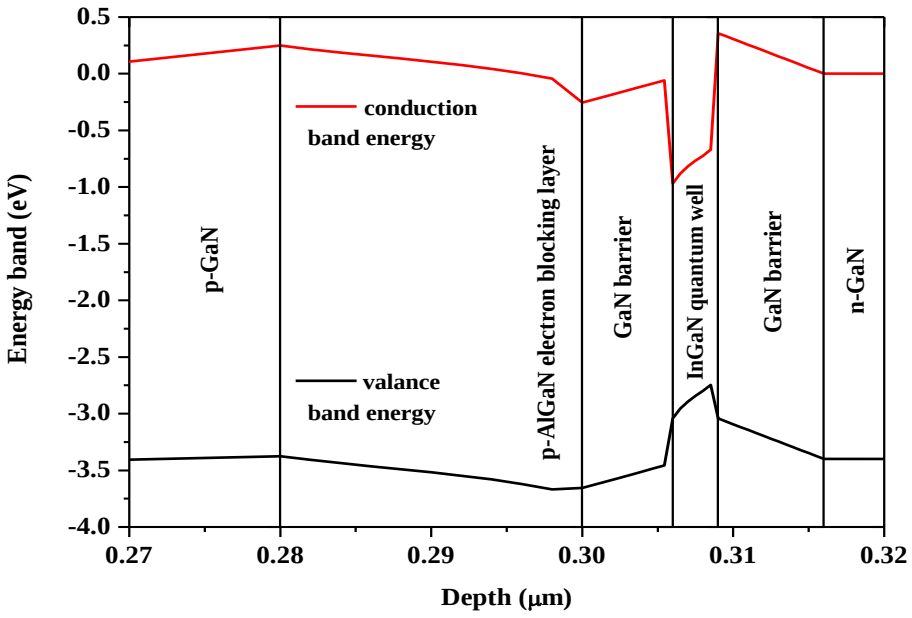

(b)

Figure V.45: The conduction and the valance band of (a) the violet SQW, and (b) the green SQW at 3.5 V F bias.

The valence and conduction band profiles are strongly influenced by the quantum confined Stark Effect (QCSE). We can see in both Figure. V.45 that the QCSE effect becomes more significant for the green SQW as compared to that of the violet one. This is due to the higher lattice mismatch between the green SQW and the GaN barrier. Moreover as the current increases, there is a reduction of the QCSE. Hence, a blue shift of the peak wavelength will happen.

Figure.V.46 shows that for the violet SQW the peak wavelengths are 422.3 nm and 420.4 nm at currents density of 1.266 KA/cm^2 and 2.449 KA/cm^2, respectively.

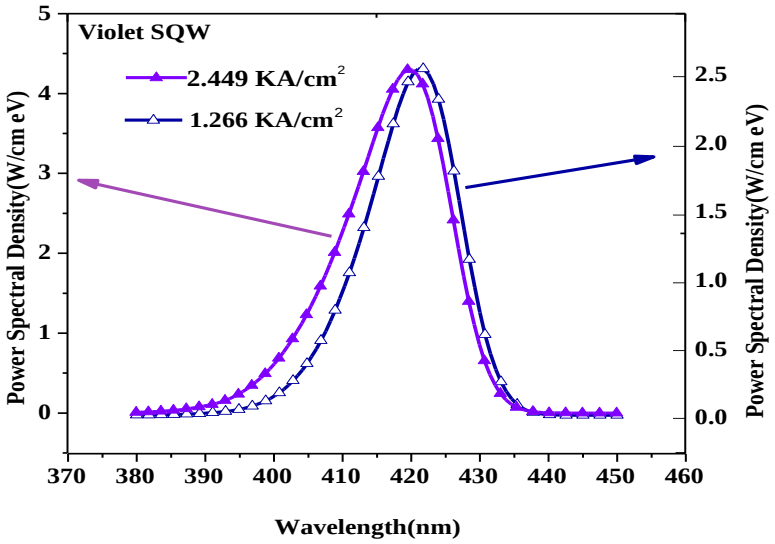

Figure V.46: Blue shift in the Power spectrum of the violet SQW as a function of the injection current density.

Figure.V.47 shows that for the green SQW the peak wavelengths are 588 nm and 564 nm at currents of 1.286 KA/cm^2 and 2.059 KA/cm^2, respectively.

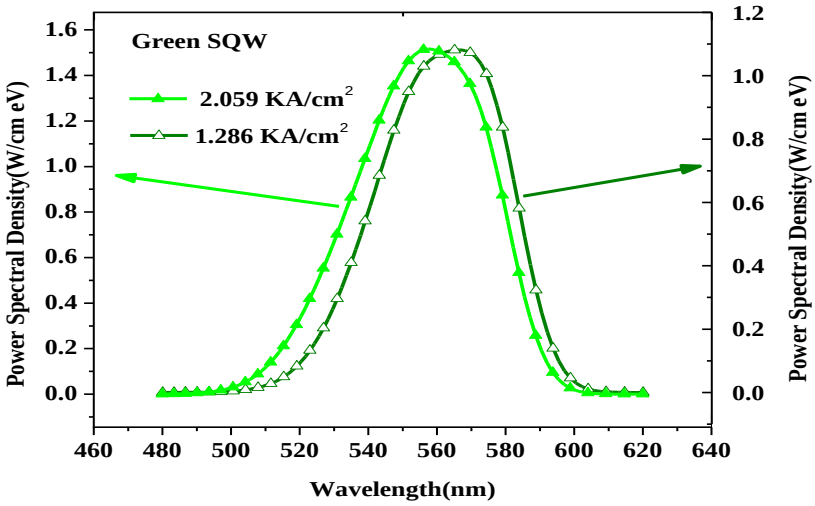

Figure V.47: Blue shift in the Power spectrum of the green SQW as a function of the injection current density.

The blue shift of the green SQW (24 nm) is bigger than of the violet SQW (2.1 nm) as seen in Figures V.46 and V.47. In fact, many published experimental works showed that there is a dependence of the peak electroluminescence (EL) emission wavelength on the drive current. This leads to blue shift, and that as the In content is high, the blue shift will be high [69-72, 74,77]. This

problem has to be taken into consideration to obtain the needed color rendering when designing white light LEDs.

V.5.4. Recapitulation

In summary, multi-junction color-tunable LED is designed and simulated. The device can emit violet or green light individually. Also, it can emit simultaneously mixture of both colors, and at certain mixture ratio, the white light is obtained. The simulated structure does not suffer from inhomogeneous carriers' distribution since the two SQW are laterally arranged. Moreover, the generated photons do not make multiple passes through the active layers with lower band gap energy, therefore, the absorption of photons will be limited, this will give good external quantum efficiency (EQE), a summarized comparison is illustrated in Table V.5.

The structures	Inhomogeneous carriers distribution		Absorption effect	Color tunable	Circuit complexity
Dual wavelength LED with two QWs	**High**		**Not reduced**	**Non controllable**	**Simple**
	Green SQW	**Violet SQW**			
	$5.6 \times 10^{19} cm^{-3}$	$1 \times 10^{19} cm^{-3}$			
Vertically stacked QW LED 1anode 2 cathode	**Low**		**Not reduced**	**Controllable**	**Complex**
	Green SQW	**Violet SQW**			
	$5 \times 10^{19} cm^{-3}$	$4 \times 10^{19} cm^{-3}$			
Laterally arranged QW LED 2anode 1 cathode	**Low**		**Reduced**	**Controllable**	**Complex**
	Green SQW	**Violet SQW**			
	$8 \times 10^{19} cm^{-3}$	$6 \times 10^{19} cm^{-3}$			

Table V.5: Summarized comparison between the designed structures.

V.6. Conclusion

All the designed structures are phosphor free but suffer from a blue shift that will affect the color rendering, in addition the first designed device shows higher inhomogeneous carriers distribution in the two active layers. Moreover the absorption effect is inevitable, in both the first and the second designed devices. The third designed structure does not suffer neither from the absorption effect nor from the inhomogeneous carriers distribution, the two last structures are color tunable.

General Conclusion

General conclusion

The main achieved works of this thesis was the design and simulation of many structures, they are studied to obtain optimal solutions for multi color and white light generation. Where the highest luminous efficiency can be obtained using the dichromatic approach, that can be achieved using a green and violet active layers. The investigations have been started by the design of two structures, they are green and violet SQW LEDs, hence, we conclude that for white light generation among many complementary Wavelengths, the two optimal choices that can be used are $\lambda_1 = 410\text{nm}$ and $\lambda_2 = 561.3\text{nm}$ with power ratio $P(\lambda_2)/P(\lambda_1) = 0.356$, or $\lambda_1 = 420\text{nm}$ and $\lambda_2 = 561.7\text{nm}$ with power ratio $P(\lambda_2)/P(\lambda_1) = 0.891$.

In the second step, a dual color LEDs with two staked QWs using conventional structure has been designed and simulated, unfortunately, the structure suffer from inhomogeneous hole distribution, and photon absorption, this will affect the performance of the device.

Next, two vertically arranged SQW LED with 1 anode, 2 cathode , the device can generate violet-green mix emissions and at certain mixture ratio the white light is obtained, the structure does not suffer from inhomogeneous hole distribution, but the photon absorption effect is inevitable.

Finally two laterally arranged SQWs LED, which can emit simultaneously mixture of both colors, and at certain mixture ratio, the white light is obtained. The structure does not suffer from inhomogeneous carriers' distribution, moreover, the photon absorption effect is limited.

The GaN substrate has been used in all structures, this has limited the drawbacks caused by the others substrates, such as the thermal expansion coefficient and lattice mismatch.

In addition because the structures are tunable, this allows to cover many color regions in the chromaticity diagram, moreover the structures are phosphor free, where many draw backs such as high correlated color temperature (CCT), low color rendering index (CRI), and slow frequency response limitation, are reduced.

In addition the low performance because of inhomogeneous carriers distribution is minimized in both last structures.

Moreover, in the last design, the generated photons do not make multiple passes through the active layers with lower band gap energy, therefore, the absorption of photons will be limited. This will give good external quantum efficiency (EQE).

Outlook:

As future work we propose to:

Design a devices using the same previous structures, but replacing the GaN by InGaN material, in the barriers and the substrate, in such away to obtain better IQE.

Design devices using the same previous structures, but replacing the SQWs by MQWs, which is better choice for high power LEDs.

Design a devices using the same structures and adding a third color active layer, by exploiting the wide energy band gap range of the III-Nitride, that can give an output between the deep ultraviolet and the infrared, meaning that it can cover all the visible color regions in the chromaticity diagram.

Design devices using the same structures but changing the used materials such as ZnO and inorganic semiconductor to obtain more choices.

References

References

[1] J. Singh . Electronic and optoelectronic properties of semiconductor structures. Cambridge University Press, 2007.

[2] Neamen, Donald A. Semiconductor physics and devices: basic principles. McGraw-hill, 2003.

[3] Pierret, Robert F., and Gerold W. Neudeck. Advanced semiconductor fundamentals. Vol. 6. Reading, MA: Addison-Wesley, 1987.

[4] Li, Sheng S. Semiconductor physical electronics. Springer Science & Business Media, 2012.

[5] Poelman, Dirk. "Fundamentals of solid state engineering, M. Razeghi." PHYSICALIA MAGAZINE 29.2: 32-33. (2007).

[6] G.F. Neumark, Igor L. Kuskovsky, and Hongxing Jiang, eds. Wide bandgap light emitting materials and devices. John Wiley & Sons, (2007).

[7] D. Skatrud, and W. K. Paul W. K. High Brightness Light Emitting Diodes. Semiconductors and Semimetals, Volume 48. Elsevier Science & Technology, (1997).

[8] E. F. Schubert. Light-Emitting Diodes. 2nd ed. New York: Cambridge University Press, (2006).

[9] S. Nakamura, S. P. DenBaars *et al.* Current status of GaN-based nonpolar/semipolar/polar blue and white LEDs, In : *Conference Poster*, (2007).

[10] S. Nakamura, M. Seno, & T. Mukai. P-GaN/N-InGaN/N-GaN double-heterostructure blue-light-emitting diodes. Jpn. J. Appl. Phys.Vol. 32, no.1A, p.L8, (1993).

[11] M. Yamada, Y. Narukawa and T. Mukai. Phosphor Free High-Luminous-Efficiency White Light-Emitting Diodes Composed of InGaN Multi-Quantum Well. Jpn. J. Appl. Phys. Vol. 41 ,pp. 246– 248 , (2002).

[12] N. Poyiatzis, M. Athanasiou, J. Bai, Y. Gong, & T. Wang. Monolithically integrated white light LEDs on (11–22) semi-polar GaN templates. Scientific reports, vol. 9, no 1, p. 1-7, (2019).

[13] Y. Li, L. Chang, H. Chen, et al. Phosphor-free InGaN white light emitting diodes using flip-chip technology. Materials, *10*(4), 432, (2017).

[14] H. Li, P. Li, H. Zhang, *et al.* Electrically driven, polarized, phosphor-free white semipolar (20-21) InGaN light-emitting diodes grown on semipolar bulk GaN substrate.*Optics express*, vol. 28, no 9, p. 13569-13575, (2020).

[15] Y. Lee, P. Lin, T. Lu, H. Kuo and S. Wang. Dichromatic InGaN-based white light emitting diodes by using laser lift-off and wafer-bonding schemes. Applied Physics Letters, vol. 90, no. 16, p. 161115, (2007).

[16] Z. Liu, et al. "Status and prospects for phosphor-based white LED packaging." *Frontiers of Optoelectronics in China* 2.2 (2009): 119-140.

[17] G. F. Yang, et al. "InGaN/GaN multiple quantum wells on selectively grown GaN microfacets and the applications for phosphor-free white light-emitting diodes." *Reviews in Physics* 1 (2016): 101-119.

[18] J. Chang, Y. Kuo and M. Tsai. Correlation of barrier material and quantum-well number for InGaN/(In)GaN blue light-emitting diodes, physica status solidi (a). 208 (3) 729-734. (2011).

[19] C. Kolper, M. Sabathil, M. Mandl, M. Strassburg and B. Witzigmann. All-InGaN Phosphorless White Light Emitting Diodes: An Efficiency Estimation, Journal of Lightwave Technology. 30 (17) 2853-2862. (2012).

[20] S. Singh, N. Rohila, S. Pal and C. Dhanavantri. Optimization towards reduction of efficiency droop in blue GaN/InGaN based light emitting diodes, Optik. 123 (14) 1287-1292. (2012)

[21] D. Kong, C. Kang, J. Lee, J. Kim and D. Lee. Color tunable monolithic InGaN/GaN LED having a multi-junction structure. Optics Express, vol. 24, no. 6, p. A667, (2016).

[22] I. Park, J. Kim, M. Kwon, C. Cho, J. Lim and S. Park. Phosphor-free white light-emitting diode with laterally distributed multiple quantum wells. Applied Physics Letters, vol. 92, no. 9, p. 091110, (2008).

[23] LI, Simon, LI, Suihua. 3D TCAD Simulation for Semiconductor Processes, Devices and Optoelectronics. Springer Science & Business Media, (2011).

[24] Sze, Simon Min. Semiconductor devices: physics and technology. John wiley & sons, 2008

[25] Ma, D., & Chen, Y. Organic Semiconductor Heterojunctions and Its Application in Organic Light-Emitting Diodes (Vol. 250). Berlin: Springer. (2017).

[26] Wang, C., Dong, H., Jiang, L., & Hu, W. Organic semiconductor crystals. Chemical Society Reviews, 47(2), 422-500. (2018).

[27] J. Piprek, Semiconductor Optoelectronic Devices: Introduction to Physics and Simulation. UCSB: Academic Press (2003): 22.

[28] F. Bernardini, V. Fiorentini, and D.Vanderbilt. Spontaneous polarization and piezoelectric constants of III-V nitrides. Phys. Rev. B, vol. 56, pp. R10024–R10027, (1997).

[29] E.F. Schubert, T. Gessmann, et J. K. Kim. Inorganic semiconductors for light-emitting diodes. Organic Light Emitting Devices, p. 1-33, (2006).

[30] Hu, H., Zhou, S., Wan, H., Liu, X., Li, N., & Xu, H. Effect of strain relaxation on performance of InGaN/GaN green LEDs grown on 4-inch sapphire substrate with sputtered AlN nucleation layer. *Scientific reports*, *9*(1), 1-9. (2019).

[31] Ryu, H. Y., Jeon, K. S., Kang, M. G., Yuh, H. K., Choi, Y. H., & Lee, J. S. A comparative study of efficiency droop and internal electric field for InGaN blue lighting-emitting diodes on silicon and sapphire substrates. *Scientific reports*, *7*(1), 1-9. (2017).

[32] Hu, H., Zhou, S., Wan, H., Liu, X., Li, N., & Xu, H. Effect of strain relaxation on performance of InGaN/GaN green LEDs grown on 4-inch sapphire substrate with sputtered AlN nucleation layer. *Scientific reports*, *9*(1), 1-9. (2019).

[33] Manikandan, M., Nirmal, D., Prajoon, P., Dhivyasri, G., & Chandran, V. Luminous power improvement in InGaN V-Shaped Quantum Well LED using CSG on SiC Substrate. In *IOP Conference Series: Materials Science and Engineering* (Vol. 906, No. 1, p. 012011). IOP Publishing. (2020).

[34] Prajoon, P., Menokey, M. A., Pravin, J. C., Ajayan, J., Rajesh, S., & Nirmal, D. Investigation of efficiency enhancement in InGaN MQW LED with compositionally step graded GaN/InAlN/GaN multi-layer barrier. *Superlattices and Microstructures*, *116*, 71-78. (2018).

[35] SaifAddin, B. K., Almogbel, A., Zollner, C. J., Foronda, H., Alyamani, A., Albadri, A., ... & Speck, J. S. Fabrication technology for high light-extraction ultraviolet thin-film flip-chip (UV TFFC) LEDs grown on SiC. *Semiconductor Science and Technology*, *34*(3), 035007. (2019).

[36] Lu, X., Zhu, S., Lin, R., Sun, D., Cui, X., & Tian, P. Performance improvement of red InGaN micro-LEDs by transfer printing from Si substrate onto glass substrate. *IEEE Electron Device Letters*, *43*(9), 1491-1494. (2022).

[37] Jiang, X., Zheng, C., Mo, C., Wang, X., Zhang, J., Quan, Z., ... & Jiang, F. Study on the performance of InGaN-based green LED by designing different preparing layers. *Optical Materials*, *89*, 505-511. (2019).

[38] Mo, C., Fang, W., Pu, Y., Liu, H., & Jiang, F. Growth and characterization of InGaN blue LED structure on Si (1 1 1) by MOCVD. *Journal of crystal growth*, *285*(3), 312-317. (2005).

Lee, M., Yang, M., Song, K. M., & Park, S. InGaN/GaN blue light emitting diodes using freestanding GaN extracted from a Si substrate. *ACS Photonics*, *5*(4), 1453-1459. (2018).

[39] Pasayat, S. S., Gupta, C., Wong, M. S., Wang, Y., Nakamura, S., Denbaars, S. P., ... & Mishra, U. K. Growth of strain-relaxed InGaN on micrometer-sized patterned compliant GaN pseudo-substrates. *Applied Physics Letters*, *116*(11), 111101. (2020).

[40] Nakamura, T., & Motoki, K. GaN substrate technologies for optical devices. *Proceedings of the IEEE*, *101*(10), 2221-2228. (2013).

[41] Ooi, Y. K., & Zhang, J. Design analysis of phosphor-free monolithic white light-emitting-diodes with InGaN/InGaN multiple quantum wells on ternary InGaN substrates. *AIP Advances*, *5*(5), 057168. (2015).

[42] Ryou, J. H., Yoder, P. D., Liu, J., Lochner, Z., Kim, H., Choi, S., ... & Dupuis, R. D. Control of quantum-confined stark effect in InGaN-based quantum wells. *IEEE Journal of Selected Topics in Quantum Electronics*, *15*(4), 1080-1091. (2009).

[43] Zhang, J., & Tansu, N. Optical gain and laser characteristics of InGaN quantum wells on ternary InGaN substrates. *IEEE Photonics Journal*, *5*(2), 2600111-2600111. (2013).

[44] Saha, M., Biswas, A., & Karan, H. Monolithic high performance InGaN/GaN white LEDs with a tunnel junction cascaded yellow and blue light-emitting structures. *Optical Materials*, *77*, 104-110. (2018).

[45] Wang, J., Meisch, T., Heinz, D., Zeller, R., & Scholz, F. Internal quantum efficiency and carrier injection efficiency of c-plane, and InGaN/GaN-based light-emitting diodes. *physica status solidi (b)*, *253*(1), 174-179. (2016).

[46] Robin, Y., Pristovsek, M., Amano, H., Oehler, F., Oliver, R. A., & Humphreys, C. J. What is red? On the chromaticity of orange-red InGaN/GaN based LEDs. *Journal of Applied Physics*,*124*(18), 183102. (2018).

[47] J. Schanda, ed. Colorimetry: understanding the CIE system. John Wiley & Sons, 2007.

[48] R. J. Mortimer, & T. S. Varley. Quantification of colour stimuli through the calculation of CIE chromaticity coordinates and luminance data for application to in situ colorimetry studies of electrochromic materials. *Displays*, vol. 32, no 1, p. 35-44, (2011).

[49] R. J. Tilley. Colour and the optical properties of materials. John Wiley & Sons,(2020).

[50] Stauss, P., Mandl, M., Rode, P., Laubsch, A., Biebersdorf, A., Windisch, R., ... & Steegmüller, U. Monolitically grown dual wavelength InGaN LEDs for improved CRI. *physica status solidi c*, *8*(7-8), 2396-2398. (2011).

[51] Yan, D., Zhao, S., Zhang, Y., Wang, H., & Zang, Z. Highly efficient emission and high-CRI warm white light-emitting diodes from ligand-modified CsPbBr 3 quantum dots. *Opto-Electronic Advances*, *5*(1), 200075-1. (2022).

[52] Iida, D., Zhuang, Z., Kirilenko, P., Velazquez-Rizo, M., & Ohkawa, K. High-color-rendering-index phosphor-free InGaN-based white light-emitting diodes by carrier injection enhancement via V-pits. *Applied Physics Letters*, *117*(17), 172103. (2020).

[53] Titkov, I. E., Yadav, A., Zerova, V. L., Zulonas, M., Tsatsulnikov, A. F., Lundin, W. V., ... & Rafailov, E. U. Internal quantum efficiency and tunable colour temperature in monolithic white InGaN/GaN LED. In *Gallium Nitride Materials and Devices IX* (Vol. 8986, pp. 271-278). SPIE. (2014).

[54] Lin, D., Zhong, P., & He, G. Color temperature tunable white LED cluster with color rendering index above 98. *IEEE Photonics Technology Letters*, *29*(12), 1050-1053. (2017).

[55] Onwukaeme, C., Lee, B., & Ryu, H. Y. Investigation into the stability condition of correlated color temperature of white illumination sources based on trichromatic light-emitting diodes.*Displays*, 102358. (2022).

[56] Akinlami, J. O., & Olateju, I. O. Reflection coefficient and optical conductivity of gallium nitride GaN. *Semiconductor physics quantum electronics & optoelectronics*. (2012).

[57] Son, J. H., Kim, J. U., Song, Y. H., Kim, B. J., Ryu, C. J., & Lee, J. L. Design Rule of Nanostructures in Light-Emitting Diodes for Complete Elimination of Total Internal Reflection. *Advanced Materials*, *24*(17), 2259-2262. (2012).

[58] ATLAS Manual., Silvaco Software Inc. (2013).

[59] Meneghini, M., Trivellin, N., Meneghesso, G., Zanoni, E., Zehnder, U., & Hahn, B. (2009). A combined electro-optical method for the determination of the recombination parameters in InGaN-based light-emitting diodes. *Journal of Applied Physics*, *106*(11).

[60] David, A., & Grundmann, M. J. (2010). Droop in InGaN light-emitting diodes: A differential carrier lifetime analysis. *Applied Physics Letters*, *96*(10).

[61] Laubsch, A., Sabathil, M., Baur, J., Peter, M., & Hahn, B. High-power and high-efficiency InGaN-based light emitters. *IEEE transactions on electron devices*, *57*(1), 79-87,(2009).

[62] Zhang, M., et al. "Direct measurement of auger recombination in In0. 1Ga0. 9N/GaN quantum wells and its impact on the efficiency of In0. 1Ga0. 9N/GaN multiple quantum well light emitting diodes." *Applied Physics Letters* 95.20 (2009).

[63] Chuang, S.L., and C.S. Chang, "k*p Method for Straind Wurtzite Semiconductors", Phys. Rev. B Vol. 54, No. 4, 15: 2491-2504. (1996).

[64] Y. Sayad and A.K. Nouiri. Electroluminescence properties of InGaN/GaN multiple quantum well light emitting diodes. Int. J. Nanoparticles, Vol. 6, Nos. 2/3, (2013).

[65] H. Jian-Jang; K. Hao-Chung; S. Shyh-Chiang. Nitride Semiconductor Light-Emitting Diodes (LEDs): Materials, Technologies, and Applications. Woodhead Publishing, (2017).

[66] G. Muziol, H. Turki, *et al.* Beyond quantum efficiency limitations originating from the piezoelectric polarization in light-emitting devices. *ACS Photonics*, vol. 6, no 8, p.1963-1971. (2019).

[67] G. A. Garrett, H. Shen, M. Wraback, A. Tyagi, S. Nakamaura, et al. Comparison of time-resolved photoluminescence from InGaN single quantum wells grown on nonpolar and semipolar bulk GaN substrates.*physica status solidi c*, *6*(S2 2), S800-S803. (2009).

[68] Y. C. Shen, G.O.Mueller, S. Watanabe, et al. Auger recombination in InGaN measured by photoluminescence, Applied Physics Letters. 91 (14) 141101-141103.(2007).

[69] S .Yamamoto, Y. Zhao, C. Pan, et al. High-Efficiency Single-Quantum-Well Green and Yellow-Green Light-Emitting Diodes on Semipolar (20$\bar{2}$1) GaN Substrates, Applied Physics Express. 3 (12) 122102.(2010).

[70] H. Sato, A. Tyagi, H. Zhong et al. High power and high efficiency green light emitting diode

on free-standing semipolar (11(2)over-bar2) bulk GaN substrate, Phys Status Solidi (RRL)– Rapid Research Letters. 1 (4) (2007) 162–164. (2007).

[71] S. Zhang, J. Zhang, J. Gao, et al. Efficient emission of InGaN-based light-emitting diodes: toward orange and red, Photonics Research. 8 (11) 1671-1675.(2020).

[72] A. Tyagi, H. ZHong, N.N. Fellows et al. High Brightness Violet InGaN/GaN Light Emitting Diodes on Semipolar (1011) Bulk GaN Substrates. Japanese Journal of Applied Physics, vol. 46, no. 7, pp. L129-L131, (2007).

[73] A. David, M. J. Grundmann, J. F. Kaeding & all. Carrier distribution in (0001) In Ga N⁄ Ga N multiple quantum well light-emitting diodes. *Applied Physics Letters*, *92*(5), 053502.(2008).

[74] Y. Jiang, Y. Li, et all. Realization of high-luminous-efficiency InGaN light-emitting diodes in the "green gap" range. Scientific reports, *5*(1), 1-7, (2015).

[75] Y. Kawaguchi, C. Y. Huang, S.Nakamura, et all. Semipolar ($20\bar{2}1$) single-quantum-well red light-emitting diodes with a low forward voltage.Japanese journal of applied physics, 52(8S), 08JC08. (2013).

[76] H. Masui, H. Yamada, K. Iso, S. Nakamura, et all. Optical polarization characteristics of m-oriented InGaN/GaN light-emitting diodes with various indium compositions in single-quantum-well structure. *Journal of Physics D: Applied Physics*, *41*(22), 225104. (2008).

[77] F. K. Yam, & Z.Hassan, InGaN: An overview of the growth kinetics, physical properties and emission mechanisms.Superlattices and Microstructures, *43*(1), 1-23. (2008).

[78] Information on https://www.ies.org/definitions/table-t-5a-color-matching-functions-and-chromaticity-coordinates-of-cie-1931-standard-colorimetric-observer/.

Appendixes

Appendixes A: CIE 1931 reference observer in the normalized reference system Distribution coefficients for the Trichromatic coefficients Wavelength stimuli of the same energy [78].

Chromaticity coordinates			Wavelenght λ [nm]	CIE color Matching functions		
x	y	z		$\bar{x}(\lambda)$	$\bar{y}(\lambda)$	$\bar{z}(\lambda)$
0.1741	0.0050	0.8209	380	0.0014	0.0000	0.0065
0.1738	0.0049	0.8213	390	0.0042	0.0001	0.0201
0.1733	0.0048	0.8219	400	0.0143	0.0004	0.0679
0.1726	0.0048	0.8226	410	0.0435	0.0012	0.2074
0.1714	0.0051	0.8235	420	0.1344	0.0040	0.6456
0.1689	0.0069	0.8242	430	0.2839	0.0116	1.3856
0.1644	0.0109	0.8247	440	0.3483	0.0230	1.7471
0.1566	0.0177	0.8257	450	0.3362	0.0380	1.7721
0.1440	0.0297	0.8263	460	0.2908	0.0600	1.6692
0.1241	0.0578	0.8181	470	0.1954	0.0910	1.2876
0.0913	0.1327	0.7760	480	0.0956	0.1390	0.8130
0.0454	0.2950	0.6596	490	0.0320	0.2080	0.4652
0.0082	0.5384	0.4534	500	0.0049	0.3230	0.2720
0.0139	0.7502	0.2359	510	0.0093	0.5030	0.1582
0.0743	0.8338	0.0919	520	0.0633	0.7100	0.0782
0.1547	0.8059	0.0394	530	0.1655	0.8620	0.0422
0.2296	0.7543	0.0161	540	0.2904	0.9540	0.0203
0.3016	.6923 0	0.0061	550	0.4334	0.9950	0.0087
0.3731	0.6245	0.0024	560	0.5945	0.9950	0.0039
0.4441	0.5547	0.0012	570	0.7621	0.9520	0.0021
0.5125	0.4866	0.0009	580	0.9163	0.8700	0.0017

Publications And Communications

I-Journal Publications

- ✓ **Ahmid Djelloul,** HAMAIZIA Zahra, "**Design and Numerical Simulation of Color Tunable Laterally Arranged Quantum Well Light Emitting Diode with Double Anode Single Cathode",** *Advanced Materials Research , Vol. 1170, pp 11-24, Online: 2022-05-24*

  DOI: https://doi.org/10.4028/p-a4ldk0

II-Conferences

- ✓ **D. Ahmid** Z. Hamaizia**,** A. Saadoune **,** "Contribution **à** la modélisation et **à** la simulation numériques des diodes électroluminescentes **à** hétérojonction multicouches ", Le 1 er Colloque Doctoral sur La Méthodologie d'Elaboration d'une Thèse et d'une Publication en Doctorat, EI-Oued : 07 Mars 2018.

- ✓ **D. Ahmid**, Z. Hamaizia**,** A. Saadoune, "Simulation of tunable laterally arranged quantum well light emitting diode", International Symposium on Technology & Sustainable Industry Development ISTSID'19, Elouad , February 24-26 2019.

- ✓ **D. Ahmid**, Z. Hamaizia , "Comparative study of violet and green InGaN-based SQW LEDs using Silvaco TCAD tool ",1st International Conference on Optoelectronics, Materials & Renewable Energy, ICOMRE22 EL OUED, December 12-13 2022.

Advanced Materials Research
ISSN: 1662-8985, Vol. 1170, pp 11-24

Submitted: 2020-10-24
Revised: 2021-12-17
Accepted: 2022-01-13
Online: 2022-05-24

Design and Numerical Simulation of Color Tunable Laterally Arranged Quantum Well Light Emitting Diode with Double Anode Single Cathode

AHMID Djelloul[1,a*], HAMAIZIA Zahra[1,b]

[1]LMSM – Mohammed Khieder University, 07000 Biskra, Algeria

[a]Ahmid.djelloul@outlook.com, [b]z.hemaizia@univ-biskra.dz

Keywords: Gallium nitride, Indium gallium nitride, Aluminum gallium nitride, Color tunable LED, Silvaco, Quantum well, Electrode, Laterally arranged SQW.

Abstract. In this paper, a color-tunable light emitting diode LED with two laterally arranged single quantum wells (SQWs) is designed, and simulated. In this work, III-nitride materials are used. The structure has been numerically investigated using the ATLAS simulation software. The proposed structure has three electrodes. This gives the opportunity to emit violet (420 nm) or green (560 nm) light individually. Furthermore, it can emit simultaneously a mixture of both colors, and at a certain mixture ratio the white light is obtained with chromaticity coordinates ($x = 0.3113$, $y = 0.3973$). The lateral arrangement of the two SQWs reduces the negative effect of photon absorption; which will give good external quantum efficiency (EQE). The structure has a big importance in the application of the solid-state lighting, especially in the white light generation.

Introduction

During the last two decades, the great achievement of energy saving, using solid-state lighting technology was very remarkable; where wurtzite nitride based light emitting diodes LEDs [1] are widely used. Furthermore, the white light and color-tunable LEDs have a big importance in modern display industry, such as high efficiency light bulbs, and flat-screen televisions.

In many researches a phosphor free monolithic white LED has been proposed, in which a multi-quantum wells (MQWs) with different indium content active layers have been used [2-5]. These structures suffer from low performance because of inhomogeneous carrier's distribution. This is reported in many works [6]. Another critical problem has been encountered where a part of the photons generated by the higher band gap active layer will be absorbed by the lower band gap active layer [7]. It is also reported that the radiative recombination efficiency decreases with increasing indium composition [8]. All of these drawbacks make the conception of white light, and different emission colors MQW LED very difficult. Many color-tunable LEDs have been designed by some researchers, generally with three terminals structure [9-11]. In these structures QWs are vertically stacked. This solution suffers from photon absorption problems as the ordinary multi-color emitting MQW LEDs.

In addition, the quantum well (QW) LEDs grown on sapphire substrates have a large polarization electric field. It is due to the large lattice mismatch that leads to the quantum confined Stark effect (QCSE). This lowers the internal quantum efficiency [12, 13]. This problem becomes more significant for longer wavelength devices such as green LEDs. To overcome this inconvenience, gallium nitride (GaN) substrate has been suggested by several groups; promising results were obtained with the peak emission ranging from 413 nm to 590 nm, where violet, blue, green, yellow and amber colors can be generated [13-16].

The main issue of this simulation work is the design of violet-green color tunable monolithic LED. The structure has a multi-junction structure with laterally arranged SQWs grown on GaN substrate. Here, white and multi-color light can be generated. Additionally, the proposed device will limit the negative effects mentioned above. The selective area growth method can be used in the fabrication process of the proposed device [17]. The structure has three electrodes; this will give the opportunity of varying the color, which is a mixture of violet and green spectra.

The LED structure has been numerically investigated using ATLAS simulation software, which is a powerful tool for understanding, and designing electronic devices. It predicts many physical

Equipe Modélisation Simulation et Optimisation des Systèmes Alternatifs et Durables

Faculté de Technologie

Unité de Recherche Matériaux Procédés et Environnement

Le 1er Colloque Doctoral Sur
La Méthodologie d'Elaboration d'une Thèse et d'une Publication en Doctorat
El-Oued : 07 Mars 2018

Attestation de Participation

Le président du comité d'organisation du 1er Colloque Doctoral atteste que

Mr. (Mme. Melle.) **AHMID Djelloul**

a présenté une communication ***Poster*** intitulée

Contribution à la modélisation et à la simulation numériques des diodes électroluminescentes à hétérojonction multicouches

Co- auteur (s): HAMAIZIA Zahra and SAADOUNE Achour

Le Doyen de la Faculté de Technologie

الجمهورية الجزائرية الديمقراطية الشعبية
People's Democratic Republic of Algeria
وزارة التعليم العالي والبحث العلمي
Ministry of Higher Education and Scientific Research

Centre de Recherche en Technologies Industrielles-Alger

جامعة الشهيد حمه لخضر - الوادي
Université Echahid Hamma Lakhdar - El-Oued

Direction Générale de la Recherche Scientifique et du Développement Technologique

Certificate of Participation

ISTSID, 24-25-26/02/2019

This Certifies That the paper entitled

Simulation of tunable laterally arranged quantum well light emitting diode

Has been presented with successfully as (Poster) presentation at the ISTSID'2019

By: AHMID Djelloul

Co-Authors: HAMAIZIA Zahra, SAADOUNE Achour

ISTSID'19 General Chair

International Symposium on Technology & Sustainable Industry Development

People's Democratic Republic of Algeria
Ministry of Higher Education and Scientific Research
Echahid Hamma Lakhdar University - El-Oued
1st International Conference on Optoelectronic, Materials & Renewable Energy
ICOMRE'22
1st Edition, December 12-13, 2022

Certificate of Participation

This Certifies that the paper entitled as

Comparative study of violet and green InGaN-based SQW LEDs using Silvaco TCAD tool

Has been presented with successfully as (Oral) presentation at the ICOMRE'22

In the Topic of: Optoelectronics

By (Mr.; Ms.) **AHMID Djelloul**

Mohammed Khieder university, LMSM laboratory, Faculty of technology, 07000 Biskra, Algeria

Co-Authors: **HAMAIZIA Zahra z.hemaizia@univ-biskra.dz**

Equipements Scientifique & Didactique

Algeria, December 12, 2022
ICOMRE'22 Chairman